学位申請論文

Studies on the Nonlinear Interactions in a Two-Layer, Quasi-Geostrophic, Low-Order Model with Topography

Shigeo Yoden

Geophysical Institute, Kyoto University

論文内容の要旨

報告番号	甲第　　号	氏名	余田成男
論文調査担当者	主査　山元龍三郎 中島暢太郎　　光田寧		

（論文題目）

Studies on the nonlinear interactions in a two-layer, quasi-geostrophic, low-order model with topography.

（地形を含む2層　準地衡　低次モデルを用いた大規模大気非線型相互作用の研究）

（論文内容の要旨）

山岳強制波を含む大規模大気運動の非線型相互作用の本格的な研究は，1979年および1980年にCharneyらによって始められた。彼らは，順圧大気中では外部パラメータが同じであっても安定平衡解が2種類ある事，そして，傾圧大気中では唯1種の安定平衡解しか存在しない事を見出した，Charneyらの研究は，大気のブロッキング現象の機構の説明を指向したものであったので，非線型相互作用の研究としては，十分に系統的なものではなかった。

申請者余田成男の主論文は，Charneyらと同様に，山岳強制波動を考慮した傾圧大気中の非線型相互作用を数値実験的に研究したものである。申請者の用いた数値モデルは，運動の鉛直分布は2層で表現し，水平分布は展開直交関数の低次項のみで表わす，いわゆる低次2層モデルである。

主論文第Ⅰ部では，山岳強制波と東西風との間の非線型相互作用を研究

している。まず，南北モードが１つの保存系については共鳴条件を確かめると共に，平衡解の不安定性には２種類－地形による不安定性と傾圧不安定性－がある事を明らかにした。非保存系では，外部パラメータのある範囲内で，時間的に変化する解の多重性を見出している。そして，安定周期解の周期が外部パラメータの変化に伴なって，２倍．４倍となる周期倍化現象の存在を明らかにした。

自由波動を追加した場合を．主論文第Ⅱ部で研究している。東西風の不安定性について，山岳と同じスケールの波に対して，他のスケールの波よりも不安定な場合には，山岳強制波は自由波動と共存する。逆の場合には，山岳強制波が時間の経過と共に減衰して，一定の振幅と位相速度をもつ自由波動のみが卓越する事を見出している。さらに，東西波数および南北モード数を増やして，詳細な数値実験を行なった。運動状態は，南北温度差や摩擦などの外部パラメータの値に依存して，４つの型に分類できるとしている。実際の大気で見られるような外部パラメータの値の場合．大きい振幅の波を含む不規則変動が現われる。長期にわたる時間積分の結果を統計処理して，その時間平均値として検出される停滞波は，自由波動の存在しない場合に平衡解として得られた山岳強制波とは，明らかに異なる構造を有している事を見出し，自由波動の役割の重要性を明らかにした。

参考論文の２篇の論文は，いずれも大規模大気運動の非線型過程を取扱ったものである。その１では，回転水槽実験で流れの模様が変化するいわゆるVacillationは，順圧過程と傾圧過程とが交互に卓越する事によってひき起こされている事を明らかにしている。その２では，東西風と傾圧不安定波の相互作用を研究し，非線型相互作用の結果として，エネルギー過程に，約15日の周期をもつ準周期的変動が生ずる事を示している。

Nonlinear interactions in a two-layer, quasi-geostrophic, low-order model with topography

Part I: Zonal flow-forced wave interactions

by Shigeo Yoden

Geophysical Institute, Kyoto University,
Kyoto, 606, Japan.

Abstract

A two-layer, quasi-geostrophic, low-order model is constructed to investigate the nonlinear interactions between the zonal flow, topographically forced waves and free baroclinic waves. In Part I free baroclinic waves are excluded to direct our attention to the zonal flow-forced wave interactions.

In the conservative case, without external thermal forcing and dissipation, equilibrium solutions are obtained and the resonance condition in the present two-layer model is examined. Multiple flow equilibria are also obtained in the non-conservative case. However, unlike the barotropic model of Charney and DeVore(1979), there do not exist two stable equilibria. A multiplicity of the time-dependent solutions is found in a certain range of the external parameters. There exist two or more stable periodic(or aperiodic) solutions for the same external conditions. The selection of a solution depends on the initial condition.

As the external thermal forcing parameter increases or decreases by bits, the period of a stable periodic solution can become doubled, quadrupled, and so on. Finally aperiodic solutions appear through the period-doubling sequence phenomenon.

1. Introduction

The nonlinear interaction between the zonal flow and free baroclinic waves was investigated in our previous paper (Yoden, 1981; hereafter referred to as Y81) using a two-layer quasi-geostrophic spectral model on a β-plane. In Y81 it was shown that the zonal flow-baroclinic wave interaction is one of the possible mechanisms for the quasi-periodic variation in the atmosphere with time scales of two to three weeks.

However, it has been well known that planetary waves forced by the large-scale topography and land-sea distributions play an important role in the general circulation of the atmosphere as well as free baroclinic waves. Especially, quasi-stationary phenomena such as the atmospheric blocking are considered to be strongly influenced by the forced planetary waves. Some numerical experiments with a realistic lower boundary condition have shown that the blocking is closely related to the topography and land-sea distributions(Kikuchi, 1969, 1971; Bengtsson, 1981).

Recently Charney and DeVore(1979; hereafter referred to as CD) studied the interaction between the zonal flow and topographically forced waves in a barotropic model with vorticity source and frictional dissipation. They treated the nonlinear interaction explicitly by using highly-truncated spectral expansions with an idealized topography of a single Fourier component. In a certain range of the external forcing they found two stable equilibrium states(i.e., steady and stationary states) for the same external conditions. One of the stable equilibrium states is a high-index circulation with a strong zonal flow and a small-amplitude wave. The other is a low-index circulation(or a blocking state) with a weak zonal flow and a large-amplitude wave. The

concept of the multiple flow equilibria shown by CD is a new departure for understanding the blocking mechanism.

Multiple equilibria in a baroclinic system were investigated by Charney and Straus(1980; referred to as CS) and Roads(1980) with a two-layer model. Both of them obtained multiple equilibrium solutions associated with a single wave with the gravest meridional mode. But only the low-index(blocking) state is stable and there do not exist multiple stable equilibria as in the barotropic model of CD. They also obtained some time-dependent solutions by numerical integrations. CS had a periodic solution which is characterized by a westward propagating wave interacting with a fluctuating zonal flow. However, their numerical experiments were not done very systematically and there still remains uncertainty in the conditions for the appearance of the steady solutions, periodic solutions and aperiodic solutions.

In this paper we study the nonlinear interactions between the zonal flow, topographically forced waves and free baroclinic waves, using the highly-truncated spectral model of Y81 with some modifications.

In Part I free baroclinic waves are excluded to direct our attention to the interaction between the zonal flow and planetary waves influenced by a topography. The system used in Part I is similar to that in CS, except for the values of the external parameters. Equilibrium solutions are obtained in cases with and without the external thermal forcing and dissipation in order to discuss the resonance condition and the multiplicity of solutions. Stability of the equilibrium solutions is also analyzed by solving an eigenvalue problem of the linearized equations. In a non-conservative case with source and sink terms, numerical

integrations are performed to investigate the time-dependent behavior of the system such as its attraction to a steady state, its periodicity and aperiodicity. The conditions for the appearance of these equilibrium solution, periodic solution and aperiodic solution are examined by varying the external parameters.

The interactions between the zonal flow, topographically forced planetary waves and baroclinically unstable waves (represented by higher harmonics of the forced wave) are investigated in Part II.

2. Model description

A two-layer quasi-geostrophic model in a mid-latitude β-channel was constructed in Y81, which was based on Lorenz's model(1963) for the study of the mechanics of vacillation in the rotating annulus experiments. Here we include an effect of the surface topography in the model through a modification of the lower boundary condition. The governing equations for the two-layer model(Fig. 1) are as follows;

the vorticity equations,

$$\frac{\partial}{\partial t}\nabla^2\psi = - J(\psi, \nabla^2\psi) - J(\tau, \nabla^2\tau) - \beta\frac{\partial\psi}{\partial x} + \frac{f_0}{2\Delta P}\omega_4$$

$$- k(\nabla^2\psi - \nabla^2\tau) \qquad (2\text{-}1)$$

$$\frac{\partial}{\partial t}\nabla^2\tau = - J(\psi, \nabla^2\tau) - J(\tau, \nabla^2\psi) - \beta\frac{\partial\tau}{\partial x} + \frac{f_0}{\Delta P}\omega_2 - \frac{f_0}{2\Delta P}\omega_4$$

$$+ k(\nabla^2\psi - \nabla^2\tau) - 2k'\nabla^2\tau \qquad (2\text{-}2)$$

the thermodynamic equation,

$$\frac{\partial}{\partial t}\theta = - J(\psi, \theta) + \frac{\bar{\bar{\sigma}}}{\Delta P}\omega_2 + H(\theta^* - \theta) \qquad (2\text{-}3)$$

the thermal wind equation,

$$\nabla^2\theta = A\nabla^2\tau \qquad (2\text{-}4)$$

and the lower boundary condition,

$$\omega_4 = - \rho_4 g J(\psi-\tau, h) \qquad (2\text{-}5)$$

Here the following notation is employed;

t	time
$J(a,b)$	horizontal Jacobian $(= \frac{\partial a}{\partial x}\frac{\partial b}{\partial y} - \frac{\partial a}{\partial y}\frac{\partial b}{\partial x})$
∇^2	horizontal Laplacian $(= \frac{\partial^2}{\partial x^2} + \frac{\partial^2}{\partial y^2})$
$\overline{\quad}$	horizontal average
$\psi(x,y,t)$	stream function for the vertically averaged wind
$\tau(x,y,t)$	stream function for the vertical wind shear
$\omega(x,y,t)$	vertical p-velocity
$\theta(x,y,t)$	mean potential temperature
$\theta^*(x,y)$	prescribed equilibrium potential temperature
$h(x,y)$	topographic height
$\overline{\overline{\sigma}}$	horizontally averaged static stability
ρ	air density ($\rho_4 = 1.225$ kg/m^3)
g	gravitational acceleration (9.8 m/s^2)
f_0	mean Coriolis parameter
β	variation of Coriolis parameter with latitudinal length
$2k$	frictional coefficient at the lower boundary
k'	frictional coefficient at the interface
H	heating coefficient for Newtonian heating
A	a constant depending on the properties of fliud, $A = f_0 [\frac{C_p}{2} \{ (\frac{P_3}{P_4})^\kappa - (\frac{P_1}{P_4})^\kappa \}]^{-1}$

where C_p is the specific heat at constant pressure and κ is the ratio R/C_p (R is the gas constant for dry air.).

In (2-3) we assume $\overline{\overline{\sigma}}$ to be constant in time. This is required in order to avoid the third order nonlinearity and is physically consistent with the fact that the static stability is determined primarily by moist convection (see CS). An analysis of energy budget shows that the sum of the potential and internal

energy is conserved when friction and heating are absent. Therefore the total energy is not conserved in this model. In such a case, however, the sum of the kinetic and available potential energy is conserved if the latter is defined by

$$APE = \frac{f_0 P_4}{gA} \frac{1}{\bar{\bar{\sigma}}} \iint (\theta - \bar{\bar{\theta}})^2 \, dx \, dy \qquad (2\text{-}6)$$

The vertical p-velocity at the surface is calculated in (2-5) by use of the stream function in the lower layer. In this formulation of ω_4 the topography does not give a net contribution to the time rate of change of kinetic energy(Yao, 1980).

We transform the equations (2-1)-(2-5) into a spectral form. First we expand the field variables in orthogonal functions as follows;

$$\left.\begin{aligned} F_0 &= 1 \\ F_{Am} &= \sqrt{2} \cos\frac{my}{L} \\ F_{Km}^n &= 2 \sin\frac{my}{L} \cos\frac{nx}{L} \\ F_{Lm}^n &= 2 \sin\frac{my}{L} \sin\frac{nx}{L} \end{aligned}\right\} \qquad (2\text{-}7)$$

which satisfy the lateral boundary conditions at $y = 0$ and $y = \pi L$. Substituting the spectral expansion into (2-1)-(2-5) and eliminating τ and ω components, we finally obtain a set of ordinary differential equations for the expansion coefficients, $\psi_i(t)$ and $\theta_i(t)$. (Here subscript i is one of A_m, K_m^n or L_m^n.)

$$\dot{\psi}_i = a_i^{-2}\Big[\sum_{j=1}^{\infty}\sum_{k>j}^{\infty} c_{ijk}\{(a_j^2 - a_k^2)(\psi_j\psi_k + \theta_j\theta_k) + (\psi_j - \theta_j)h_k - (\psi_k - \theta_k)h_j\} + \beta\sum_{j=1}^{\infty} b_{ij}\psi_j\Big] - k(\psi_i - \theta_i) \tag{2-8}$$

$$(1+\frac{1}{\sigma_0 a_i^2})\dot{\theta}_i = a_i^{-2}\Big[\sum_{j=1}^{\infty}\sum_{k>j}^{\infty} c_{ijk}\{(a_j^2 - a_k^2 - \frac{1}{\sigma_0})\psi_j\theta_k + (a_j^2 - a_k^2 + \frac{1}{\sigma_0})\theta_j\psi_k - (\psi_j - \theta_j)h_k + (\psi_k - \theta_k)h_j\} + \beta\sum_{j=1}^{\infty} b_{ij}\theta_j\Big] + k(\psi_i - \theta_i) - 2k'\theta_i - \frac{H}{\sigma_0 a_i^2}(\theta_i^* - \theta_i) \tag{2-9}$$

Here ψ is non-dimensionalized by $L^2 f_0$; θ and σ by $AL^2 f_0$; β by f_0/L; k, k' and H by f_0; and t by $1/f_0$. The coefficients a_i, b_{ij} and c_{ijk} are given by

$$L^2\nabla^2 F_i = -a_i^2 F_i \tag{2-10}$$

$$L\frac{\partial}{\partial x}F_j = \sum_{i=1}^{\infty} b_{ij}F_i \quad , \quad b_{ij} = \overline{\overline{LF_i\frac{\partial}{\partial x}F_j}} \tag{2-11}$$

$$L^2 J(F_j, F_k) = \sum_{i=1}^{\infty} c_{ijk}F_i \quad , \quad c_{ijk} = \overline{\overline{L^2 F_i J(F_j, F_k)}} \tag{2-12}$$

We truncate the expansion by retaining a few components of the meridional mode $m=1,2,..,M$ and the wavenumber $n=n_0, 2n_0, .., Nn_0$. Then (2-8) and (2-9) constitute a set of $2M\times(2N+1)$ ordinary differential equations. In this paper we set $M=1$ or 2 and $N=1$, 2 or 3. Hence we have a dynamical system with 28 degrees of freedom for least severely truncated case ($M=2$ and $N=3$). Table 1 shows the interaction coefficient c_{ijk} with non-

zero value. The systems for M=1 can depict the wave-zonal flow interactions, while those for M=2 can depict both the wave-zonal flow and the wave-wave interactions. If we put M=2 and N=1, we obtain the same spectral equations as in CS except for the values of constant coefficients.

The parameter values used in the present model are given in the remainder of this section. As in Y81 we adopt an infinite channel on a β-plane with lateral boundaries at 20°N and 70°N. Then the Coriolis parameter f_0 and β are given as values at 45°N:

$$\begin{aligned} f_0 &= 1.03 \times 10^{-4}\ s^{-1} \\ \beta &= 1.61 \times 10^{-11} m^{-1} s^{-1} \end{aligned} \qquad (2\text{-}13)$$

The wavenumber n is related to the zonal wavenumber $\tilde{n}$ in the latitude circle at 45°N by

$$\tilde{n} = a \cdot n \cdot \cos 45^\circ / L \qquad (2\text{-}14)$$

where a is the radius of the earth. Hereafter $\tilde{n}$ will be used in practice.

Unless otherwise mentioned, we use the same values of frictional and heating coefficients as in Y81. Then

$$\left.\begin{aligned} 2k &= 0.02 \\ k' &= 0.005 \\ H &= 0.01 \end{aligned}\right\} \quad \text{(non-dimensional)} \qquad (2\text{-}15)$$

which correspond to e-decaying times of 5.63 days, 22.5 days and 11.3 days, respectively.

We restrict the prescribed potential temperature to its first zonal component $\theta^*_{A_1}$. As a control external parameter, $\theta^*_{A_1}$ will be varied from 0 to 0.2 . The corresponding temperature difference across the channel is from 0 K to 150 K at the radiative equilibrium state. In this paper we do not discuss an effect of the variation of diabatic heating in the longitudinal direction.

As for the static stability we set $\sigma_0 = 5.64 \times 10^{-2}$, and in dimensional form $2\overline{\overline{\sigma}}/\Delta P = 30$ K/500 mb.

We describe the surface topography by a single component of $h_{K_1^{\tilde{n}}}$, which is the lowest zonal wavenumber($\tilde{n}_0$) and the gravest meridional mode. The amplitude of the topography is fixed at 1 km (non-dimensionalized value $h_{K_1^{\tilde{n}_0}} = 6.01 \times 10^{-2}$). (For the earth's topography in middle latitudes, the amplitudes of the zonal wavenumbers $\tilde{n} = 1$ and 2 are roughly 1 km, and that of $\tilde{n} = 3$ is 600 m. Amplitudes for $\tilde{n} \geq 4$ are much smaller.)

3. Multiple equilibria and their stability(M=1)

In Part I we set N=1 and investigate the interaction between the zonal flow and topographically forced waves. In most highly truncated case(M=1, N=1), we obtain a dynamical system of six equations as follows;

$$\dot{\psi}_A = h^0(\psi_L-\theta_L) - k(\psi_A-\theta_A)$$

$$\dot{\psi}_K = -\alpha(\psi_A\psi_L + \theta_A\theta_L) + \beta'\psi_L - k(\psi_K-\theta_K)$$

$$\dot{\psi}_L = \alpha(\psi_A\psi_K + \theta_A\theta_K) - h^n(\psi_A-\theta_A) - \beta'\psi_K - k(\psi_L-\theta_L)$$

$$(1+F^0)\dot{\theta}_A = \gamma^0(\psi_K\theta_L - \theta_K\psi_L) - h^0(\psi_L-\theta_L) + k\psi_A - \ell^0\theta_A + F^0H\theta_A^*$$

$$(1+F^n)\dot{\theta}_K = -(\alpha+\gamma^n)\psi_A\theta_L - (\alpha-\gamma^n)\theta_A\psi_L + \beta'\theta_L + k\psi_K - \ell^n\theta_K$$

$$(1+F^n)\dot{\theta}_L = (\alpha+\gamma^n)\psi_A\theta_K + (\alpha-\gamma^n)\theta_A\psi_K + h^n(\psi_A-\theta_A) - \beta'\theta_K + k\psi_L - \ell^n\theta_L$$

where the superscripts and subscripts of A_1, K_1^n and L_1^n are omitted. The positive constants in (3-1)-(3-6) are given by

$$\alpha = -\frac{n^2}{n^2+1}c_{AKL}$$

$$\beta' = \frac{n}{n^2+1}\beta$$

$$\left.\begin{aligned} F^i &= \frac{1}{\sigma_0(i^2+1)} \\ \gamma^i &= -F^i c_{AKL} \end{aligned}\right\} \quad i = 0 \text{ or } n$$

$$h^i = -\frac{h_K}{i^2 + l} c_{AKL}$$

$$\ell^i = k + 2k' + F^i H$$

where $c_{AKL} = -\frac{8\sqrt{2}}{3\pi} n$.

a. Resonance in the conservative case

First we consider the conservative case by setting k, k' and H equal to zero. If we put the time derivatives in (3-1)-(3-6) equal to zero, we obtain two sets of equilibrium solutions.

One of them is given by

$$\psi_A = \theta_A = \frac{\beta'}{2\alpha} \tag{3-7}$$

$$\psi_K = \theta_K \tag{3-8}$$

$$\psi_L = \theta_L \tag{3-9}$$

where K and L components can be determined arbitrarily. There is no flow in the lower layer because every ψ component is equal to the corresponding θ component and $\theta_i = \tau_i$ due to the thermal wind relation. In the upper layer the zonal flow($\psi_A + \theta_A$) is $\frac{\beta'}{\alpha}$ and the wave component has arbitrary amplitude and phase. In this equilibrium state, the Jacobian term is balanced with the beta term and no topographic effect appears because there is no flow in the lower layer. The zonal flow in the upper layer has the value for which a Rossby wave with the same scale as that of the

topography becomes stationary. This value corresponds to the resonant value for the barotropic case in CD. But the equilibrium state in the present case is not a resonance because the wave in the upper layer is independent of the topography. Note that the resonance condition obtained in CS is incorrect, which is identical to (3-7) in the present notation.

The other set is

$$\begin{cases} \psi_K = h^n(\psi_A - \theta_A)\{(\alpha+\gamma^n)\psi_A - \beta' + \alpha\theta_A\}/D & (3\text{-}10) \\ \theta_K = -h^n(\psi_A - \theta_A)\{\alpha\psi_A - \beta' - (\gamma^n-\alpha)\theta_A\}/D & (3\text{-}11) \\ \psi_L = \theta_L = 0 & (3\text{-}12) \\ D = (\alpha\psi_A - \beta')\{(\alpha+\gamma^n)\psi_A - \beta'\} + \alpha(\gamma^n-\alpha)\theta_A^2 & (3\text{-}13) \end{cases}$$

where the zonal components ψ_A and θ_A have arbitrary values. In this equilibrium state three terms in (3-3) and (3-6), i.e., the Jacobian term, the topographic term and the beta term, are balanced for any zonal wind. The wave components are purely in phase or out of phase with the topography depending on their sign of K components. When the numerator in (3-10) or (3-11) is not zero and the denominator D tends to zero, the amplitudes of the wave become positive or negative infinity. Therefore the condition for resonance is

$$D = 0 \text{ and } h^n \neq 0 \qquad (3\text{-}14)$$

except for the indefinite cases of $(\psi_A, \theta_A) = (\frac{\beta'}{2\alpha}, \frac{\beta'}{2\alpha})$ and

$(\frac{\beta'}{\gamma^n}, \pm\frac{\beta'}{\gamma^n})$. The condition D=0 is an ellipse in ψ_A- θ_A plane for $\alpha<\gamma^n$. This inequality is transformed to $\sigma_0 n^2<1$, and $\tilde{n}<11$ for the parameters given in the previous section.

The magnitudes of ψ_K and θ_K for $\tilde{n}=3$ are shown in Figs.2-(a) and (b). The resonance curve (3-14) and some other characteristic lines are also shown in Fig.2-(c). Positive ψ_A indicates the westerly mean zonal wind and positive θ_A means that the zonally-averaged temperature decreases with latitude. Resonance occurs only in the westerly mean zonal flow($\psi_A>0$) and the greater part of resonance curve exists for the westerly flow in the lower layer($\psi_A-\theta_A>0$). If the zonal wavenumber $\tilde{n}$ is increased, the resonance curve shifts toward the origin and the resonant area decreases, because the value β'/α is decreased in proportion to $1/\tilde{n}^2$.

Next we analyze the linear stability of the equilibrium solutions. Equations (3-1)-(3-6) are linearized for small perturbations from the equilibrium state. Compared with the conventional baroclinic instability analysis, the present system has three differences: (1) a perturbation of zonal components, (2) a basic state with wave components, and (3) an inclusion of topographic term. Letting the perturbation be proportional to $e^{\sigma t}$, we obtain the growth rate σ_r as a real part of the complex eigenvalues of the 6x6 coefficient matrix. If the eigenvalue σ is real and positive, the perturbation grows without propagation. This instability was termed orographic form-drag instability by CS(Hereafter the term 'topographic instability' is used in place of 'orographic form-drag instability'.). If σ is a complex number with positive real part, such an instability is a topographically-modified, baroclinic instability(We use the term

'modified baroclinic instability' instead of 'topographically-modified, baroclinic instability' for simplicity.).

Fig.2-(d) shows the growth rate for the most unstable mode. Dotted area is the region of the topographic instability, oblique-lined area the region of the modified baroclinic instability and the rest of the domain is a neutral region. The equilibrium solutions are topographically unstable outside the resonance curve and neutral inside it with some exceptions near the origin. In the topographically unstable region the growth rate becomes large either as the zonal components ψ_A and θ_A approach the resonance condition, or as the zonal flow in the lower layer ($|\psi_A - \theta_A|$) becomes large in the off-resonant area. The modified baroclinic instability surpasses the topographic instability in the region of large θ_A and small $|\psi_A - \theta_A|$. In other words, the zonal flow profile with large vertical shear and weak flow in the lower layer is preferred by that mode. The growth rate of the modified baroclinic disturbance becomes large as the zonal flow in the lower layer becomes weak.

These stability properties of the equilibrium solutions remain similar in cases of other zonal wavenumbers. But the area where the modified baroclinic instability surpasses the topographic instability increases as the zonal wavenumber is increased.

b. Non-conservative case

If we take account of the effects of heating and friction described in section 2, the system has energy sources and sinks

due to the zonally symmetric Newtonian heating, the frictional dissipation and the eddy components of the diabatic heating. For such a non-conservative case we can obtain all equilibrium solutions of equations (3-1)-(3-6) using the same method as that in CS.

Presented in Fig.3 are all the equilibrium solutions within the range of $0 \leq \theta_A \leq \theta_A^*$ for $0 < \theta_A^* \leq 0.2$. The zonal wavenumber is again $\tilde{n}=3$. For $0 < \theta_A^* < 0.09$ there exists only the Hadley solution with no wave components. In the same way as in CS, the Hadley solution is given by

$$\psi_A = \theta_A = \frac{H}{2k'\sigma_0 + H}\,\theta_A^* \tag{3-15}$$

$$\psi_K = \theta_K = \psi_L = \theta_L = 0 \tag{3-16}$$

There is no topographic effect for this solution because there is no flow in the lower layer.

When the parameter of differential heating θ_A^* exceeds the critical value($(\theta_A^*)_c = 0.09$), there appear two wavy equilibrium solutions indicated by W1 and W2. As the heating parameter θ_A^* increases, the amplitudes of the wave components become large, while those of the zonal components change a little. The zonal components of the equilibrium solutions are plotted in ψ_A-θ_A plane of Fig.2-(c). Both wavy solutions are bifurcated from the Hadley solution at a point close to $(\psi_A, \theta_A) = (\frac{\beta'}{2\alpha}, \frac{\beta'}{2\alpha})$. The W1 solutions are located inside the resonance curve in the conservative case while the W2 solutions outside it.

As the zonal wavenumber increases, the magnitude of the zonal components at the bifurcation point decreases: $\psi_A = \theta_A = 0.084$ for

$\tilde{n}$=3, 0.048 for $\tilde{n}$=4 and 0.031 for $\tilde{n}$=5. These values are also close to $\beta'/2\alpha$ for each wavenumber. For $\tilde{n}$=4 and $\tilde{n}$=5 there exist four wavy equilibrium solutions for the same θ_A^* in a small range near the bifurcation point. Additional two wavy solutions appear as a result of bending of the branch of W2 solutions. The appearance of new wavy solutions is similar to that in CS. However, the appearance is not connected to the existence of both of baroclinic and topographic instability of the Hadley solution contrary to their conclusion. For $\tilde{n}$=1 or $\tilde{n}$=2, on the other hand, there is no wavy solution in the range of $0<\theta_A^*\leq 0.2$. Because the value of $\beta'/2\alpha$ is 0.750 for $\tilde{n}$=1 and 0.187 for $\tilde{n}$=2.

The stream functions of three equilibrium solutions for $\tilde{n}$=3 and θ_A^*=0.15 are presented in Fig.4. The Hadley solution has no flow in the lower layer(Eqs. (3-15) and (3-16)). The W1 solution is nearly out of phase with topography and the W2 solution is nearly in phase. In both wavy solutions, the trough line has a westward tilt with height. The stationary wave transports heat northward. The sum of the convergence of the heat flux due to the meridional circulation and the stationary wave balances the time rate of the diabatic heating. Compared with the Hadley solution, the rate of the heating is large because of the small value of θ_A.

Next we analyze the linear stability of the equilibrium solutions in the non-conservative case. Fig.5 shows the growth rates(σ_r) of the perturbation. Pure real eigenvalue is denoted by a dot and eigenvalues of complex conjugate are denoted by a plus-sign. The Hadley solution is stable for $0<\theta_A^*<0.09$, topographically unstable for $0.09\leq\theta_A^*\leq 0.11$, and baroclinically unstable(influenced by the topography) for $0.11<\theta_A^*$. Note that

the point at which the topographic instability arises coincides with the bifurcation point of the wavy solutions, $(\theta_A^*)_c$. The broken line in the figure shows the growth rate in the case of no topography, i.e., the purely baroclinic instability. Topographic effect reduces the growth rate and then shifts the critical value to larger θ_A^*.

All the W1 solutions are stable, while W2 solutions are baroclinically or topographically unstable. These stability properties correspond to those in the conservative case: Equilibrium solutions inside the resonance curve are neutral and those outside it are unstable(see Figs.2-(c) and (d)).

In the present case there do not exist multiple stable equilibria like the high-index and blocking states in CD. The only stable equilibrium solution is the Hadley solution for $\theta_A^* < (\theta_A^*)_c$ and the W1 solution for $\theta_A^* \geq (\theta_A^*)_c$.

This is similar for $\tilde{n}=4$ or $\tilde{n}=5$ with a small exception near the bifurcation point. Both wavy solutions are stable near that point. Indeed two stable equilibrium solutions exist in the small range around $\theta_A^*=0.052$ for $\tilde{n}=4$ and $0.034 \leq \theta_A^* \leq 0.036$ for $\tilde{n}=5$. However, near the bifurcation point two wavy solutions have only small difference from each other. Therefore the multiple stable equilibria in the present two-layer model are different from those in the CD's barotropic model.

Some numerical integrations are performed to clarify the global structure of the system (3-1)-(3-6). Trajectories of the time-dependent behavior are projected onto $\psi_A - \psi_K$ and $\psi_A - \psi_L$ planes(Fig.6). Initial states are unstable equilibrium solutions(the Hadley and the W2 solutions) with small perturbations. The initial behavior depends on the initial condotion. But

once captured by the attractor basin of the W1 solution, the dependent variables asimptotically approach the W1 solution with a similar trajectory. This behavior agrees with the linear stability analysis(Fig.5): The W1 solution is a stable focus. Attraction to the W1 solution requires about 1,000 time steps(in dimensional 112.5 days).

4. System with two meridional modes(M=2)

a. Role of the second meridional mode

In the previous section we restricted the meridional mode to only one component. In such a case it is impossible to depict the barotropic process by eddy momentum flux, because the wave is symmetric in the horizontal plane without tilting of the trough and ridge lines. Time-variation of the zonal component is determined by the eddy heat flux, the topographic term and the forcing and dissipation terms(Eqs. (3-1) and (3-4)). If the second meridional mode is permitted, it becomes possible to depict the barotropic process. Interactions betweèn the waves of the first and the second meridional modes contribute to the time variation of zonal flow of the second mode(Table 1).

When we permit the second meridional mode by setting M=2, we obtain a dynamical system with 12 degrees of freedom. Equations (3-1)-(3-6) for the case of M=1 constitute a sub-system of the present system when we take all the second mode components equal to zero. Therefore, the equilibrium solutions obtained in the previous section(Fig.3) form a part of the equilibrium solutions in the present system(M=2).

However, this is not the case for M=3,4,..., because the interaction between the lowest modes produces the higher modes. For example, in the case of M=3 the interaction between K_1 and L_1 components produces A_3 component as well as A_1 component because of $c_{A_3K_1L_1} \neq 0$ (see Yoden, 1979). In such an extended system of M=3 the equilibrium solutions in the system of M=1 are no longer one part of the equilibrium solutions.

In the present system of M=2 it is difficult to obtain all

the equilibrium solutions by a similar manner as that adopted in CS. Therefore we are not concerned with the equilibrium solutions with the second meridional mode except for the solutions obtained by numerical integrations.

The stability of the equilibrium solutions is examined by solving an eigenvalue problem of the 12x12 coefficient matrix of the linearized equations. For the equilibrium solutions of the first meridional mode, the characteristic equation can be re-written in the product of two sixth-order equations of for the first and the second meridional mode perturbations. The stability properties for the first mode perturbation are identical to the result obtained in the M=1 case(Fig.5 for $\tilde{n}$=3). The growth rate for the second mode perturbation is shown in Fig.7. The Hadley solution is topographically unstable for the second mode perturbation in the range of $0.04 \leqq \theta_A^* < 0.054$ and baroclinically unstable for $0.054 \leqq \theta_A^*$. In the case of $\tilde{n}$=3 the Hadley solution is more unstable with respect to the second mode perturbation than the first mode for $\theta_A^* \leqq 0.174$. However, the selection of the most unstable mode depends on the wavenumber(e.g., for $\tilde{n}$=5 the first mode perturbation has a larger growth rate than the second mode for most of θ_A^*). This is due to the dependency of the stability criteria and the growth rate on the square of wavenumber(m^2+n^2).

Both of the wavy solutions are baroclinically unstable (topographically affected). Here we use the term 'baroclinically unstable' in the sense of instability with $\sigma_i \neq 0$ (propagating disturbance). Indeed barotropic conversion terms are also included in the perturbation equations as well as baroclinic conversion terms. Note that the W1 solution is unstable with respect to the perturbations of the second meridional mode. Therefore all

the equilibrium solutions which was obtained in the system of the first mode components(M=1) are unstable for $0.04 \leqq \theta_A^*$ in the present system of M=2.

b. Numerical solutions

When all the equilibrium solutions of the first meridional mode are unstable in the M=2 system, there may exist equilibrium solutions with the second meridional mode or time dependent solutions which are either periodic or aperiodic. Some numerical integrations were performed to find thèm. Appearance of these solutions depends on the external parameters. In this subsection the dependency on the external forcing parameter θ_A^* is investigated by changing the parameter bit by bit.

The result is summarized in Fig.8. For $\theta_A^* \leqq 0.038$ there appears the Hadley solution even if we include the second mode perturbation. When the Hadley solution becomes unstable($\theta_A^*=0.04$ and 0.042), twelve variables in the system converge to either of the two steady solutions with wave components depending on the initial conditions. The equilibrium values of each component are listed in Table 2. Two stable equilibrium solutions have the same first meridional components and have the opposite sign of the second components each other. Zonal components of the first meridional mode and wave components of the second meridional mode have large amplitude in the equilibrium. It is impossible, however, to confirm that these two solutions are all the equilibrium solutions with both of the meridional modes, because they were obtained by numerical integrations with several initial

conditions.

For θ_A^*=0.044 and 0.046 there appear two periodic solutions depending on the initial condition. Trajectories for θ_A^*=0.046 projected on three phase planes(ψ_{A_1}-ψ_{A_2}, ψ_{A_1}-ψ_{K_2} and ψ_{A_1}-ψ_{L_2} planes) are shown in Fig.9-(a). Two periodic solutions are oscillations around the unstable equilibrium solutions and they are symmetric with respect to the axis of the second mode components ψ_{X_2}=0(X is A, K or L). Namely one periodic solution has the second mode components with opposite sign of that of the other solution. Period of the oscillation is 74.3 days for θ_A^*=0.044 and 79.4 days for θ_A^*=0.046. In these periodic states the amplitude and phase of the wave components fluctuate around a mean value and the wave does not propagate to one direction.

For θ_A^*=0.048, two periodic solutions are coalescent and the trajectories are complicated(Fig.9-(b)). This is a transition stage from (a) unsymmetric oscillation with respect to the second meridional modes to (c) symmetric oscillation. Symmetric oscillation (b) has both of the properties of the periodic solutions (a) and (c). Period of the oscillation is 181.7 days for the first mode variables.

For further increased θ_A^*($\geqq$0.05) there appears another symmetric oscillation with respect to the second meridional mode(Fig.9-(c)). The variables of the second meridional mode oscillates with a double period(157.4 days) of the first mode(78.7 days). In this periodic state all the wave components propagate westward. There is no structural change of the periodic behavior in the range of $0.05 \leqq \theta_A^* \leqq 0.2$. As θ_A^* increases, wave amplitudes of the second mode components become large but other components change a little. Namely the increase of the differen-

tial heating is mainly compensated by the increase of the eddy heat flux by the second mode wave. The period of the oscillations does not depend on θ_A^* so much and are 60-70 days.

These periodic solutions are not similar to those obtained in CS, in which the first meridional mode wave propagated westward while the second mode wave propagated eastward. The difference between the periodic solutions is discussed in detail in the next subsection.

c. Some other results with halved frictional parameters

For the external parameters given in section 2, there appears only one periodic solution for $0.048 \leqq \theta_A^*$. However, two or more periodic solutions are discovered in the cases with a smaller frictional parameter for the same external conditions. In this subsection we halve the value of frictional parameters used so far; $2k=0.01$ and $k'=0.0025$. Figs.10 show the two periodic solutions for $\theta_A^*=0.14$. If the Hadley solution or the W1 solution with small perturbation is taken as an initial condition, there appears the periodic solution (A). On the other hand, the periodic solution (B) appears for the initial condition of the W2 solution. Here the equilibrium solutions of the first meridional mode components do not change substantially by halving the frictional parameters, except for the appearance of two additional wavy solutions by the bending of the W2 branch.

The first mode components of the solution (A) have a period of 49.9 days and those of the solution (B) have a period of 10.1 days. In the periodic solution (A) the second mode wave has a

large amplitude and both of the wave components propagate westward. In the periodic solution (B), on the other hand, the first mode wave has larger amplitude than the second mode and the second mode wave propagates eastward. The periodic solutions obtained in the previous subsection are similar to (A) and those in CS are similar to (B).

As θ_A^* increases or decreases, the periodic solution (A) does not have a structural change of the periodic behavior. On the other hand, the solution (B) has a quite different behavior depending on the external parameter θ_A^*. The period of the oscillating solutions is plotted in Fig.11 and some typical trajectories projected on ψ_{A_1}-ψ_{K_2} plane are presented in Figs.12.

There appears the periodic solution or aperiodic solution of the type (B) for $\theta_A^* \geqq 0.132$. Here the discrimination between periodic and aperiodic solutions were taken in the integrations for 30,000 non-dimensional time steps(in dimensional 3,375 days). Aperiodic solution is denoted by a cross on the abscissa in Fig.11. Figs.12-(1) and (2) are trajectories for both of the periodic solutions (A) and (B) for $\theta_A^*=0.135$. The solution (A) is symmetric with respect to the second meridional mode but the solution (B) is not symmetric.

However, the solution (B) becomes symmetric in the range of $0.1356 \leqq \theta_A^* \leqq 0.1454$(Fig.12-(3)). When θ_A^* exceeds a critical value(=0.1455), the symmetry of the periodic solution breaks down again with respect to the second mode components. There appear two periodic solutions of type (B), which have the second mode components with opposite signs each other. One of them are shown in Fig.12-(4). Period of the first mode components is doubled and equal to that of the second mode components. With increasing θ_A^*

the period-doubling bifurcations take place and there finally appears an aperiodic solution for $0.1508 \leq \theta_A^* \leq 0.153$ (Figs.12-(5) and (6)).

When θ_A^* is increased further, there appears another periodic solution of 78.7 days ($\theta_A^*=0.1531$) and the period-halving transitions take place at $\theta_A^*=0.15325$ and $\theta_A^*=0.15448$ (Figs.12-(7), (8) and (9)). Again aperiodic solutions appear within the range of $0.1548 \leq \theta_A^* \leq 0.1685$ (Fig.12-(10)). At $\theta_A^*=0.1686$ periodic solution appears as shown in Fig.12-(11) and the period-halving transition takes place at $\theta_A^*=0.1819$ (Fig.12-(12)).

For a wide range of θ_A^* there exist at least two time-dependent solutions: Periodic solution (A), and periodic or aperiodic solution(s) of type (B). There is a large difference in the time-dependent behavior between the two solutions of (A) and (B).

5. Discussion

In the conservative case of M=1 we obtained the resonance condition(Fig.2). Contrary to CS's result, there is an infinite number of combinations of mean zonal wind ψ_A and mean wind shear $\tau_A(=\theta_A)$ which satisfy the resonance condition (3-14). This is a distinctive feature of the baroclinic atmosphere. It was shown by Tung and Lindzen(1979) that there is an infinite number of wind configurations that can satisfy the single resonance condition: The resonance condition is a function of the mean zonal wind over the whole region between the ground and the turning level. The resonance condition obtained in section 3 is a specified one for the present two-layer model. The resonance condition for the barotropic case is $\psi_A = \beta'/\alpha$ in the present notation and is included in (3-14) with $\theta_A=0$. For the case of $(\psi_A, \theta_A) = (\frac{\beta'}{\alpha}, 0)$, wave component ψ_K has infinite value and $\theta_K=-h^n/\gamma^n$.

As regards the topographic instability we analyzed the linear stability of the equilibrium states obtained in the conservative case. Most of the wavy equilibria outside the resonance curve in Fig.2 are found to be topographically unstable. Namely the perturbation embedded in the wavy equilibria grows without propagation. The growth rate is large even in the off-resonant area and e-folding time is of the order of 0.5-2.0 days. The topographic instability is very interesting in connection with the amplification of large-scale planetary waves. An analysis of the NMC tropospheric data shows that in wintertime planetary wave of $\tilde{n}=3$ amplifies with time-scale of several days in a quasi-stationary state(Itoh, 1983).

In the non-conservative case with source and sink terms, we obtained the multiple equilibrium solutions(Fig.3). It is also

interesting to note that the type of bifurcation in the present two-layer model is different from that in the barotropic model. In the present model new wavy solutions(W1 and W2 solutions) branch from the Hadley solution when the primary Hadley solution becomes unstable(cf. Fig.5). The lowering of the degree of symmetry in the system takes place in connection with the bifurcation: The Hadley solution has no wave component but the wavy solutions branch off from it. This is one type of the bifurcations appearing in the steady problem of the fluid dynamics(see Matsuda(1982b) as for a general account on the bifurcations and symmetry breaking in fluid phenomena). An example of this type is the Bénard problem, in which the convection solution branches off from the heat conduction solution.

As shown in Fig.13 for CD's barotropic result, on the other hand, the equilibrium solutions appears above the snap point(denoted by S). These are slightly above resonance solution (2) and high-index solution (3). There exist three equilibria together with pre-existing, slightly below resonance solution (1). For a large external forcing parameter ψ_A^*, the branches (1) and (2) are coalescent and there exists only the solution (3) above the critical value(out of range in Fig.13). Because the branches (1) and (3) are always stable and the branch (2) is unstable, this type of bifurcation is characterized by the appearance and disappearance of a pair of stable and unstable solutions. An example of this type is found in the model of the circulation systems in the Venus atmosphere(Matsuda, 1980, 1982a).

If the second meridional mode components are permitted(section 4), there exist several types of solutions depending on the external parameters. As shown in Fig.8, there

takes place a transition of solutions with increasing θ_A^* : the Hadley solution → steady solution → unsymmetric periodic-solution (vacillation) → symmetric periodic-solution (vacillation). This transition resembles that in the zonal flow-baroclinic wave interaction model without topography(Lorenz, 1963; Yoden, 1979). However, in the present parameter range of θ_A^*, there does not appear the corresponding upper Hadley regime for a large thermal Rossby number($\propto\theta_A^*$). This difference is probably due to the assumption of constant static stability. In the interaction model of Lorenz(1963), the static stability σ_0 is determined dynamically and has a large value for large θ_A^* . This stabilization suppresses the baroclinic instability in the upper Hadley regime.

For smaller values of frictional parameters there appear irregular solutions. This is also consistent with the result in the interaction models of Lorenz and Yoden, in which the transition from vacillation to irregular regime takes place with increasing the Taylor number. The Taylor number is inversely proportional to the square of frictional coefficient. The transitions from the Hadley solution to the irregular solutions via steady and periodic solutions are general properties of the nonlinear baroclinic systems, although there are some differences due to the inclusion of the topography and the assumption of constant static stability.

The period-doubling sequence phenomenon was found in cases with smaller frictional parameters(Figs.11 and 12). As the external forcing parameter θ_A^* increases or decreases by bits, period of the stable periodic solution becomes doubled, quadrupled, and so on. This phenomenon is interesting in connection with the transition from periodic solution to irregular one. The period-

doubling sequence is also obtained in the barotropic model of CD. Fig.14 is a result for the barotropic case with 6 degrees of freedom(M=2 and N=1 in CD). When the external forcing ψ_A^* exceeds a critical value(=0.205), there appear periodic solutions by a Hopf bifurcation (see e.g., Marsden and McCracken, 1976). As ψ_A^* increases, the period-doubling bifurcations take place and finally aperiodic solution appears. The dependency of the solutions on the external forcing parameter is more complicated in the two-layer model(Fig.11) than in the barotropic model. Similar period-doubling phenomena were also found in the numerical analyses of the amplitude equations governing the dynamics of a weakly unstable finite-amplitude baroclinic waves(Pedlosky and Frenzen, 1980; Pedlosky, 1981). They discussed the relation between their results and the work of Feigenbaum(1978) on the universality of the period-doubling structure in a large class of recursion relations $x_{n+1}=\lambda f(x_n)$. However, it is difficult to clarify the strict relations between the result obtained here and the work of Feigenbaum(1978). We only gave some numerically analyzed results for the dynamical systems applied to a problem of the atmospheric circulation.

6. Summary

A two-layer, quasi-geostrophic, low-order model in a mid-latitude β-plane was constructed to study the nonlinear interactions between the zonal flow and waves in the presence of the surface topography. In Part I only one wave component was permitted in zonal direction(N=1) and one or two meridional modes(M=1 or 2) were considered for the zonal component and the wave.

In most highly truncated case(M=1), the model becomes a dynamical system with 6 degrees of freedom. First of all we obtained the equilibrium solutions in the conservative case without the external thermal forsing and dissipation. It was shown that there is an infinite number of wind configurations which satisfy the resonance condition. Two kinds of instability of the equilibrium solutions were also obtained; topographic instability(growing in place) and topographically-modified baroclinic instability.

For the non-conservative case multiple flow equilibria were obtained in our two-layer model. However, the stable equilibrium solution is only the low-index (blocking) state as in CS and Roads(1980). There is no counterpart of the stable high-index state of the CD's barotropic case. Therefore it is difficult to connect the multiple stable equilibria in CD directly to the blocking phenomena in the atmosphere.

If the second meridional mode components are included(M=2), all the equilibrium solutions of the first mode components become unstable except for the weak Hadley solutions. By some numerical integrations, several types of solutions were obtained depending on the external parameters. There take place the transitions of

solutions(Hadley solution -> steady solution -> unsymmetric vacillation -> symmetric vacillation) with increasing the thermal Rossby number or with increasing the Taylor number. These transitions are general properties of the nonlinear baroclinic systems as in Lorenz(1963) and Yoden(1979). The period-doubling sequence phenomenon was found in the transition from periodic solution to irregular one.

Besides it, we found the multiplicity of time-dependent solutions in a certain range of external parameters. There exist two or more stable periodic(or aperiodic) solutions for the same external conditions. One of which is similar to the periodic solutions obtained in CS. Characteristics of the time-dependent behavior are different in these solutions. The selection of a solution depends on the initial condition. However, there is a possibility of the transition form one periodic state to the other state if the external thermal forcing θ_A^* slowly varies with time like a seasonal variation.

References

Bengtsson, L., 1981: Numerical prediction of atmospheric blocking - A case study. Tellus, 33, 19-42.

Charney, J. G. and J. G. DeVore, 1979: Multiple flow equilibria in the atmosphere and blocking. J. Atmos. Sci., 36, 1205-1216.

——— and D. M. Straus, 1980: Form-drag instability, multiple equilibria and propagating planetary waves in baroclinic, orographically forced, planetary wave systems. J. Atmos. Sci., 37, 1157-1176.

Feigenbaum, M. J., 1978: Quantitative universality for a class of nonlinear transformations. J. Statis. Phys., 19, 25-52.

Itoh, H., 1983: An observational study on the amplification of planetary waves in the troposphere. XXXXX.

Kikuchi, Y., 1969: Numerical simulation of the blocking process. J. Meteor. Soc. Japan, 47, 29-54.

———, 1971: Influence of mountains and land-sea distribution on blocking action. J. Meteor. Soc. Japan, 49, 564-572.

Lorenz, E. N., 1963: The mechanics of vacillation. J. Atmos. Sci., 20, 448-464.

Marsden, J. E., and M. McCracken, 1976: The Hopf bifurcation and its applications. Springer-Verlag. pp. 408.

Matsuda, Y., 1980: Dynamics of the four-day circulation in the Venus atmosphere. J. Meteor. Soc. Japan, 58, 443-470.

———, 1982a: A further study of dynamics of the four-day circulation in the Venus atmosphere. J. Meteor. Soc. Japan, 60, 245-254.

———, 1982b: Classification of critical points and symmetry

breaking in fluid phenomena and its application to dynamic meteorology.YYYYY.

Pedlosky, J. and C. Frenzen, 1980: Chaotic and periodic behavior of finite-amplitude baroclinic waves. J. Atmos. Sci., 37, 1177-1196.

———, 1981: The effect of β on the chaotic behavior of unstable baroclinic waves. J. Atmos. Sci., 38, 717-731.

Roads, J. O., 1980: Stable near-resonant states forced by orography in a simple baroclinic model. J. Atmos. sci., 37, 2381-2395.

Tung, K. K. and R. S. Lindzen, 1979: A theory of stationary long waves. Part II: Resonant Rossby waves in the presence of realistic vertical shears. Mon. Wea. Rev., 107, 735-750.

Yao, M. S., 1980: Maintenance of quasi-stationary waves in a two-level quasi-geostrophic spectral model with topography. J. Atmos. Sci., 37, 29-43.

Yoden, S., 1979: Some dynamical properties of nonlinear baroclinic waves in a quasi-geostrophic model. J. Meteor. Soc. Japan, 57, 493-504.

———, 1981: Quasi-periodic energy variation in a zonal flow-baroclinic wave interaction model. J. Meteor. Soc. Japan, 59, 291-302.

Table 1 Subscripts of non-zero interaction coefficients, c_{ijk}.

($c_{ijk} = c_{jki} = c_{kij}$ and $c_{ijk} = - c_{ikj}$). Integer in square brackets denotes meridional mode or wavenumver.

M	interaction	N		
		1 [n]	2 [n,2n]	3 [n,2n,3n]
1 [1]	wave-zonal flow	$A_1K_1^nL_1^n$	$A_1K_1^{2n}L_1^{2n}$	$A_1K_1^{3n}L_1^{3n}$
2 [1,2]	wave-zonal flow	$A_1K_2^nL_2^n$ $A_2K_1^nL_2^n$ $A_2K_2^nL_1^n$	$A_1K_2^{2n}L_2^{2n}$ $A_2K_1^{2n}L_2^{2n}$ $A_2K_2^{2n}L_1^{2n}$	$A_1K_2^{3n}L_2^{3n}$ $A_2K_1^{3n}L_2^{3n}$ $A_2K_2^{3n}L_1^{3n}$
	wave-wave		$K_1^nK_2^nL_1^{2n}$ $K_1^nL_2^nK_1^{2n}$ $L_1^nK_2^nK_1^{2n}$ $L_1^nL_2^nL_1^{2n}$	$K_1^nK_1^{2n}L_2^{3n}$ $K_1^nK_2^{2n}L_1^{3n}$ $K_2^nK_1^{2n}L_1^{3n}$ $K_1^nL_1^{2n}K_2^{3n}$ $K_1^nL_2^{2n}K_1^{3n}$ $K_2^nL_1^{2n}K_1^{3n}$ $L_1^nK_1^{2n}K_2^{3n}$ $L_1^nK_2^{2n}K_1^{3n}$ $L_2^nK_1^{2n}K_1^{3n}$ $L_1^nL_1^{2n}L_2^{3n}$ $L_1^nL_2^{2n}L_1^{3n}$ $L_2^nL_1^{2n}L_1^{3n}$

Table 2 Equilibrium solutions with both of the meridional modes obtained by some numerical integrations.

Θ_A^*	ψ_{A_1} ψ_{A_2}	ψ_{K_1} ψ_{K_2}	ψ_{L_1} ψ_{L_2}	θ_{A_1} θ_{A_2}	θ_{K_1} θ_{K_2}	θ_{L_1} θ_{L_2}
0.04	0.0381 ±0.0014	-0.0008 ∓0.0014	0.0001 ±0.0064	0.0368 ∓0.0002	-0.0012 ±0.0004	-0.0000 ±0.0053
0.042	0.0399 ±0.0019	-0.0016 ∓0.0011	0.0003 ±0.0103	0.0373 ∓0.0003	-0.0023 ±0.0015	-0.0000 ±0.0080

Figure captions

Fig. 1 Two-layer representation of the model atmosphere.

Fig. 2 (a): Equilibrium values of ψ_K for combinations of ψ_A and θ_A ($\tilde{n}$=3). The regions of equilibrium values greater than 1.0 are shaded. (b): Equilibrium values of θ_K. (c): Resonance curve and three lines of $\psi_A - \theta_A = 0$, $(\alpha+\gamma^n)\psi_A - \beta' + \alpha\theta_A = 0$ and $\alpha\psi_A - \beta' - (\gamma^n - \alpha)\theta_A = 0$. There is also shown the equilibrium solutions in the non-conservative case(the Hadley, W1 and W2 solutions). (d): Linear stability of the equilibrium solutions. Growth rate σ_r for the most unstable mode is contoured.

Fig. 3 Equilibrium solutions in the non-conservative case ($\tilde{n}$=3).

Fig. 4 Stream functions of the equilibrium solutions ($\tilde{n}$=3 and θ_A^*=0.15). Phase of the forced wave λ and phase difference between the layers $\Delta\lambda$ are presented. Surface topography is shown in right-bottom with negative region shaded.

Fig. 5 Linear stability of the equilibrium solutions ($\tilde{n}$=3). Pure real eigenvalue is denoted by a dot and eigenvalues of complex conjugate are denoted by the plus sign. Broken line shows the growth rate in the case of no topography.

Fig. 6 Projection of the trajectory of amplitude coefficients onto $\psi_A - \psi_K$(top) and $\psi_A - \psi_L$ (bottom) planes($\tilde{n}$=3 and

θ_A^*=0.2). Initial conditions are denoted by an asterisk (left: Hadley solution, right: W2 solution).

Fig. 7 Linear stability of the equilibrium solutions ($\tilde{n}$=3) with respect to the perturbation of the second meridional mode. Notations are the same as in Fig.5. Note that the scale of the ordinate is half of that in Fig.5.

Fig. 8 Numerical solutions depending on θ_A^*. Trajectories of the periodic solutions(a-c) are shown in Fig.9.

Fig. 9 Projection of the trajectories of periodic solutions onto $\psi_{A1}-\psi_{A2}$ (top), $\psi_{A1}-\psi_{K2}$ (middle) and $\psi_{A1}-\psi_{L2}$ (bottom) planes. Scales in (b) and (c) are the same as in (a).

Fig.10 Two periodic solutions for the same external conditions (θ_A^*=0.14 and frictional parameters are halved; 2k=0.01 and k'=0.0025). The first integer in each parenthesis refers to the meridional mode and the second one the zonal wavenumber. Initial conditions are (A): Hadley or W1 solution, and (B): W2 solution with small perturbations. 1,000 nondimensional time corresponds to 112.5 days.

Fig.11 Periods of the oscillating solutions of (A) (denoted by a broken line) and (B) (denoted by a dot). Simbol X on the abscissa denotes the aperiodic solution. Integer in each parenthesis refers to the number in Fig.12.

Fig.12 Projection of the trajectories of periodic and ap-

eriodic solutions onto $\psi_{A_1} - \psi_{K_2}$ plane. Scales in (2)-(12) are the same as in (1).

Fig.13 Equilibrium solutions of the first meridional mode in the barotropic model of CD. External parameters are same as those in their Table 1.

Fig.14 Periods of the oscillating solutions in the barotropic model of CD. Values of external forcing parameter at which the period-doubling phenomenon takes place are also listed.

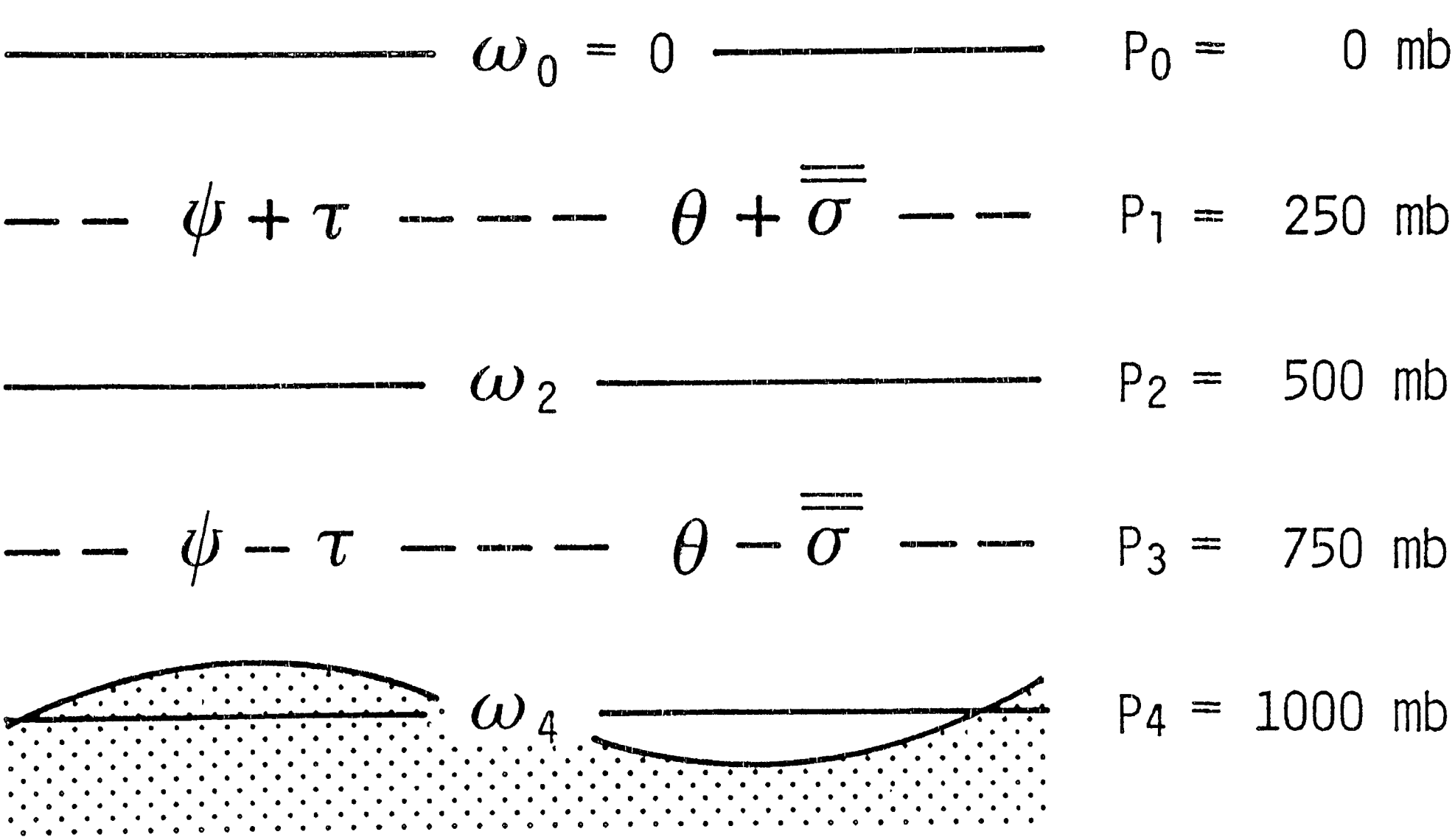
$\omega_0 = 0$
$P_0 =$ 0 mb
$\psi + \tau$
$\theta + \overline{\overline{\sigma}}$
$P_1 =$ 250 mb
ω_2
$P_2 =$ 500 mb
$\psi - \tau$
$\theta - \overline{\overline{\sigma}}$
$P_3 =$ 750 mb
ω_4
$P_4 =$ 1000 mb

Fig. 1

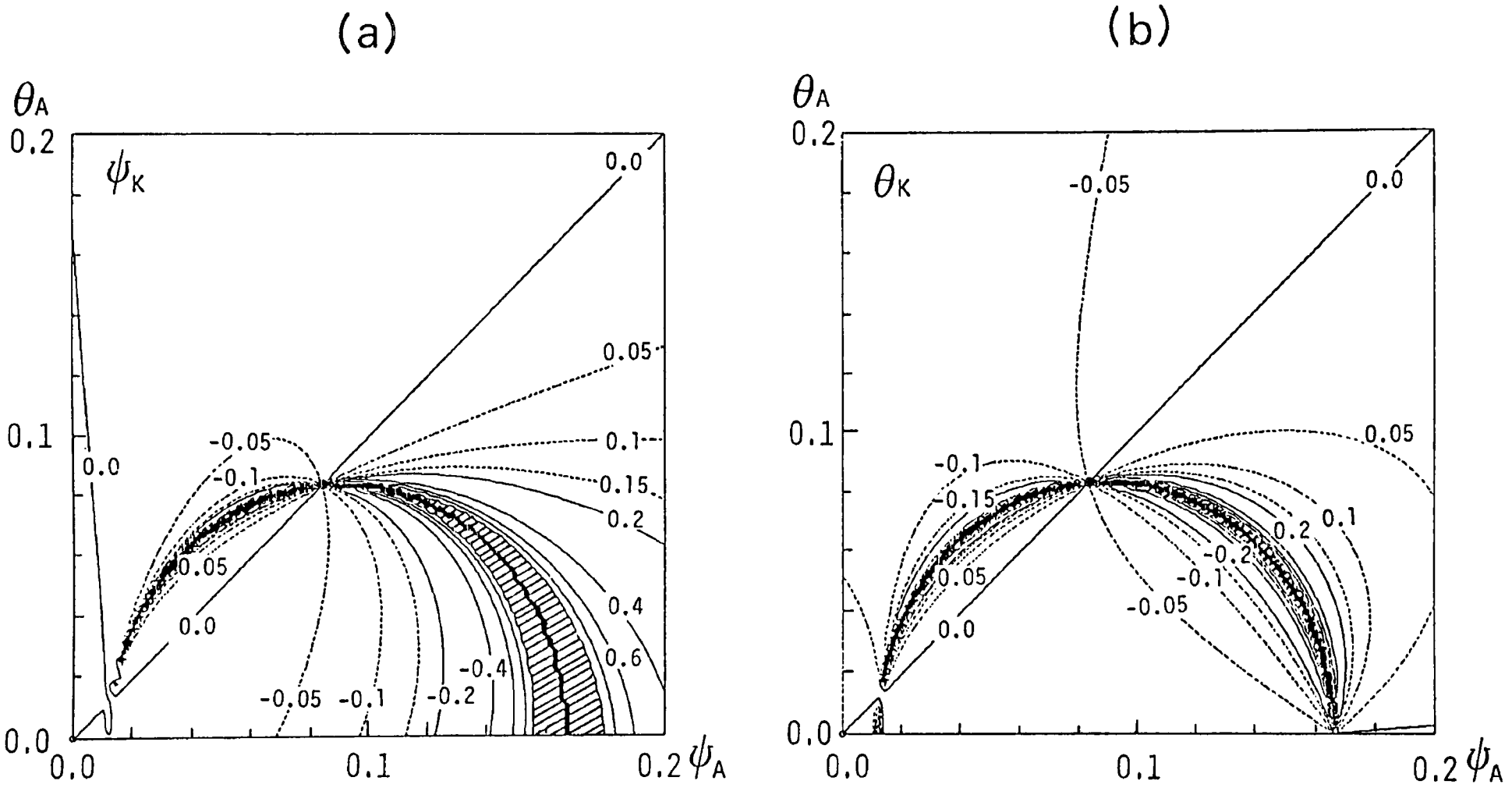

Fig. 2-(a), (b)

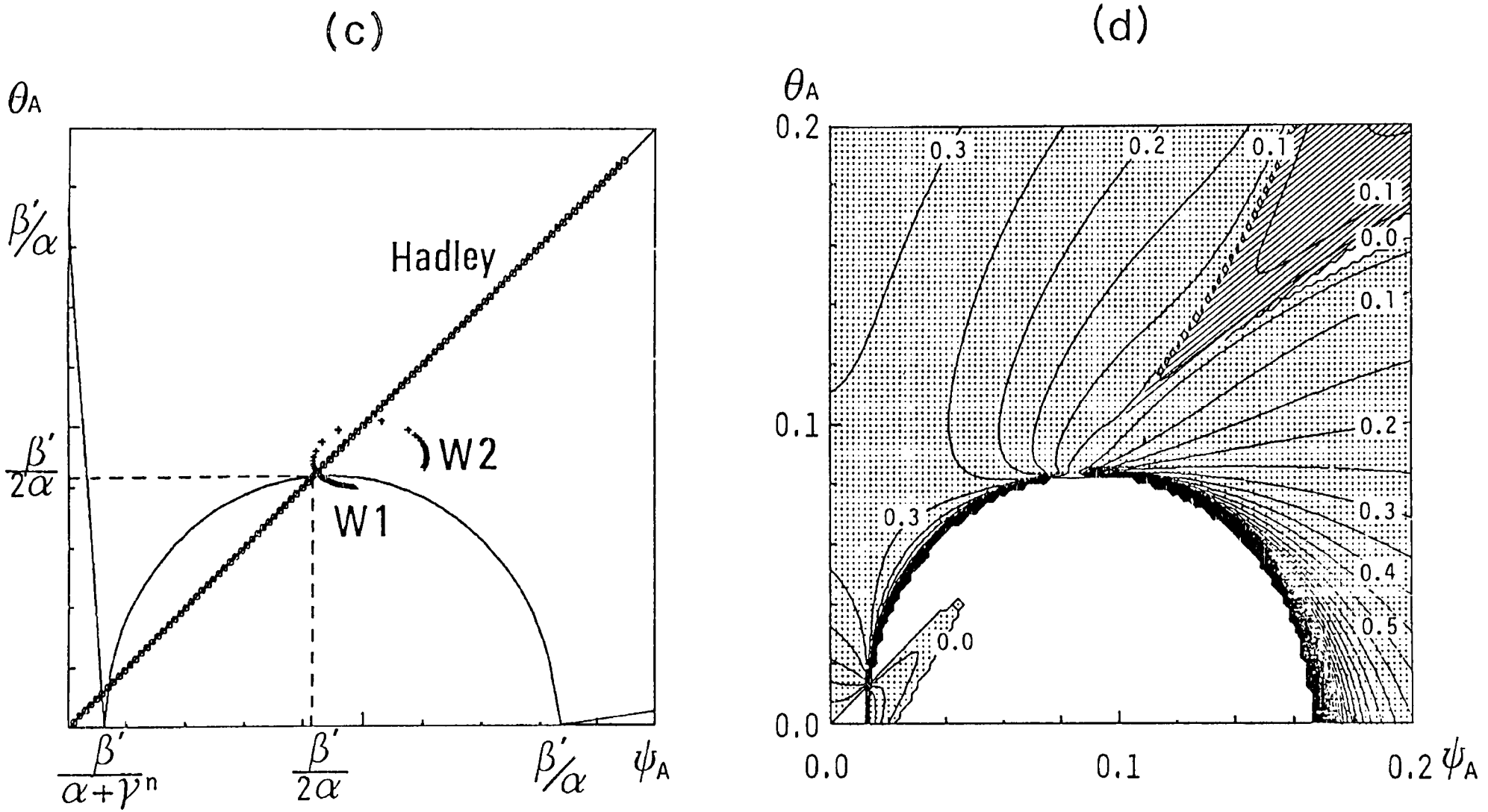
(c)
(d)
θA
β′/α
Hadley
β′/2α
W2
W1
β′/(α+γ^n)
β′/2α
β′/α
ψA
0.2
0.1
0.0
0.0
0.1
0.2 ψA
0.3
0.2
0.1
0.1
0.0
0.1
0.2
0.3
0.4
0.5
0.3
0.0

Fig. 2-(c), (d)

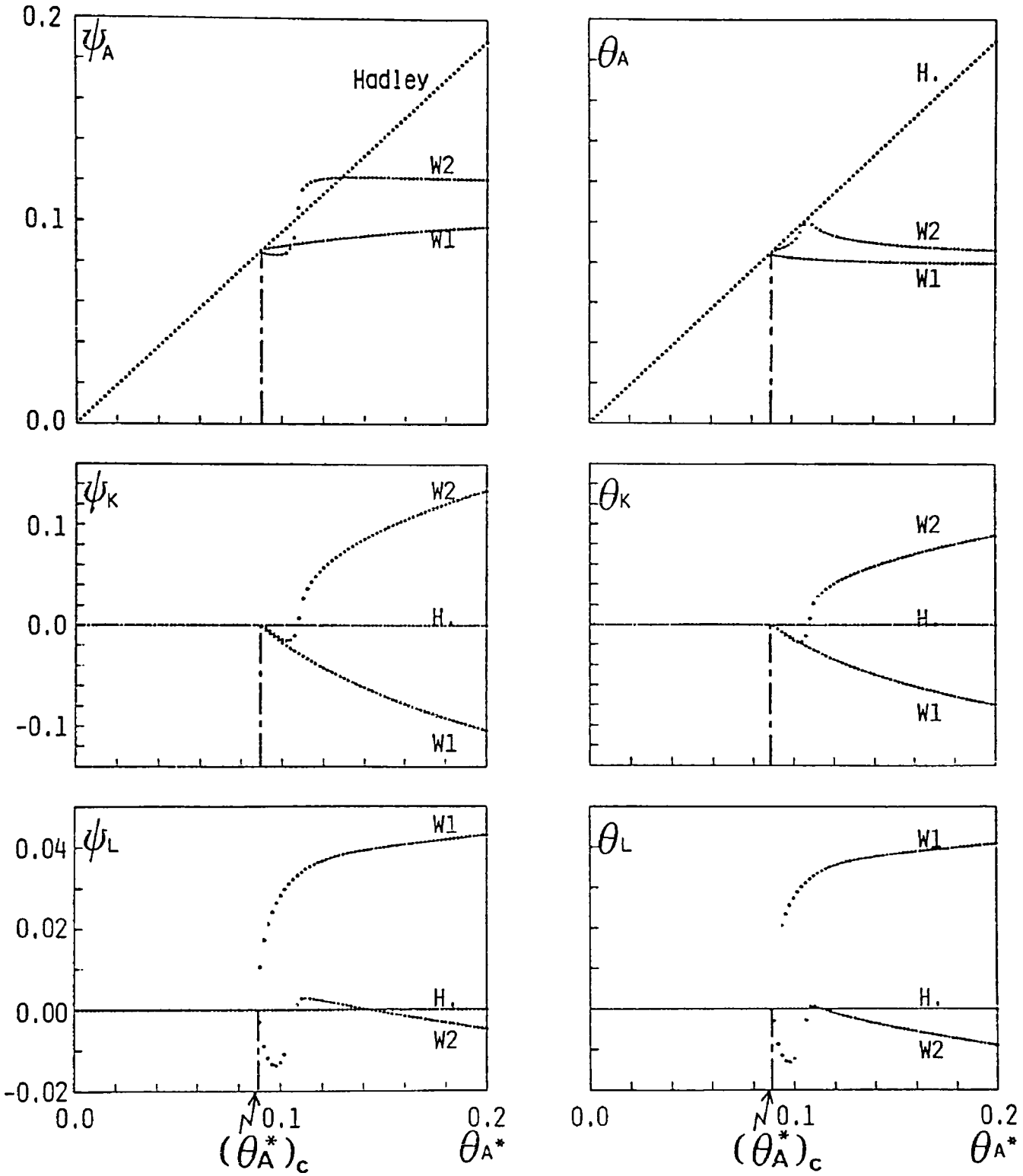
0.2
0.1
0.0
ψ_A
Hadley
W2
W1
θ_A
H.
W2
W1
ψ_K
0.1
0.0
-0.1
W2
H.
W1
θ_K
W2
H.
W1
ψ_L
0.04
0.02
0.00
-0.02
W1
H.
W2
θ_L
W1
H.
W2
0.0
0.1
0.2
$(\theta_A^*)_c$
θ_A^*

Fig. 3

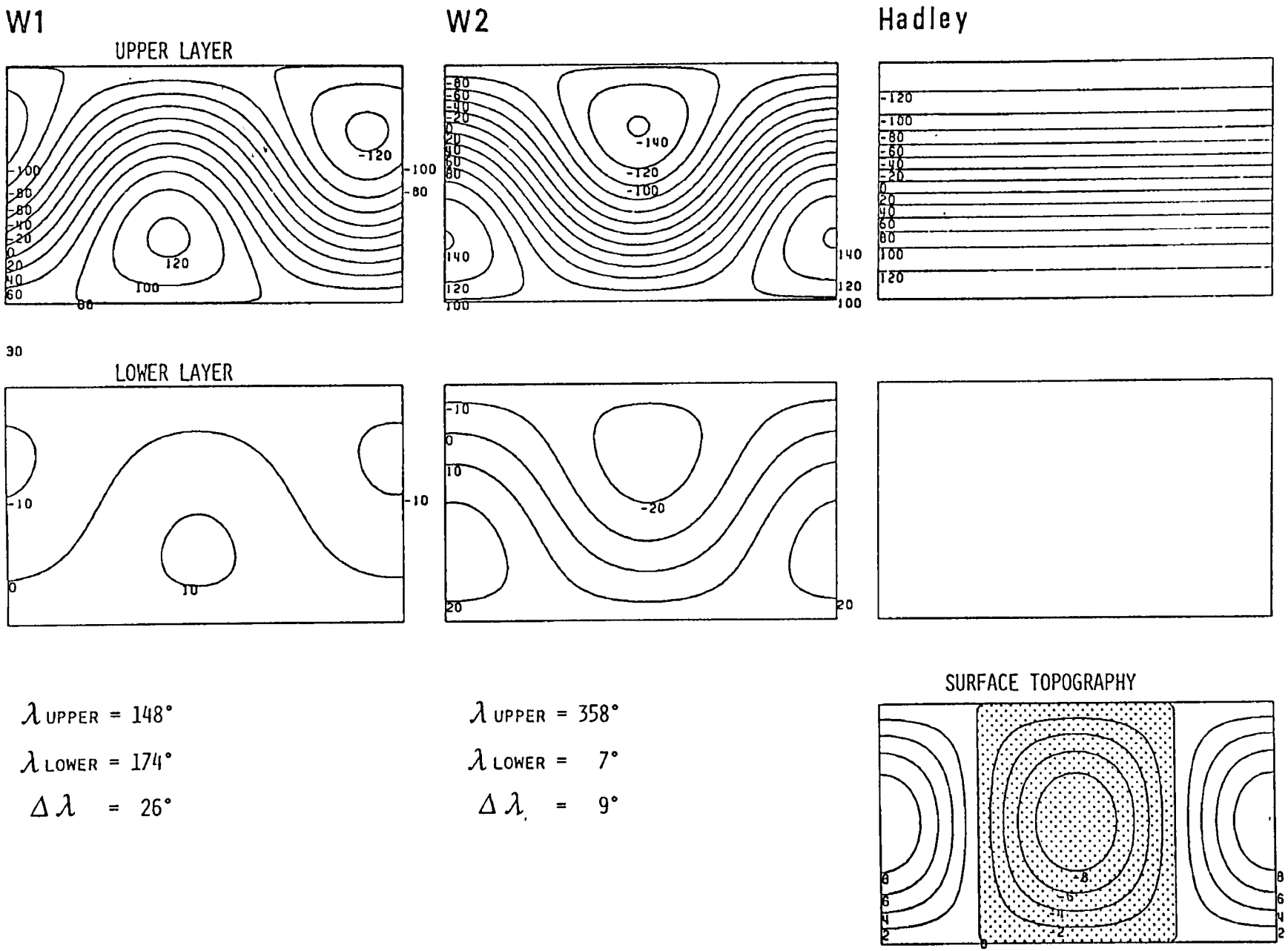
W1
W2
Hadley
UPPER LAYER
LOWER LAYER
30
λ_{UPPER} = 148°
λ_{LOWER} = 174°
$\Delta\lambda$ = 26°
λ_{UPPER} = 358°
λ_{LOWER} = 7°
$\Delta\lambda$ = 9°
SURFACE TOPOGRAPHY

Fig. 4

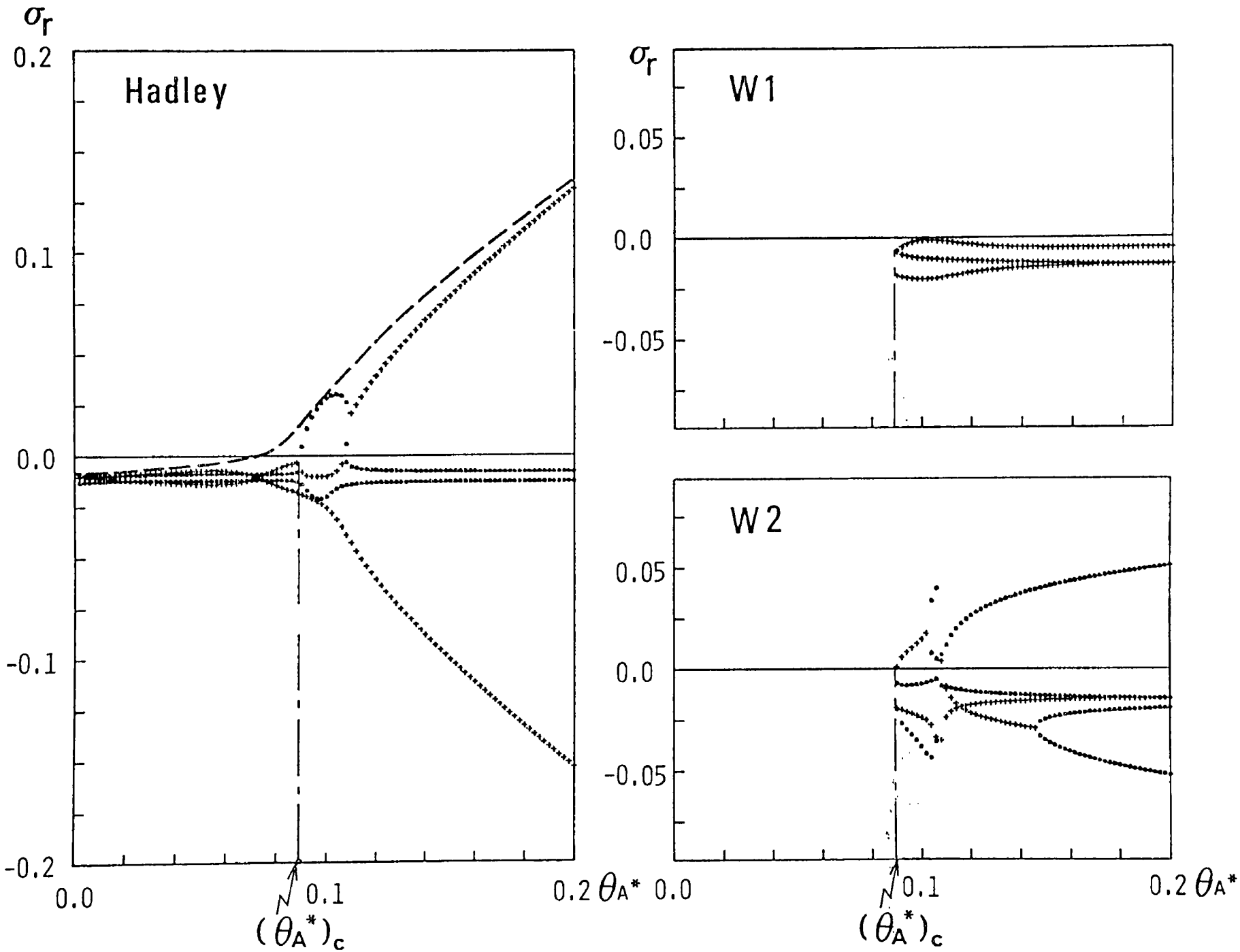
σ_r
0.2
Hadley
0.1
0.0
-0.1
-0.2
0.0
0.1
0.2 θ_A^*
$(\theta_A^*)_c$
σ_r
W1
0.05
0.0
-0.05
W2
0.05
0.0
-0.05
0.0
0.1
0.2 θ_A^*
$(\theta_A^*)_c$

Fig. 5

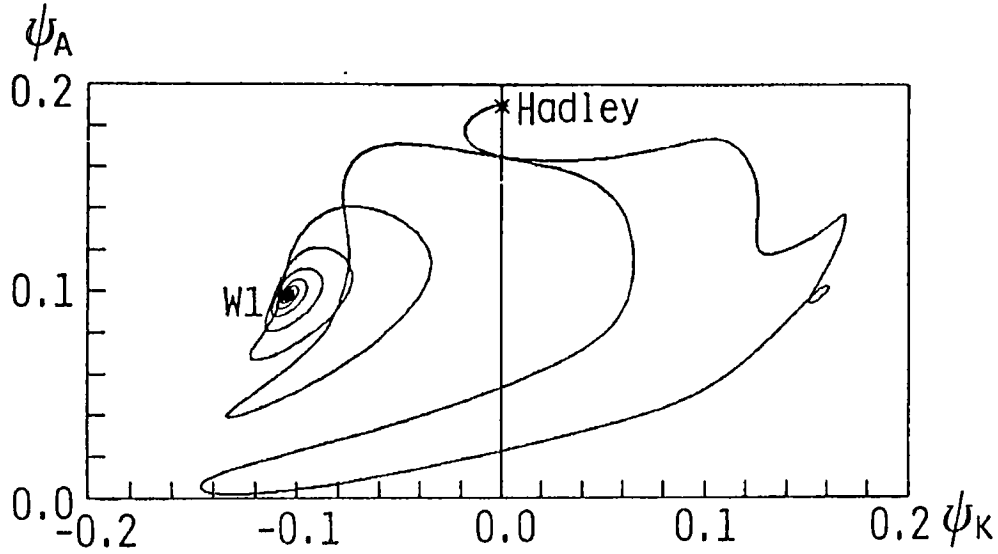
ψ_A
0.2
0.1
0.0
Hadley
W1
-0.2
-0.1
0.0
0.1
0.2 ψ_K

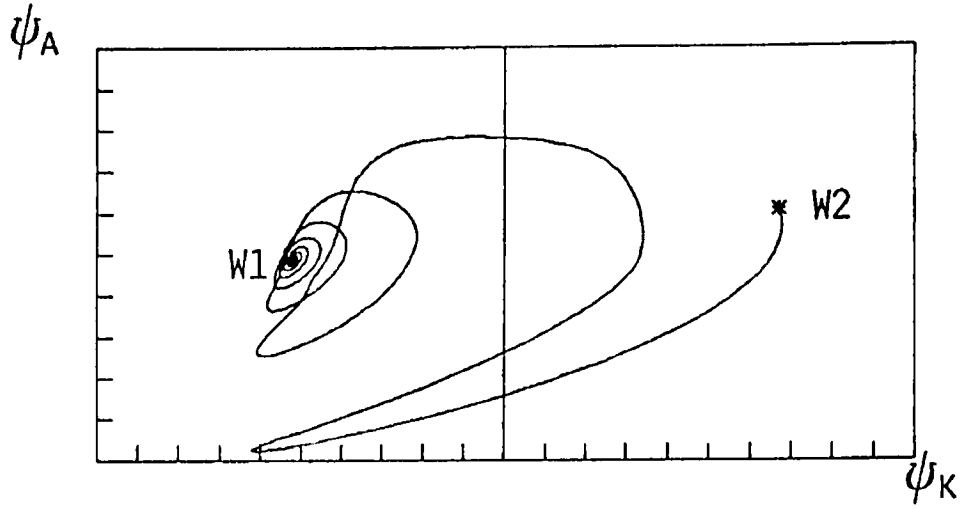
ψ_A
W1
W2
ψ_K

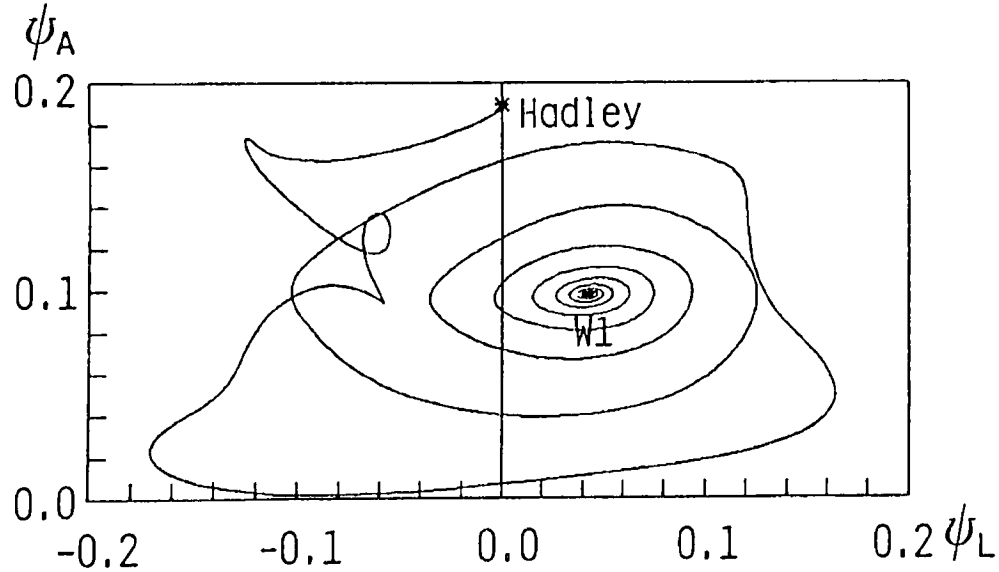
ψ_A
0.2
0.1
0.0
Hadley
W1
-0.2
-0.1
0.0
0.1
0.2 ψ_L

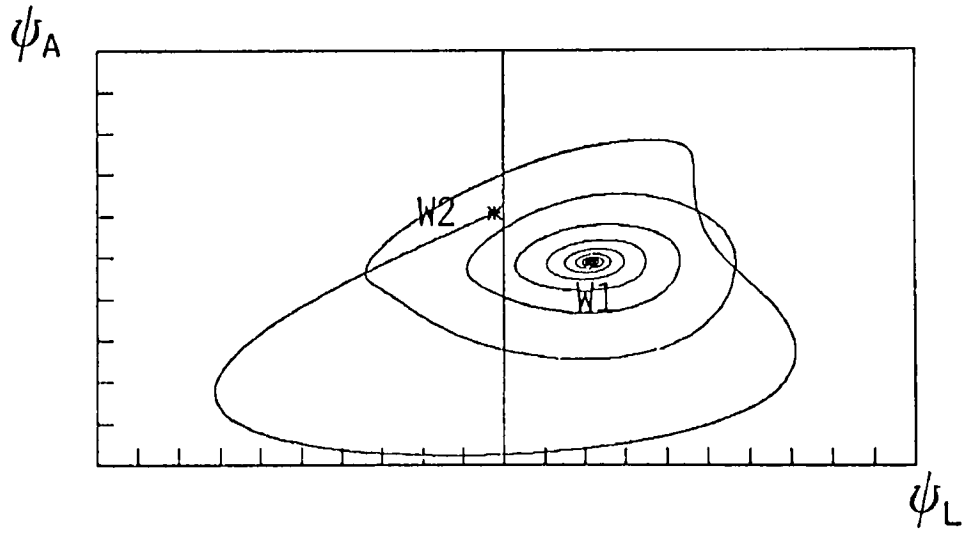
ψ_A
W2
W1
ψ_L

Fig. 6

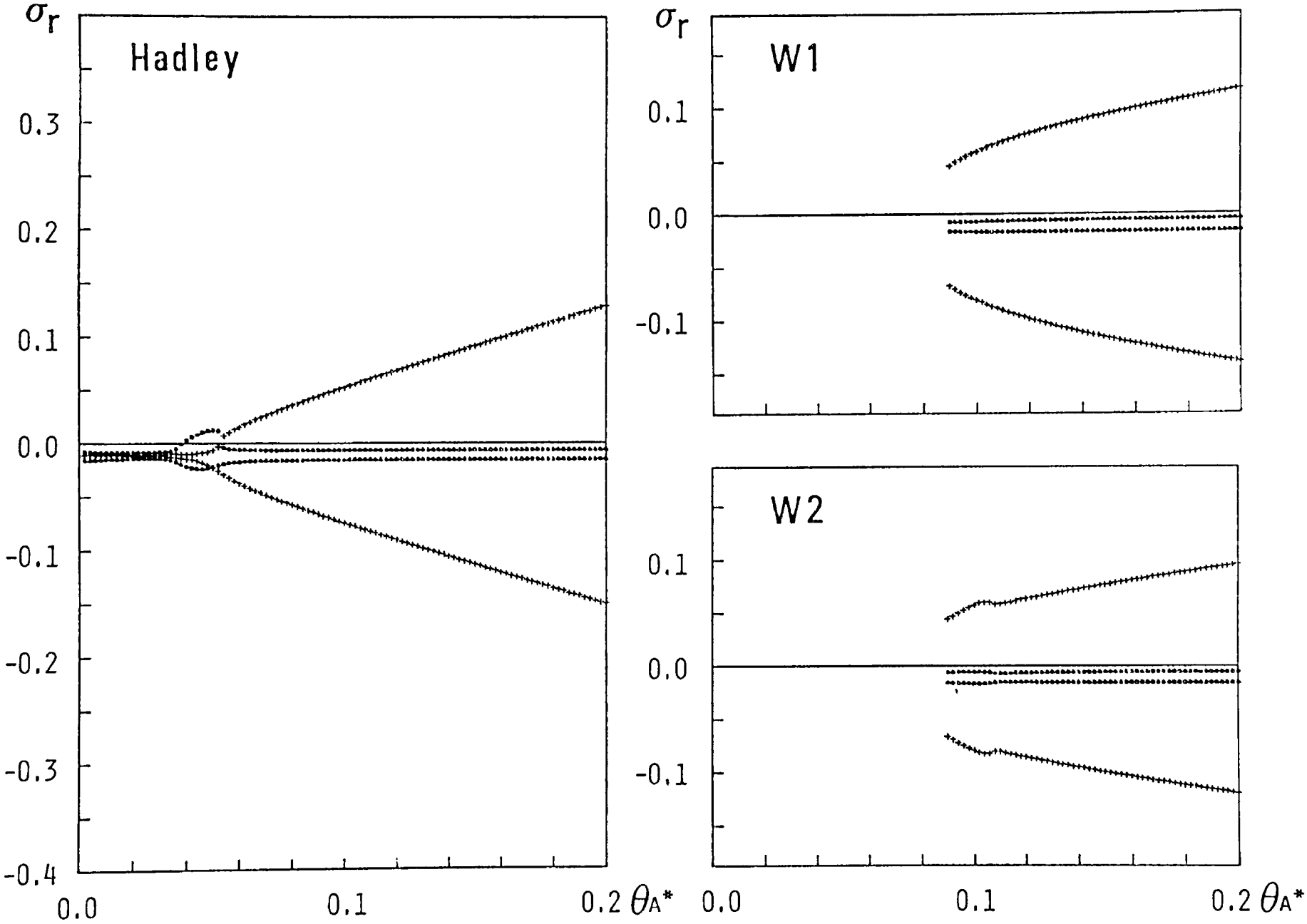
σ_r
Hadley
0.3
0.2
0.1
0.0
-0.1
-0.2
-0.3
-0.4
0.0
0.1
0.2 θ_{A^*}
σ_r
W1
0.1
0.0
-0.1
W2
0.1
0.0
-0.1
0.0
0.1
0.2 θ_{A^*}

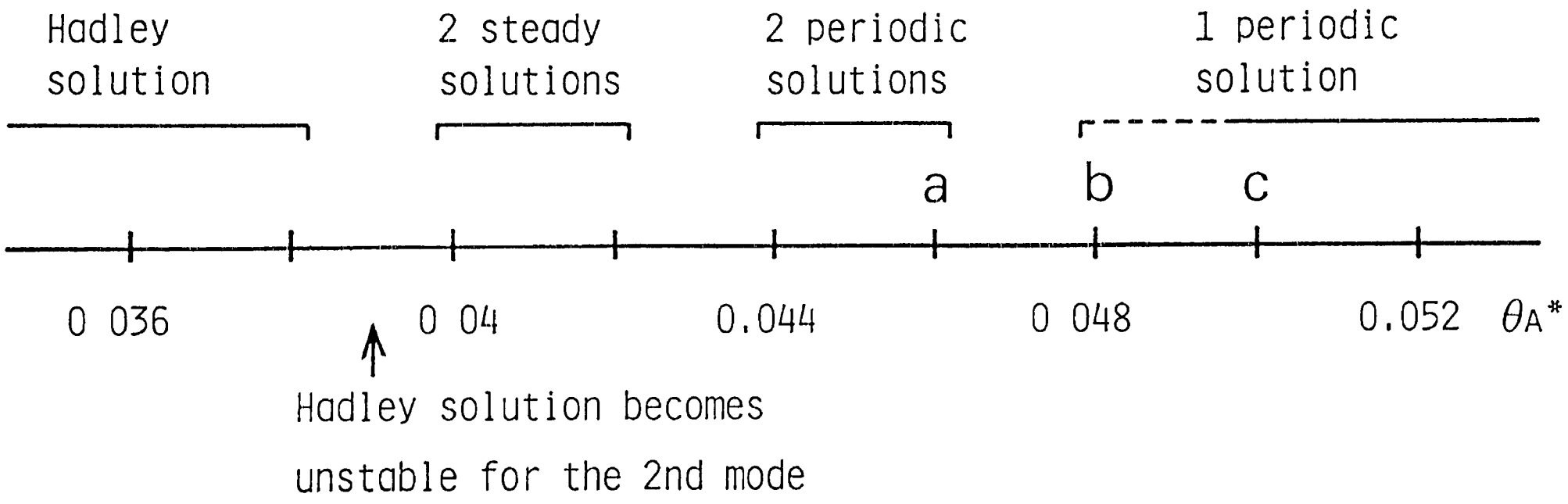
Hadley solution
2 steady solutions
2 periodic solutions
1 periodic solution
a
b
c
0 036
0 04
0.044
0 048
0.052
θA*
Hadley solution becomes unstable for the 2nd mode

Fig. 8

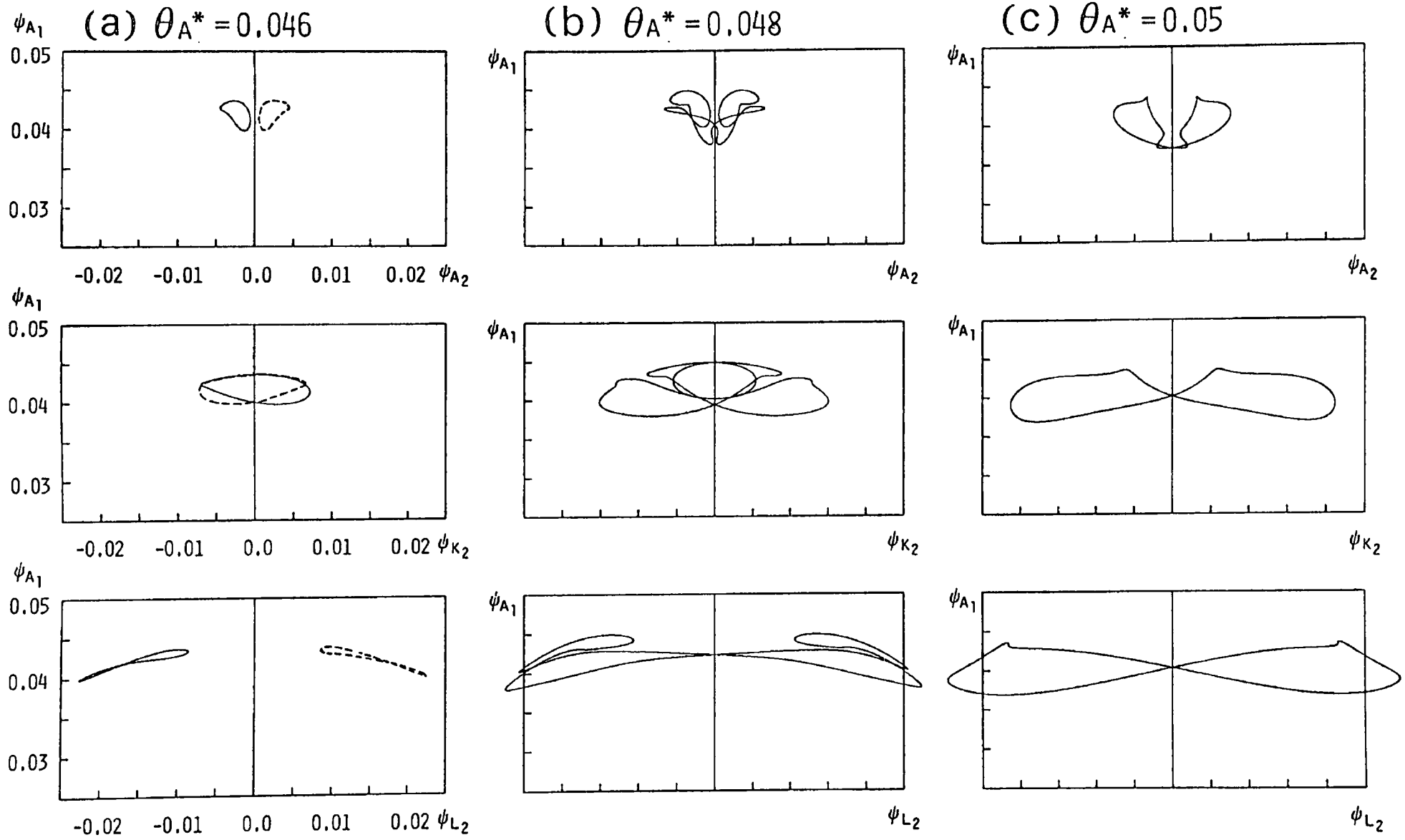
(a) $\theta_A^* = 0.046$
(b) $\theta_A^* = 0.048$
(c) $\theta_A^* = 0.05$
ψ_{A_1}
ψ_{A_2}
ψ_{K_2}
ψ_{L_2}
0.05
0.04
0.03
-0.02
-0.01
0.0
0.01
0.02

Fig. 9

(A)

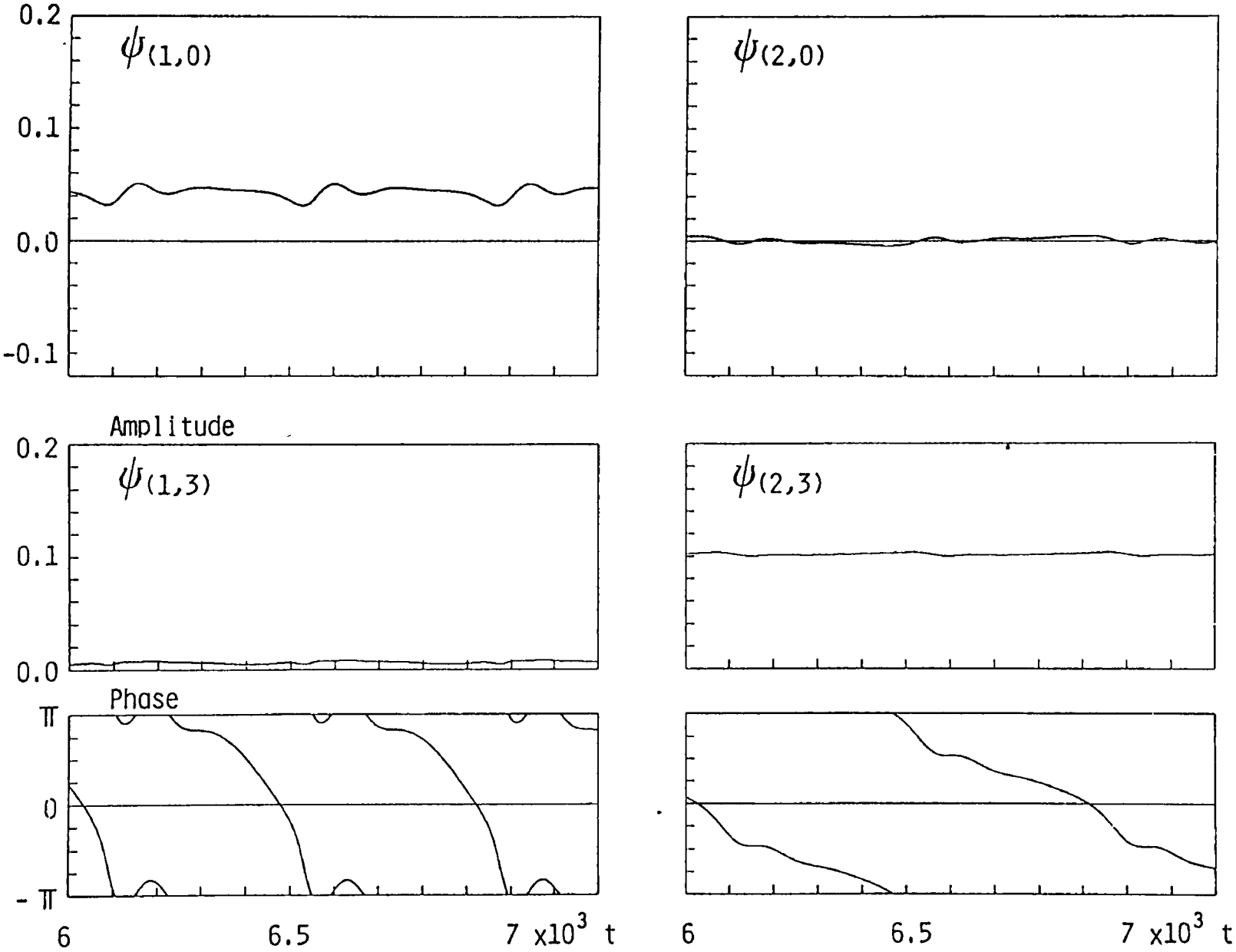
0.2
0.1
0.0
-0.1
ψ(1,0)
ψ(2,0)
Amplitude
0.2
0.1
0.0
ψ(1,3)
ψ(2,3)
Phase
π
0
- π
6
6.5
7 x10^3 t
6
6.5
7 x10^3 t

Fig. 10-(A)

(B)

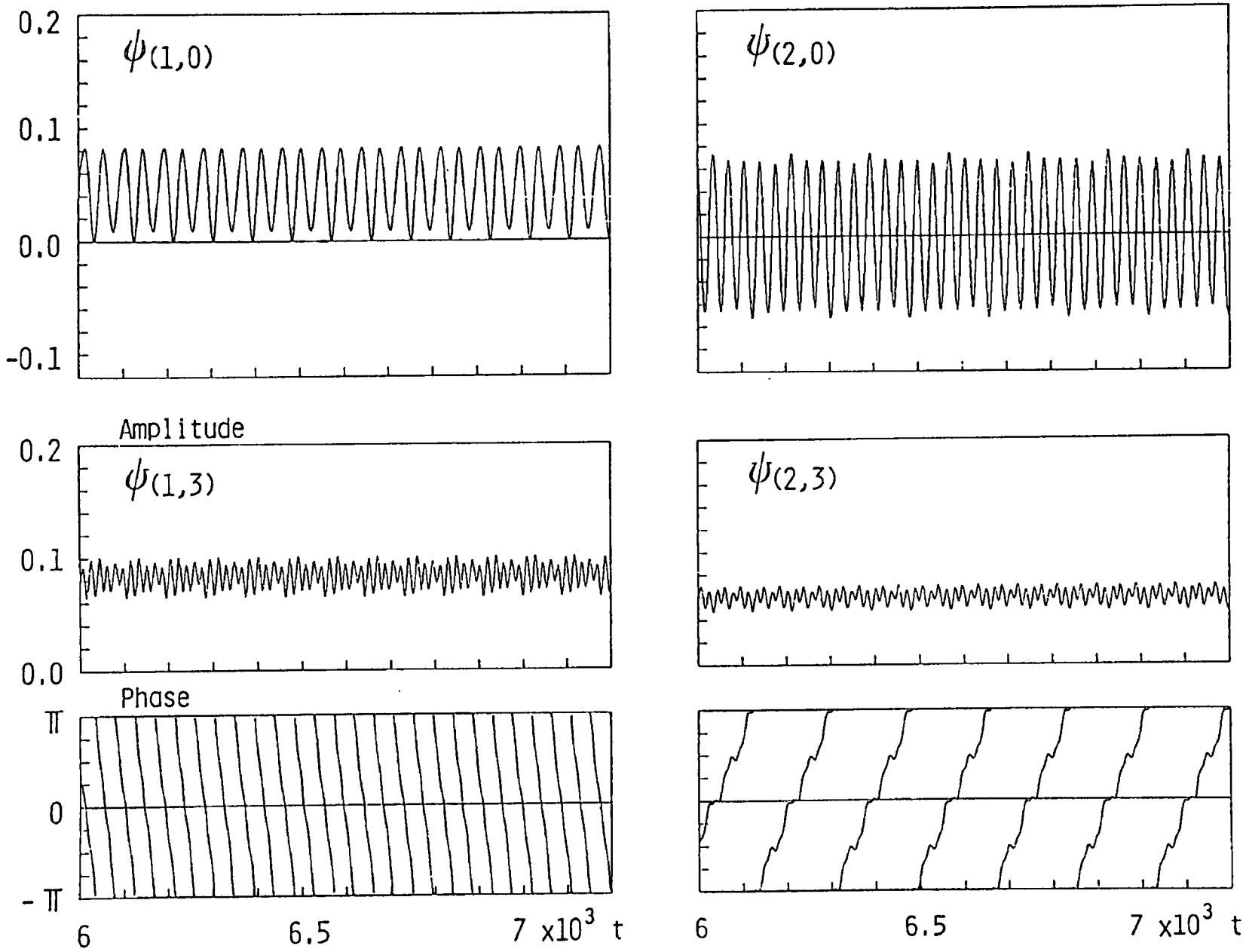
0.2
0.1
0.0
-0.1
ψ(1,0)
ψ(2,0)
Amplitude
0.2
0.1
0.0
ψ(1,3)
ψ(2,3)
Phase
π
0
-π
6
6.5
7 x10^3 t
6
6.5
7 x10^3 t

Fig. 10-(B)

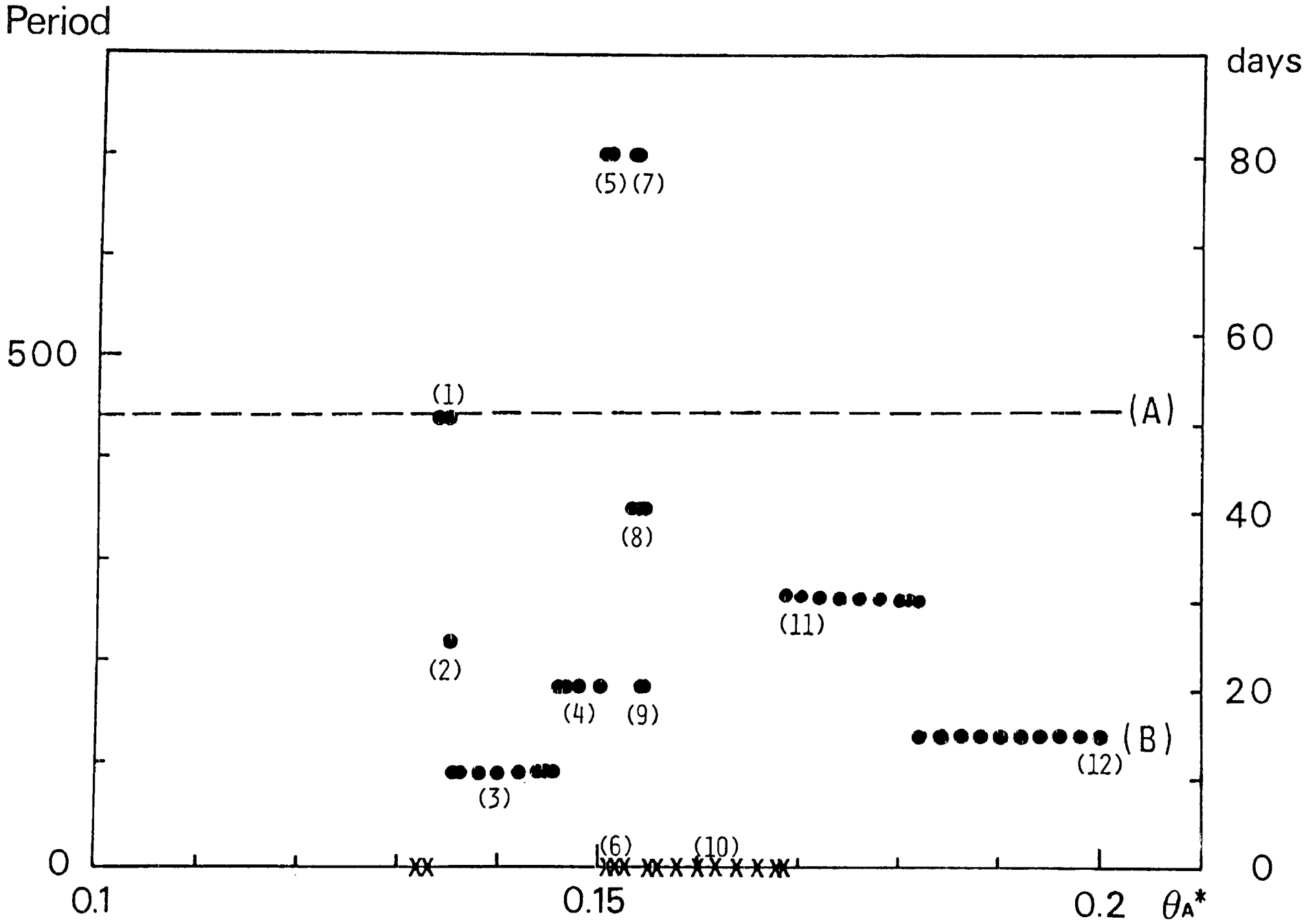
Period
days
500
80
60
40
20
0
0.1
0.15
0.2
θ_A^*
(1)
(2)
(3)
(4)
(5)(7)
(6)
(8)
(9)
(10)
(11)
(12)
(A)
(B)

Fig. 11

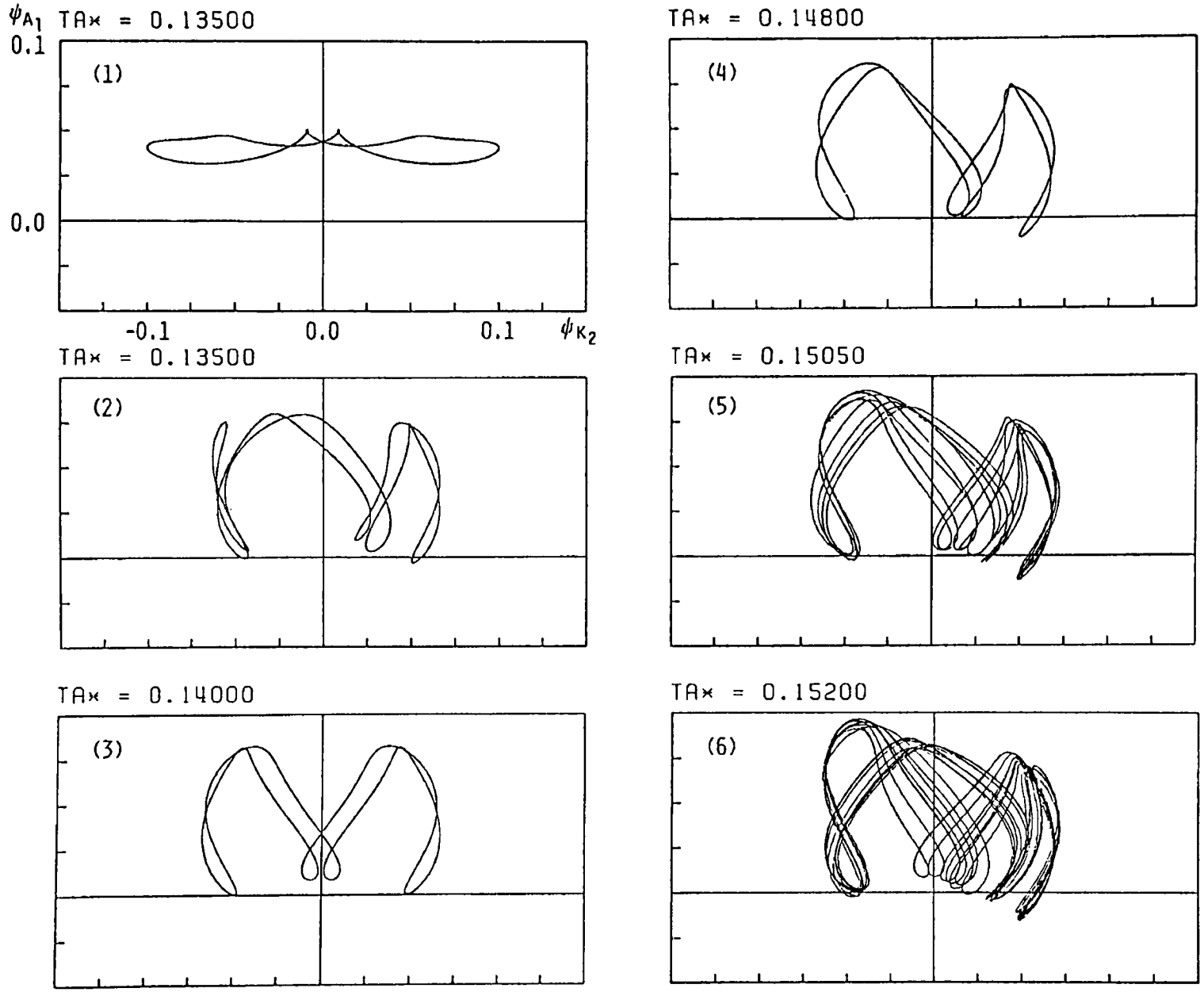
ψ_{A_1}
TA* = 0.13500
0.1
0.0
(1)
-0.1
0.0
0.1
ψ_{K_2}
TA* = 0.13500
(2)
TA* = 0.14000
(3)
TA* = 0.14800
(4)
TA* = 0.15050
(5)
TA* = 0.15200
(6)

Fig. 12-(1)~(6)

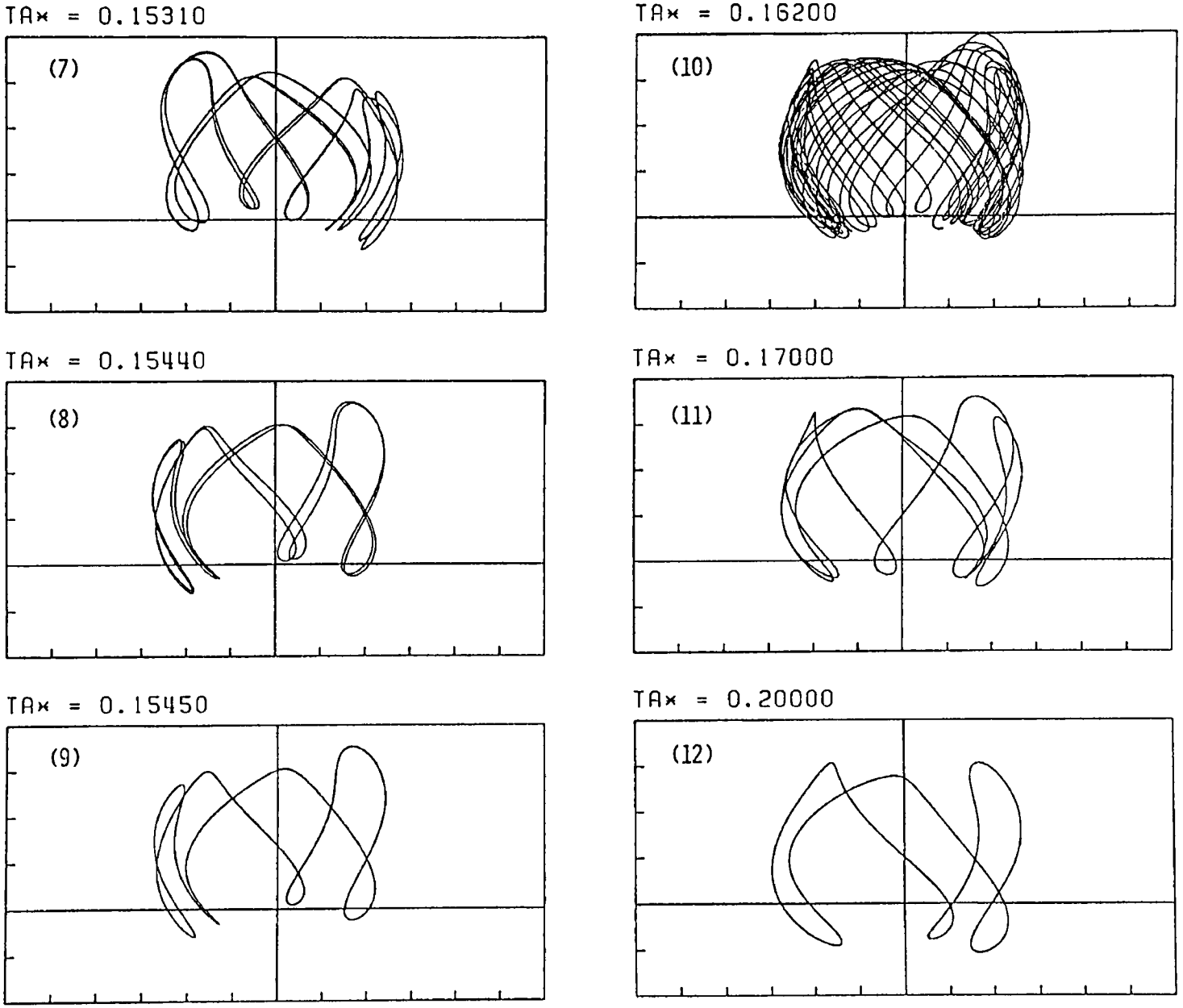
TA× = 0.15310
(7)
TA× = 0.16200
(10)
TA× = 0.15440
(8)
TA× = 0.17000
(11)
TA× = 0.15450
(9)
TA× = 0.20000
(12)

Fig. 12-(7)~(12)

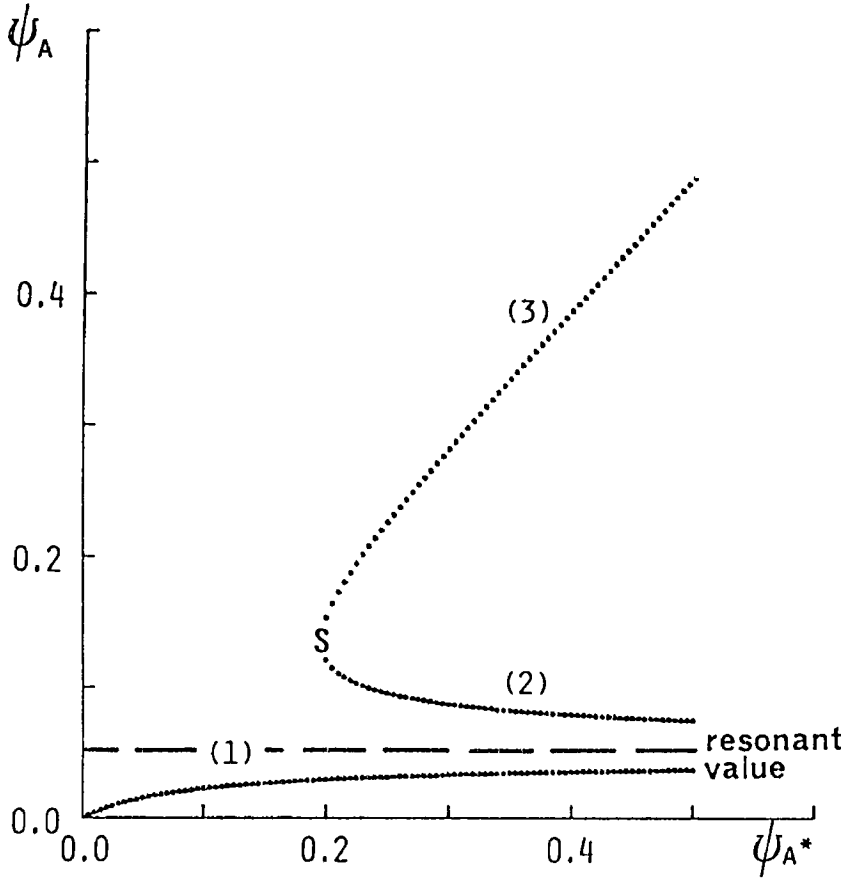
ψ_A
0.4
0.2
0.0
0.0
0.2
0.4
ψ_{A^*}
(3)
S
(2)
(1)
resonant
value

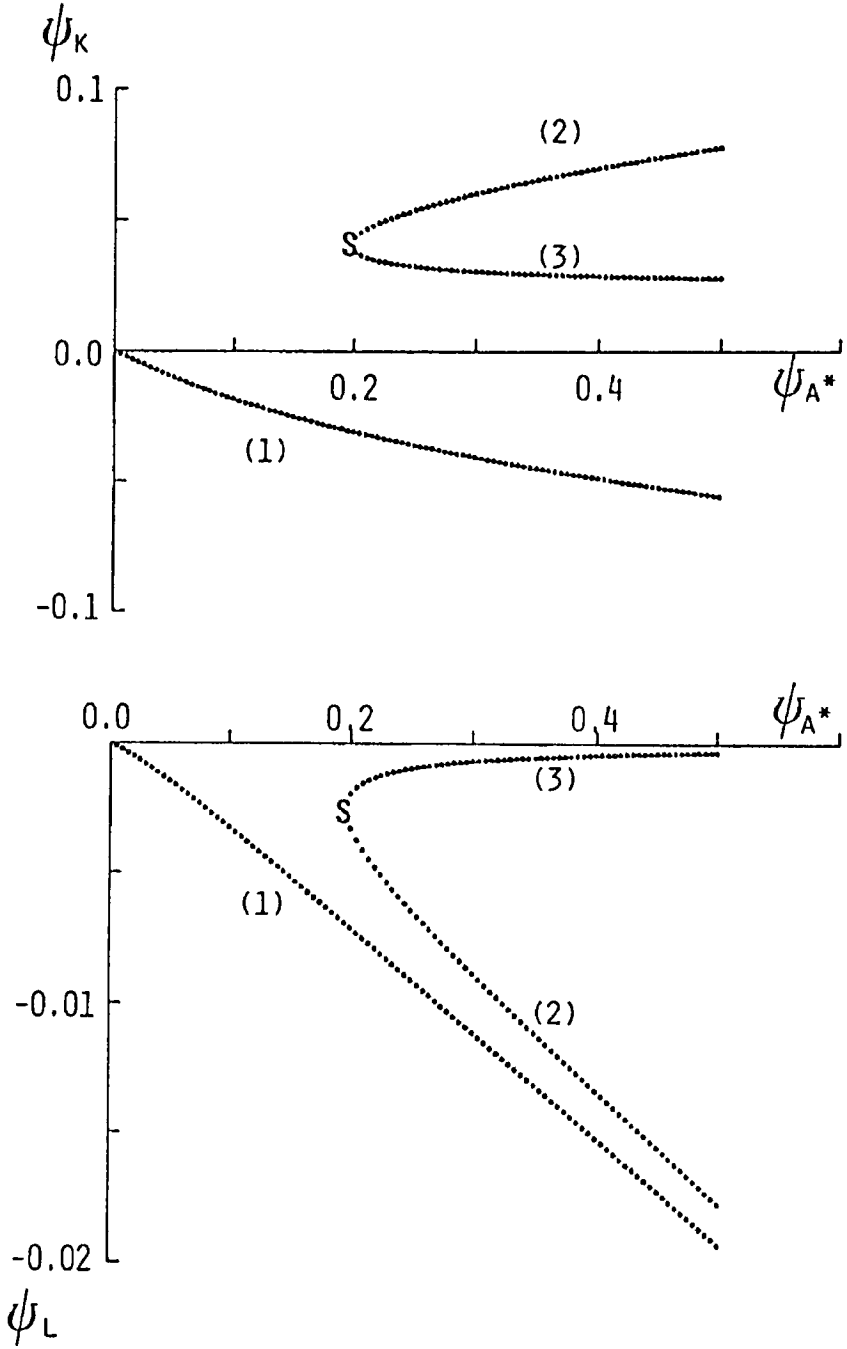
ψ_K
0.1
0.0
-0.1
(2)
S
(3)
0.2
0.4
ψ_{A^*}
(1)
0.0
0.2
0.4
ψ_{A^*}
(3)
S
(1)
(2)
-0.01
-0.02
ψ_L

Fig. 13

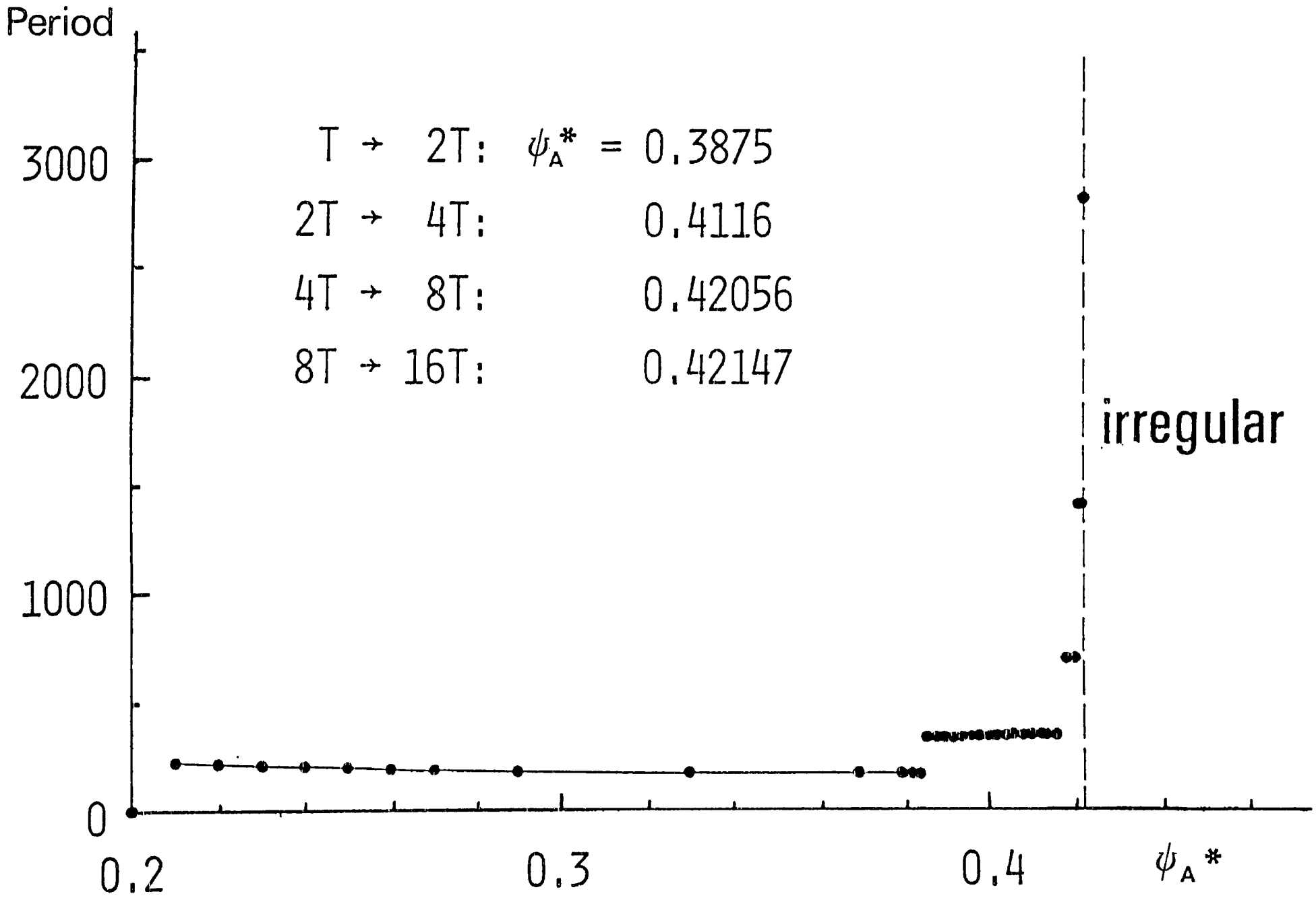
Period
3000
2000
1000
0
T → 2T: ψ_A^* = 0.3875
2T → 4T: 0.4116
4T → 8T: 0.42056
8T → 16T: 0.42147
irregular
0.2
0.3
0.4
ψ_A^*

Fig. 14

地形を含む二層準地衡低次モデルにおける非線型相互作用

I：帯状流と強制波の相互作用

余田成男

京都大学理学部地球物理学教室

帯状流と地形による強制波および傾圧不安定波の間の非線型相互作用を調べるために，二層の準地衡風近似をした低次モデルを作成した．少数のスペクトル成分のみを残すことにより得られた連立非線型常微分方程式系である．第I部では，帯状流と強制波の相互作用に着目して，地形以外の規模の波は除外する．

外部加熱による強制と摩擦による散逸のない保存系の場合について，平衡解を求め，波の振幅が無限大となる共鳴条件を調べた．次に，強制と散逸を含む非保存系の場合に，平衡解を求め解の多重性を調べた．この傾圧モデルでは，チャーニィとデボーア（1979）の順圧モデルで得られたような，複数の安定平

衡解が同時に存在することはない。しかし、時間に依存する解の多重性が、ある外部パラメータの範囲で見つかった。全く同じ外部条件に対して、2つまたはそれ以上の安定な周期解（または非周期解）が存在し、その選択は初期条件のみに依存している。

外部加熱のパラメータを少しずつ変化させて時間積分を繰り返したとき、安定周期解の周期が2倍・4倍・8倍…となって、やがて不規則な非周期解が出現する場合があった。低次モデルで、周期倍化現象を経て周期解から不規則変動へと遷移する実例を得た。

Nonlinear interactions in a two-layer, quasi-geostrophic, low-order model with topography

Part II: Interactions between zonal flow, forced waves and free waves

by Shigeo Yoden

Geophysical Institute, Kyoto University,
Kyoto, 606, Japan.

Abstract

Nonlinear interactions between the zonal flow, topographically forced waves and free baroclinic waves are investigated by using the two-layer, quasi-geostrophic, low-order model constructed in Part I(Yoden, 1983). An idealized topography is given by a Fourier component with the largest scale permitted in the present model.

When the zonal flow is more unstable with respect to a free wave than to the forced wave, there appears a final steady state in which the finite amplitude free wave with a constant phase velocity balances with the marginally stable zonal flow and the forced wave decays out. On the other hand, when the flow is more unstable with respect to the wave component directly coupled with the topography, the flow system has both of the forced and free wave components.

All the wave components are coupled with the topography in least severely truncated case in this paper(two meridional modes and three zonal wavenumbers of $\tilde{n}$, $2\tilde{n}$ and $3\tilde{n}$ are permitted). Then the flow system has several types of time-dependent behavior depending on the external parameters such as the external thermal forcing, the frictional dissipation and the static stability: Steady flow with constant forced wave and propagating free wave, periodic or quasi-periodic oscillation and irregular fluctuation.

For the external parameters corresponding to the real atmosphere, there appears an irregular fluctuation with large-amplitude waves. Statistical relation between the zonal flow and waves in the irregular fluctuation is investigated over a long time-span. The flow pattern at each time step is classified into

one of three categories in terms of the magnitude of the mean zonal flow. Composite fields in three categories are characterized by the zonality in the high-index state and the moderate state and by the meander of the flow in the low-index state. When the flow is in the low-index state, both of the mean value and vertical shear of the zonal flow are small, the stationary waves have larger amplitudes, and the transient waves have smaller amplitudes compared with the high-index and the moderate states. The structure of the stationary waves in the irregular fluctuation is different from that of the forced wave in the equilibrium solutions in Part I.

1. Introduction

This paper is the second part of a two-part report on the nonlinear interactions between the zonal flow and long waves in a two-layer quasi-geostrophic model with topography. In Part I(Yoden, 1983) a low-order model(i.e., a highly-truncated spectral model) was constructed and the zonal flow-forced wave interaction was investigated by neglecting the components of free baroclinic waves. It was revealed that the multiple stable equilibria as in the barotropic model (Charney and DeVore, 1979) do not exist in the parameter range of the earth's atmosphere. However, the multiplicity of time-dependent solutions were found in the topographically forced planetary wave system. In this Part II free baroclinic waves are included to study the interactions between the zonal flow, topographically forced waves and free baroclinic waves.

From a standpoint of the interactions between the zonal flow and long waves some different theories have been proposed to explain the blocking phenomena(see e.g., Austin, 1980; Treidl et.al., 1981 as to recent observational studies). Charney and DeVore(1979) and Charney and Straus(1980) obtained multiple equilibrium states in low-order models with topography and insisted that two stable states correspond to high and low indices in the atmosphere. Solitary Rossby wave theory was applied to the blocking by McWilliams(1980) and Patoine and Warn(1982). Implications of the linear and nonlinear resonance of stationary long waves were discussed by Tung and Lindzen(1979) and Trevisan and Buzzi(1980). For the onset of blocking Frederiksen(1982) considered the instability characteristics of three dimensional flow with stationary long waves.

Numerical experiments have also been performed to study the dynamics of blocking or quasi-stationary waves. Egger(1978) proposed that nonlinear interactions between forced waves and slowly moving free waves lead to a development of the blocking and examined the idea by using barotropic and baroclinic(two-layer) models with a constant topographic forcing. Further development of Egger's work was performed by Schilling(1982). He obtained model-generated blockings in a series of numerical integrations and discussed the flow configuration and energetics. Yao(1980) also studied the energetics for the maintenance of the quasi-stationary waves. Two types of energy cycle were obtained depending on the magnitude of differential heating with latitude. For a small gradient of the heating the flow is less irregular and kinetic energy of the stationary wave is mainly converted from that of the zonal component through the topographic effect in the form of a vertical geopotential flux at the surface. On the other hand, the flow becomes highly irregular for a larger gradient of the heating and the quasi-stationary waves are generated mainly by the baroclinic instability of the forced waves. There are some differences between their numerical models and the present model on the parameterizations of friction and heating, the formulation of the topographic effect and the truncation of spectral components.

The goal of our present study is to investigate the interactions between the zonal flow, forced waves and free baroclinic waves for a better understanding of the blocking phenomena. In Part I it was pointed out that the multiple flow equilibria in the low-order models are not directly related to the atmospheric blocking. However, there is a possibility that time-dependent

solutions in the low-order models may give an insight to the nature of the blocking.

The influence of the free baroclinic waves on the equilibrium and time-dependent solutions in the zonal flow-forced wave system will be investigated by a stepwise relaxation of the truncation level. Fig.1 shows the schematic representation of the interactions permitted in the systems of several truncation level. Three cases are considered in the present study. The surface topography is given by a single component of the lowest zonal wavenumber($\tilde{n}$) with the gravest meridional mode(m=1). (In Part II the same notations are adopted as in Part I.) The most simplified system(case 1) with both of the forced and free waves is limited to one meridional mode(M=1) and two waves(N=2). In this case each wave component interacts with the zonal component independently. If we permit the second meridional mode and harmonics of the lowest wavenumber, it becomes possible to describe the wave-wave interactions. In the case 2 of M=2 and N=2, there is only one type of wave-wave interaction, in which (1,$\tilde{n}$), (2,$\tilde{n}$) and (1,2$\tilde{n}$) components are combined with one another by the Jacobian term and the topographic term. Hereafter the first integer in each parenthesis refers to the meridional mode and the second one the zonal wavenumber. In the case 3 of M=2 and N=3, another type of interaction is possible, i.e., triad interactions between the waves of $\tilde{n}$, 2$\tilde{n}$ and 3$\tilde{n}$. In this truncation level all the wave components interact with the topography of (1,$\tilde{n}$) component.

Effects of the truncation are examined in section 2 for three cases shown in Fig.1. In section 3 dependency on the external parameters such as the external differential heating, the

static stability and the frictional time constants is examined by changing the parameter values. We can obtain an irregular fluctuation with a similar energy spectrum to the atmosphere in least severely truncated case and in some ranges of the external parameters. In section 4 some numerical integrations are performed for 2,800 model days to investigate the relation between the zonal flow and long waves statistically. Discussion and conclusion are in sections 5 and 6.

2. Effects of truncation

In this section we will show how the gross features of the interactions between the zonal flow, forced waves and free waves are affected by the truncation(Fig.1). Ordinary differential equations of the present low-order model are Eqs. (2-8) and (2-9) in Part I. Then the degrees of freedom of the systems are 10 for case 1, 20 for case 2 and 28 for case 3.

a. case 1 (M=1,N=2)

In the case of M=1, each wave component interacts with the zonal component independently(Fig.1). Therefore the equilibrium solutions obtained in most severely truncated case(Fig.3 in Part I) are one part of the equilibrium solutions in the present system when we take all the free wave components equal to zero.

First we examine the linear stability of the equilibrium solutions in the present system. The growth rate σ_r is obtained as a real part of complex eigenvalues of the 10x10 coefficient matrix. The characteristic equation can be rewritten in the product of the sixth-order equation of σ for the zonal flow and forced wave part and the forth-order equation for the free wave part. The stability properties for the zonal flow and forced wave part are identical to the result obtained in the case of M=1 and N=1 in Part I. Because the forced wave and the topography do not directly interact with the free wave, the characteristic equation for the free wave contains only the zonal flow components of the equilibrium solutions. Therefore the stability of the equilibrium solutions with respect to the perturbations of the free wave is

determined by the conventional baroclinic stability analysis of the zonal flow.

The growth rate of the most unstable perturbation embedded in the equilibrium solution of $\tilde{n}$=3 is shown in Fig.2 for the zonal wavenumber $\tilde{n}$=1-12. Note that the ordinate is the external forcing parameter θ_A^* (not the vertical shear of the zonal wind), although the vertical shear depends on θ_A^* linearly only in the Hadley solution(Eq. (3-15) in Part I). The growth rate for $\tilde{n}$=3 must be excluded(broken lines in the figure), because the perturbation of $\tilde{n}$=3 feels the surface topography and then it is not free. The Hadley solution is most unstable with respect to the perturbation of $\tilde{n}$=9 in the range of $0.016 \leqq \theta_A^* \leqq 0.018$, $\tilde{n}$=8 in $0.02 \leqq \theta_A^* \leqq 0.048$ and $\tilde{n}$=7 in $0.05 \leqq \theta_A^*$. Both of the equilibrium solutions with wave components(W1 and W2 solutions shown in Fig.3 in Part I) are unstable with respect to the free waves of $4 \leqq \tilde{n} \leqq 11$ and most unstable for $\tilde{n}$=7. Because the zonal flow of the W1 solution does not depend on θ_A^* so much, the growth rate is almost independent of θ_A^* for the W1 solutions.

Almost all the equilibrium solutions obtained in the zonal flow-forced wave system are baroclinically unstable with respect to a perturbation of free wave. If a free wave perturbation is added to the unstable equilibrium state, it will grow up and interact with the zonal flow. Then the zonal flow will change and the forced wave will also change in time.

Some numerical integrations are performed to elucidate the time-dependent behavior of each component. Time-variations of the zonal flow and the waves are presented in Fig.3. The zonal wavenumber of the topography is $\tilde{n}$=3 and that of the free wave is $\tilde{n}'$=7. The external forcing parameter θ_A^* is fixed to 0.2 and the

initial state is the W1 solution with a small perturbation of the free wave. Initially the free wave grows up with eastward phase-propagation of 16 m/s in dimensional value and the zonal-mean meridional temperature difference $\theta(1,0)$ decreases. These features are in agreement with those predicted by the linear baroclinic instability theory. Simultaneously vertically averaged zonal flow $\psi(1,0)$ increases and the amplitudes of the forced wave $\psi(1,3)$ and $\theta(1,3)$ decrease due to the changes in the topographic and Jacobian terms.

After some fluctuations of each component(about 500 non-dimensional time steps), the zonal flow converges to a small value and the forced wave decays out. The free wave converges to a constant amplitude with the westward phase velocity of 0.92 m/s (see also Table 1). Because the zonal flow in the lower layer is equal to zero(i.e., $\psi(1,0)-\theta(1,0)=0$), there is no effect of the topography. The same final steady state of the weak zonal flow and free wave with constant amplitude and constant phase velocity is also obtained for other initial conditions(e.g., the Hadley solution and the W2 solution).

Similar final steady states are obtained for other forcing parameter θ_A^*(Table 1). It is found that the zonal flow components($\psi(1,0)$ and $\theta(1,0)$), the phase difference between the upper and lower layers($\Delta\phi$) and phase velocity(c) of the free wave are independent of the external forcing. As the forcing parameter θ_A^* increases, only the amplitude of the free wave($\psi_1(1,7)$ and $\psi_3(1,7)$) becomes large to compensate the increment of differential heating.

Note that the magnitudes of the zonal flow are equal to those at the critical point where the Hadley solution becomes

baroclinically unstable with respect to the free wave. The value of θ_A^* at the critical point is 0.01813 for $\tilde{n}'=7$, which is substituted into the equation (3-15) in Part I to obtain the critical value of $\psi(1,0)= \theta(1,0)=0.01716$. At the critical point the phase velocity of the perturbation is equal to zero in the case without friction(see the baroclinic stability analysis in the two-layer model by e.g., Pedlosky, 1979). But in the present model the phase velocity has a small negative value due to the friction and diabatic heating of the eddy component.

If we vary the zonal wavenumber of the free wave in the range of $4 \leqq \tilde{n}' \leqq 11$, we obtain a final steady state in which the zonal flow with the critical value balances with the finite-amplitude free baroclinic wave. Dependency of the phase velocity(c) on the zonal wavenumber reminds us of the dispersion relation of free Rossby waves. On the other hand, when we put $\tilde{n}' \leqq 2$ or $\tilde{n}' \geqq 12$, the dependent variables asymptotically approach the W1 solution as in the zonal flow-forced wave system(Part I).

In this truncation level of M=1 and N=2, there finally appears either the W1 solution with forced wave or the final steady state with free wave. There does not appear such a state that both of the forced and free waves exist together and interact with the zonal flow.

b. case 2 (M=2,N=2)

If we permit the second meridional mode and the harmonic of the lowest zonal wavenumber, we obtain a dynamical system with 20 degrees of freedom, which contains the wave-wave and wave-

topography interactions between $(1,\tilde{n})$, $(2,\tilde{n})$ and $(1,2\tilde{n})$ components(broken line in Fig.1).

Time-variation of vertically averaged zonal flow and wave components is shown in Fig.4. The zonal wavenumber of the topography is $\tilde{n}=3$ and the harmonic wavenumber $2\tilde{n}=6$. The initial condition is the W1 solution with small perturbations of every components. The external forcing θ_A^* is again 0.2.

Variations of the zonal flow and forced wave of the first meridional mode resemble those obtained in case 1(Fig.3). Initially $\psi(1,0)$ increases and the forced wave becomes weak. After some fluctuations the zonal flow converges to a weak state and the forced wave decays out. All the free wave components grow up first due to the baroclinic instability of the zonal flow. However, as the zonal component of $\psi(1,0)$ converges to a small value, all other components except for $\psi(2,6)$ decay out. The final steady state of a weak zonal flow and free wave of constant amplitude and constant phase velocity is similar to that obtained in case 1. The meridional mode of the free wave, however, is the secondary mode which has no interaction with the topography. Similar final steady states are obtained for other external forcing parameter θ_A^* and only the amplitude of the free wave increases with increasing θ_A^*.

For the topographic wave of $\tilde{n}=4$ there appears a similar final steady state but for $\tilde{n}=5$ corresponding steady state does not appear. All the variables go on fluctuating irregularly in the $\tilde{n}=5$ case. Meanwhile, if the static stability parameter σ_0 is changed to a larger value(1.25 times or 1.5 times of the value given in Part I), the final steady state is obtained as well. However, when the static stability exceeds a critical value,

e.g., doubled σ_0 ($2\bar{\bar{\sigma}}/\Delta P$=60K/500mb), there appears an irregular fluctuation. In these situations (1,2$\tilde{n}$) component is more unstable than (2,2$\tilde{n}$) component and interacts with the topography and other waves as well as the zonal flow. The linear baroclinic instability theory(Eady, 1949) shows that stability criterion is proportional to the product of the static stability and square of wavenumber ($\propto \sigma_0 \times (m^2+n^2)$). Therefore the most unstable wavenumber shifts toward a small value with increasing the static stability σ_0.

In the present truncation level, there appears either a final steady state or an irregular fluctuation. Only (1,0) and (2,2$\tilde{n}$) components have non-zero values in the final steady state and then there do not exist the wave-wave and wave-topography interactions. On the other hand, in the irregular fluctuation all the components fluctuate with interactions of zonal flow-wave, wave-wave, zonal flow-topography and wave-topography. The alternative of two flow regimes depends on the horizontal scale of the topography(and therefore that of the forced and free waves) and the static stability but is independent of the external forcing parameter.

c. case 3 (M=2,N=3)

Because (2,2$\tilde{n}$) component is not coupled with the topography in case 2, the final steady state is possible. In case 3 of M=2 and N=3, however, all the wave components are coupled with the topography by the $\tilde{n}$-2$\tilde{n}$ interaction and the triad interactions between $\tilde{n}$, 2$\tilde{n}$ and 3$\tilde{n}$. Therefore, if one of the wave components is

not zero, another wave component will be induced by the wave-topography interaction. Final steady states like those in cases 1 and 2, in which there is no topographic effect, are not possible in the present case.

Time-variations of the vertically averaged zonal flow and wave components are presented in Fig.5 for the same external parameters as those in Figs.3 and 4. There appears the same periodic solution for the initial conditions of the Hadley, W1 and W2 equilibrium solutions with small perturbations. As in cases 1 and 2, the zonal flow of the first meridional mode $\psi(1,0)$ has a small magnitude and the wave of the smallest scale $\psi(2,9)$ has the largest wave amplitude. However, other wave components also have non-zero values by the triad interactions. The amplitude of $\psi(2,6)$ is about a half of that of $\psi(2,9)$ and other four components have rather small amplitudes(see also Table 3).

The zonal flow of the first meridional mode $\psi(1,0)$ fluctuates with the periods of 7.6 days and 85 days. The amplitude of the wave components have the same periodicity. Wave components of $\psi(2,6)$ and $\psi(1,9)$ propagate eastward with the period of 85 days. The characteristics of the time-variations are different depending on the external parameters such as the external forcing θ_A^*, the static stability σ_0 and the frictional coefficients k and k'. This dependency will be discussed in the next section.

Effects of the truncation were investigated in three cases with different truncation level. It is not possible for the sys-

tem of case 1 (M=1,N=2) to depict such a state that both of the forced and free waves exist and interact with the zonal flow. In case 2 (M=2,N=2), such a state is obtained for a small-scale topography($\tilde{n} \geq 5$) or a large static stability($\sigma_0 \times 2$). For the parameter values given in Part I(which are typical in the atmosphere), however, there appears the final steady state in which the zonal flow and a free wave have non-zero values and the topography has no contribution. On the other hand, both of the forced and free waves exist and interact with each other in case 3, because all the waves are coupled with the topography(Fig.1). At least 28 degrees of freedom(case 3) are necessary for the system to depict the coexistence of both the forced and free waves and the interactions with each other. In the next two sections we will investigate the interactions between the zonal flow and these waves at the truncation level of case 3.

3. Dependency on external parameters

In Part I we tentatively fixed the external parameters such as the frictional and heating coefficients, the static stability and the amplitude of the topography. As a control parameter, only the external forcing parameter θ_A^* was varied from 0 to 0.2(The corresponding temperature difference across the channel is from 0K to 150K at the radiative equilibrium state.). In this section we will show the effects of θ_A^*, σ_0, k and k' on the behavior of the zonal flow and waves. The zonal wavenumber of the topography is fixed to $\tilde{n}$=3; wavenumbers permitted in the present model are 3, 6 and 9.

The characteristics of the time-variations are different depending on the external parameters. In Table 2 the time-dependency is classified into four categories: Steady flow with wave components (S), periodic oscillation (P), quasi-periodic oscillation (Q) and irregular fluctuation (I). Some typical variations of the zonal component $\psi(1,0)$ for each category are presented in Fig.6. Here quasi-periodic oscillation is subjectively discriminated from irregular fluctuation by looking over the time series of the amplitudes as in Fig.6.

For a wide range of θ_A^* there appears a periodic oscillation in the cases with external parameters given in Part I. As the frictional parameters decrease, there appears a quasi-periodic oscillation or an irregular fluctuation instead of the periodic oscillation. The time-dependency is influenced by the external forcing parameter θ_A^* and frictional parameters k and k'. However, as shown in Table 3, the dominant components such as (1,0),(2,6) and (2,9) are insensitive to the changes in these external parameters. Here the mean zonal flow($\overline{\psi}(m,0)$) and the mean

amplitude of the wave($\overline{\psi}(m,n)$) are given by

$$\overline{\psi}(m,0) = \frac{1}{N}\sum_{i=1}^{N} \psi_{Am}(t_0+i\Delta t) \qquad (3\text{-}1)$$

$$\overline{\psi}(m,n) = \frac{1}{N}\sum_{i=1}^{N} [\psi_{Km}^{n}(t_0+i\Delta t)^2 + \psi_{Lm}^{n}(t_0+i\Delta t)^2]^{1/2} \qquad (3\text{-}2)$$

The dependency of the time-dependent behavior of solutions on the static stability σ_0 is shown in Table 2-(b). For a small σ_0 there appears a steady flow(Fig.6-(g)) , in which the westward propagating wave $\psi(2,9)$ is dominant and the forced wave $\psi(1,3)$ is stationary. As the static stability increases, there take place transitions from the steady flow to the periodic oscillation and from the periodic oscillation to the irregular fluctuation(Figs.6-(c), (h) and (i)). For a large σ_0, there appears another type of the periodic oscillation(Fig.6-(j)).

With increasing σ_0, the magnitude of the zonal component with the first meridional mode increases and wave components of small zonal wavenumbers($\tilde{n}$=3 and 6) become dominant(Table 3). For the case of σ_0x 4, $\overline{\psi}(1,3)$, $\overline{\psi}(2,3)$ and $\overline{\psi}(1,6)$ have large amplitudes. Difference of the periodic solutions between the cases of σ_0x1 and σ_0x4 is clearly seen in the mean values of the wave amplitudes. The dependency of the dominant wavenumber on the static stability is reminiscent of the linear baroclinic instability theory(Eady, 1949) mentioned in the previous section: The stability criterion and the most unstable mode are dependent on the product of the static stability and the square of the wavenumber.

For the external parameters given in Part I, the amplitude of the wave (1,3) with the same scale as the topography is rather

small compared with (2,6) and (2,9) components. This is not the case in the real atmospheric circulation, where ultra-long waves in general have larger amplitude than long waves in the mid-latitude troposphere. External parameters must be change in the present system of N=3 in order to obtain a similar energy spectrum like that of the atmosphere.

As shown in Table 3, mean amplitudes of wave components of small zonal wavenumbers become large with increasing the static stability σ_0. Although $\sigma_0=5.64\times10^{-2}$ (in dimensional $2\overline{\overline{\sigma}}/\Delta P$ = 30K/500mb) adopted in Part I is a typical value in mid-latitudes, a larger value is usual in winter (see e.g., Tomatsu, 1979). Charney and Straus (1980) adopted the value $2\overline{\overline{\sigma}}/\Delta P$ = 43.6K/500mb and Yao (1980) did 31.8K/500mb. Increase of the static stability parameter to 1.25 times (37.5K/500mb) or 1.5 times (45K/500mb) is not far from the atmospheric conditions.

Fig.7 shows the time-variations of vertically averaged zonal flow and wave components for the case of the increased static stability ($\sigma_0\times1.25$). All the components have large amplitudes and fluctuate in a highly irregular manner. The behavior of the zonal flow and the forced wave does not resemble to that obtained in the zonal flow-forced wave system.

The zonal component $\psi(1,0)$ fluctuates around the mean value (denoted by broken line) and sometimes has extremely large or small values. Such extreme states continue during the period ranging from several days to several ten days. The amplitude and the phase of each wave also vary in connection with the fluctuations of the zonal flow and other waves. After t=7,000, for example, $\psi(1,0)$ takes extremely small values for 140 nondimensional time (about 15 days). In this period $\psi(1,3)$ has a small amplitude

but the phase is rather quasi-stationary. While, $\psi(1,9)$ has a large amplitude and is quasi-stationary.

In the next section we will clarify the relation between the zonal flow and waves statistically over a long time-span. We have so far used the term 'forced wave' to the wave (1,3) because it has the same sizes in both x and y directions as those of the topography. But this usage is not the conventional one except when the wave happens to be steady and stationary. In the present truncation level of case 3, all the wave components are affected by the topography and the topographic effects vary in time due to the variation of flow itself. Therefore the 'forced wave' is not appropriate in the present problem and is not used in the next section. We will define 'stationary wave' as a mean wave over a time and direct our attentions to the relation between the zonal flow and the stationary waves.

4. Zonal flow and stationary waves in irregular fluctuations

Numerical integrations for three combinations of external parameters(Table 4) are performed for 25,000 time steps(in dimensional 2,813 days). Three initial conditions are taken in each case, i.e., W1, W2 and Hadley solutions with small perturbations. Mean value(MV) and standard deviation(SD) of $\psi(1,0)$ over 23,750 time steps except for initial stage are listed in Table 4. As the forcing parameter θ_A^* increases or the static stability σ_0 increases, MV and SD also increase with a few exceptions. SD is smaller than MV in the cases of $\sigma_0 \times 1.25$ but is comparable with MV in the case of $\sigma_0 \times 1.5$ and $\theta_A^*=0.2$. In each case MV and SD have variations of 1-15% depending on the initial conditions.

We classify the flow at each time step into three categories in terms of $\psi(1,0)$ component. The threshold values are MV $\pm$ SD as denoted by dotted lines in Fig.7. We term the state with $\psi(1,0)>$MV+SD high-index state (H), the state with MV+SD $\geq \psi(1,0) \geq$MV-SD moderate state (M), and the state with MV-SD $> \psi(1,0)$ low-index state (L). Mean zonal component $\psi(1,0)$ fluctuates irregularly and transits between these categories. The ratio of the time span in each category is almost (H):(M):(L) = 15:70:15 independently of the initial conditions(Table 5).

The composite fields of stream function in three categories are shown in Fig.8 for the case of $\sigma_0 \times 1.25$ and $\theta_A^* =0.2$(the W2 initial conditions). In the high-index state (H) the flow pattern is nearly zonal in both layers. In the moderate state (M) the zonal flow component is dominant in the upper layer but there is almost no motion in the lower layer. In the low-index state (L) the flow pattern is wave-like and the ridge of the dominant component is located in the western slope of the mountain. The zonal

flow in the lower layer is easterly in this category. The distinctive feature of the composite flow pattern is the zonality in (H) and (M) and the meander in (L).

Magnitude of the zonal components averaged in each category is listed in Table 5. Of cource, the vertically averaged zonal flow $\psi(1,0)$ has the largest value in the category (H) and the smallest(negative) value in (L). The meridional difference of the zonal potential temperature $\theta(1,0)$ (i.e., mean vertical shear of the zonal wind by the thermal wind relation) also decreases with the decrease of $\psi(1,0)$: $\theta(1,0)$ in (L) is about 80% of that in (H). On the other hand, zonal components of the second meridional mode ($\psi(2,0)$ and $\theta(2,0)$) are very small in all the categories.

The stationary waves are defined in three categories; cosine and sine components are given by

$$\overline{\psi}_c(m,n) = \frac{1}{N'} \sum^{N'} \psi_{Km}^{n} \qquad (4\text{-}1)$$

$$\overline{\psi}_s(m,n) = \frac{1}{N'} \sum^{N'} \psi_{Lm}^{n} \qquad (4\text{-}2)$$

where N' is the total number in the category. Fig.9 shows the amplitude and phase of the stationary waves in three categories. Only the lowest mode (1,3) with the same scale as the topography has large amplitude. Other components have small amplitudes with a few exceptions and have phase variations of 40°-70° depending on the initial conditions. The stationary wave of $\psi(1,3)$ has a large amplitude in (H) and (L) and small value in (M). Note that the phase in (L) is very close to each other(<8°) in the three numerical integrations. While, $\theta(1,3)$ has a large amplitude and nearly the same phase in (L) and (M). The phase difference be-

tween $\psi(1,3)$ and $\theta(1,3)$ is 115° in (L) and very small in (H). In the category (L) the heat flux by this stationary wave is southward(counter-gradient for the zonal mean temperature).

We obtain similar result in other cases in Table 4. The composite fields of stream function in the upper layer are shown in Figs.10. For a smaller forcing parameter(θ_A^*=0.15, Fig.10-(1)), the zonal flow becomes weak a little in (H). In (L) similar flow patterns are obtained like those in Fig.8. The amplitude and the phase of (1,3) components are not influenced by the external forcing parameter, although there are some differences in small scales. In the case of the increased static stability(σ_0x1.5, Fig.10-(2)), stationary waves of small scales have small amplitude and the flow pattern is smoothed out. The amplitude of the (1,3) components in (L) increases a little with increasing the static stability and the phase of $\psi(1,3)$ is shifted westward about 60° without a change in the phase of $\theta(1,3)$.

A control experiment is performed to verify the effect of surface topography. We set the amplitude of topography equal to zero in the case of σ_0x1.25 and θ_A^*=0.2. Mean value and standard deviation of $\psi(1,0)$ are listed in Table 4. MV has nearly the same value as in the case with topography but SD is small about one order. The surface topography produces a large variability of the vertically averaged zonal flow $\psi(1,0)$ in the present model. Composite fields for the control experiment are shown in Fig.10-(3). The amplitude of all the stationary waves is small and the phase of them is dependent on the initial conditions. Especially the amplitude of $\psi(1,3)$ is small about one order or more compared with the cases with the topography.

5. Discussion

Almost all the equilibrium solutions obtained in the zonal flow-forced wave system in Part I are baroclinically unstable with respect to a perturbation of free wave with $4 \leqq \tilde{n}' \leqq 11$ (Fig.2). When a perturbation of the free wave is added to the unstable equilibrium states, the free wave grows up and the forced wave decays out as shown in Fig.3. Finally there appears a steady state in which finite amplitude free wave with a constant phase velocity balances with the marginally stable zonal flow. This steady state is independent of the forcing parameter θ_A^*, and has no topographic effect because the zonal flow in the lower layer is zero. In case 2 with the second meridional mode and the harmonic of the lowest zonal wavenumber, the wave-wave or wave-topography interaction is possible between $(1,\tilde{n})$, $(2,\tilde{n})$ and $(1,2\tilde{n})$ components. However, we obtained a similar final steady state as in case 1 with only $(1,0)$ and $(2,2\tilde{n})$ components for the external parameters given in Part I and the zonal wavenumber $\tilde{n}=3$ and 4. There is again no topographic effect because the zonal flow in the lower layer is zero and the amplitudes of $(1,\tilde{n})$, $(2,\tilde{n})$ and $(1,2\tilde{n})$ are also zero.

These final steady states are reminiscent of the baroclinic adjustment process proposed by Stone(1978). He hypothesized that baroclinic waves adjust the meridional gradient of the zonal mean temperature so as to keep it just above the threshold value for instability in a two-layer quasi-geostrophic model, and he obtained an observational result that the meridional temperature gradient in the northern troposphere is consistent with the hypothesis in all the seasons. The final steady states obtained in section 2 reveals that the baroclinic adjustment process oper-

ates completely in these cases of the present low-order model.

In contrast to the final steady states in cases 1 and 2, all the wave components have non-zero values in case 3, because all the wave components are coupled with the topography by the $\tilde{n}$-$2\tilde{n}$ interaction and the triad interactions. There appear various flow patterns(i.e., a steady flow, a periodic oscillation and an irregular fluctuation) depending on the external parameters such as the external forcing parameter θ_A^*, the frictional coefficients k and k', and the static stability σ_0(Table 2 and Fig.6). Dependency of the flow patterns on these parameters is consistent with that in the rotating annulus experiments with differential heating and bottom topography(Leach, 1981; Jonas, 1981) and with that in the numerical experiments by Yao(1980): The flow becomes irregular with increasing the Taylor number($\propto k^{-2}$) or with increasing the thermal Rossby number($\propto \theta_A^*$ or σ_0).

The wave component (1,3) with the same scale of the topography fluctuates like a standing oscillation(Fig.5) or in a highly irregular manner(Fig.7). The behavior of the wave does not resemble that in the zonal flow-forced wave system(Fig.10 in Part I). Isolated zonal flow-forced wave systems as in Part I and Charney and Straus(1980) are not sufficient to depict the behavior of forced waves when the flow system is more unstable with respect to another disturbance with different scale(in the present case baroclinic waves of $2\tilde{n}$ and $3\tilde{n}$). Charney and DeVore(1979) hypothesized that the baroclinic instability produces an additional forcing which ultimately drives the flow system from one metastable equilibrium state to another. However, the present two-layer model which contains the baroclinic waves explicitly

does not depict such a transition from one metastable state to another.

When the static stability σ_0 was increased to 1.25 times or 1.5 times, we obtained an irregular fluctuation of which the energy spectrum is similar to that in the real atmosphere. Marcus(1981) examined the effects of truncation in a problem of thermal convection in a sphere. His numerical examples indicate that, as long as the kinetic energy spectrum decreases with wavenumber, a truncation gives a qualitatively correct solution. It is not possible to apply his conclusion directly to our model. However, it is thought that the present model with the truncation level of case 3 and the increase of the static stability can depict a qualitatively correct behavior of the zonal flow and the waves in the atmosphere.

Irregular fluctuations obtained in some numerical integrations in the model with an increased static stability were analyzed in section 4 to elucidate the relation between the zonal flow and the stationary waves. However, the transient waves in each category were not mentioned there. Mean amplitude of the transient wave in each category is given by

$$\overline{\psi}_t(m,n) = \frac{1}{N'} \sum^{N'} [\{ \psi_{Kmn} - \overline{\psi}_c(m,n) \}^2 + \{ \psi_{Lmn} - \overline{\psi}_s(m,n) \}^2]^{1/2} \quad (5\text{-}1)$$

The mean amplitudes of the transient waves are rather large compared with those of the stationary waves. However, transient wave components in the low-index state (L) are smaller than those in the moderate state (M) with some exceptions. $\overline{\overline{\psi}}_t(1,3)$ component in three categories are as follows; (H):0.0313, (M):0.0323 and (L):0.0293(σ_0x1.25 and $\theta_A{}^*$=0.2). In the 9 numerical integrations

the decrease of the amplitude in (L) is 5-12% of that in (M). This decrease is consistent with the decrease of mean vertical shear $\theta(1,0)$ mentioned in section 4.

If the low-index state is related to the blocking phenomena, appearance of such a extreme state is not periodic but unexpectedly(Fig.7). Irregularity of the present system is more complicated than the 'deterministic nonperiodic flow'(the strange attractor) in the Lorenz's system of three ordinary nonlinear differential equations(Lorenz, 1963). Lorenz found that non-periodic solutions are ordinarily unstable with respect to small perturbations, so that slightly differing initial states can evolve into considerably different states. His conclusion about the predictability may be applied to the present system. Namely the prediction of the 'blocking state'(low-index state) for a very long range is impossible unless the initial conditions are known exactly. In Lorenz's study(1965) of the predictability with a 28-variable model, which is essentially identical to the present model except the topography, the time required for initial errors such as observational errors to grow to intolerable errors is in the range from a few days to a few weeks.

6. Conclusion

Nonlinear interactions between the zonal flow, topographically forced waves and free baroclinic waves were investigated by using the two-layer, quasi-geostrophic, low-order model in a mid-latitude β-plane(Yoden, 1983). An idealized surface topography was included in the model by retaining only one Fourier component of the zonal wavenumber $\tilde{n}=3$ with the gravest meridional mode.

First of all, effects of the truncation were examined by a stepwise relaxation of the truncation level. It was revealed that at least 28 degrees of freedom(case 3 in Fig.1) are necessary for the system to depict the coexistence of both of the forced and free waves and interactions with each other. For more severely truncated cases, there appears a final steady state with no forced waves, because the baroclinic adjustment process(Stone, 1978) operates completely and the topographic effect is absent.

For the system in case 3, there appear several types of time-dependent flow patterns depending on the external parameters such as the external thermal forcing, the frictional coefficients and the static stability: Steady flow, periodic or quasi-periodic oscillation and irregular fluctuation. There appears an irregular fluctuation with large amplitude waves for the external parameters corresponding to the real atmosphere.

Irregular fluctuations obtained in the numerical integrations over a long time-span were analyzed to elucidate the relation between the zonal flow and stationary waves. The flow pattern at each time step was classified into one of three categories, i.e., the high-index state (H), the moderate state (M) and the low-index state (L), in terms of the vertically

averaged zonal flow $\psi(1,0)$. The ratio of the time span in each category is 15:70:15 for 9 cases in Table 4 when the threshold values are taken as the mean value(MV) ± standard deviation(SD).

The composite fields of stream function are characterized by the strong and moderate zonal flows in (H) and (M) and the meander of the flow in (L). In the low-index state (L) the dominant stationary wave of (1,3) with the same scale as the topography has a larger amplitude than in (H) and (M). The ridge is located in the western slope of the topography. The effects of the surface topography on this stationary wave is obvious from the control experiment without the topography(Fig.10). The stationary waves in the irregular fluctuation are different from the forced waves in the equilibrium solutions(Fig.4 in Part I) in their magnitude and structure. The difference between the equilibrium solutions and the time-averaged states was already pointed out by Yao(1980).

In summary, the present model similar to the atmospheric conditions is characterized by the irregularity(or transiency): The flow varies irregularly and transits between the categories. When the flow is in a low-index state, both of the mean value and the vertical shear of the zonal flow decrease, the stationary wave has a larger amplitude, and free waves have smaller amplitudes.

In the present study only the effect of the topography was investigated. However, the land-sea distributions may play an important role in producing the forced planetary waves. Simple representation of the diabatic heating due to the land-sea distributions will be incorporated into the present model by using the Newtonian heating with longitudinal differential equilibrium

temperature. It is a future problem to investigate the effect of the land-sea distributions and the coupled effect with the topography by using a simple low-order model.

Acknowledgements

The present paper is the main part of the author's doctoral dissertation submitted to Kyoto University in 1982. He is indebted to Prof. I. Hirota of the Geophysical Institute of Kyoto University and Prof. R. Yamamoto of the Laboratory for Climatic Change Research of Kyoto University for their continuing guidance and encouragement through that dissertation work. Thanks are also due to Prof. A. Arakawa of the University of California, Los Angels, for his helpful discussion.

The computations were performed with the use of the FACOM M-200 computer at the Data Processing Center of Kyoto University.

References

Austin, J. F., 1980: The blocking of middle latitude westerly winds by planetary waves. Quart. J. R. Met. Soc., 106, 327-350.

Charney, J. G. and J. G. DeVore, 1979: Multiple flow equilibria in the atmosphere and blocking. J. Atmos. Sci., 36, 1205-1216.

——— and D. M. Straus, 1980: Form-drag instability, multiple equilibria and propagating planetary waves in baroclinic, orographically forced, planetary wave systems. J. Atmos. Sci., 37, 1157-1176.

Eady, E. T., 1949: Long waves and cyclone waves. Tellus, 1, 33-52.

Egger, J., 1978: Dynamics of blocking highs. J. Atmos. Sci., 35, 1788-1801.

Frederiksen, J. S., 1982: A unified three-dimensional instability theory of the onset of blocking and cyclogenesis. J. Atmos. Sci., 39, 969-982.

Jonas, P. R., 1981: Laboratory observations of the effects of topography on baroclinic instability. Quart. J. R. Met. Soc., 107, 775-792.

Leach, H., 1981: Thermal convection in a rotating fluid: effects due to bottom topography. J. Fluid Mech., 109, 75-87.

Lorenz, E. N., 1963: Deterministic nonperiodic flow. J. Atmos. Sci., 20, 130-141.

———, 1965: A study of the predictability of a 28-variable atmospheric model. Tellus, 17, 321-333.

McWilliams, J. C., 1980: An application of equivalent modons to

atmospheric blocking. Dyn. Atmos. Oceans, 5, 43-66.

Marcus, P. S., 1981: Effects of truncation in modal representation of thermal convection. J. Fluid Mech., 103, 241-255.

Patoine, A. and T. Warn, 1982: The interaction of long, quasi-stationary baroclinic waves with topography. J. Atmos. Sci., 39, 1018-1025.

Pedlosky, J., 1979: Geophysical Fluid Dynamics. Springer-Verlag. 485-492.

Treidl, R. A., E. C. Birch and P. Sajecki, 1981: Blocking action in the northern hemisphere: A climatological Study. Atmosphere-Ocean, 19, 1-23.

Schilling, H. D., 1982: A numerical investigation of the dynamics of blocking waves in a simple two-level model. J. Atmos. Sci., 39, 998-1017.

Stone, P. H., 1978: Baroclinic adjustment. J. Atmos. Sci., 35, 561-571.

Tomatsu, K., 1979: Spectral energetics of the troposphere and lower stratosphere. Adv. Geophys., 21, 289-405.

Trevisan, A. and A. Buzzi, 1980: Stationary response of barotropic weakly nonlinear Rossby waves to quasi-resonant orographic forcing. J. Atmos. Sci., 37, 947-957.

Tung, K. K. and R. S. Lindzen, 1979: A theory of stationary long waves. Part I: A simple theory of blocking. Mon. Wea. Rev., 107, 714-734.

Yao, M. S., 1980: Maintenance of quasi-stationary waves in a two-level quasi-geostrophic spectral model with topography. J. Atmos. Sci., 37, 29-43.

Yoden, S., 1983: Nonlinear interactions in a two-layer, quasi-geostrophic, low-order model with topography. Part I: Zonal flow-forced wave interaction. J. Meteor. Soc. Japan, XXXXX.

Table 1 Final steady states obtained by some numerical integrations in case 1($\tilde{n}=3$). Amplitude of free wave component($\tilde{n}'$) in the upper layer is denoted by $\psi_1(1,\tilde{n}')$ and that in the lower layer by $\psi_3(1,\tilde{n}')$. Phase difference between the layers and phase velocity of the free wave are $\Delta\phi$ and c, respectively. Positive value of $\Delta\phi$ corresponds to the westward tilt of the phase lines with height. For $\tilde{n}'\leq 2$ or $\tilde{n}'\geq 12$, free waves do not grow up and there appears the W1 equilibrium solution of $\tilde{n}=3$.

$\tilde{n}$	$\Theta_{A_1}^*$	$\psi(1,0)$	$\theta(1,0)$	$\psi_1(1,\tilde{n}')$	$\psi_3(1,\tilde{n}')$	$\Delta\phi$	c
		[	x 10^{-4}		]	[°]	[m/s]
7	0.05	172	172	488	154	14.9	-0.91
7	0.1	172	172	782	247	14.9	-0.92
7	0.15	172	172	993	314	14.9	-0.92
7	0.2	172	172	1166	369	14.9	-0.92
2	0.2	977	797	[W1 equilibrium solution]			
4	0.2	422	422	1849	419	12.3	-3.92
6	0.2	213	213	1338	382	14.2	-1.62
8	0.2	150	150	1040	365	14.9	-0.29
10	0.2	163	163	933	419	11.5	1.50
11	0.2	347	347	1137	615	5.2	6.76
12	0.2	977	797	[W1 equilibrium solution]			

Table 2 Classification of time-dependent behavior for some combinations of external parameters. Four categories are denoted by S: steady flow with propagating wave, P: periodic oscillation, Q: quasi-periodic oscillation, and I: irregular fluctuation. Subscripts 5 and a-j denote corresponding figure in Fig.5 and Fig.6(a)-(j).

(a)

$k \cdot k' \times$ \ Θ_A^*	0.02	0.04	0.06	0.08	0.1	0.12	0.14	0.16	0.18	0.2
1.0	Q_a	P	P	P	P_c	P	P	P	P	P_5
0.75	Q	P	P	P	P	Q	I	Q	I	I_e
0.5	I_b	I	I	Q	Q_d	I	I	I	I	I_f

(b)

Θ_A^* \ $\sigma_0 \times$	0.5	0.8	1.0	1.25	1.5	2.0	4.0
0.1	S	S_g	P_c	I_h	I	I_i	P_j
0.2	S	S	P_5	I	I	I	I

Table 3 Mean values of the zonal flow and amplitudes of wave component.

Averaged period is from 3,750 to 7,500 in non-dimensional time.

Θ_A*	k·k'×	σ_0×	$\overline{\psi}(1,0)$	$\overline{\psi}(2,0)$	$\overline{\psi}(1,3)$	$\overline{\psi}(2,3)$	$\overline{\psi}(1,6)$	$\overline{\psi}(2,6)$	$\overline{\psi}(1,9)$	$\overline{\psi}(2,9)$
			[			x 10^{-4}				]
0.02	1.0	1.0	177	0	3	10	10	6	31	43
0.08	"	"	233	0	12	6	7	86	4	417
0.14	"		264	-0	15	8	14	191	9	584
0.2	"		279	-0	17	14	27	325	20	689
0.1	1.0	1.0	241	0	13	7	8	106	5	484
"	0.75	"	284	0	27	22	37	233	13	511
"	0.5	"	315	0	72	55	93	265	36	592
0.1	1.0	0.8	112	-0	6	9	8	0	1	452
"	"	1.0	241	0	13	7	8	106	5	484
"	"	1.25	270	3	189	185	188	150	189	311
"	"	1.5	357	18	219	213	222	207	200	194
"	"	2.0	414	-21	258	231	269	192	111	93
	"	4.0	795	-0	56	111	41	3	3	2

Table 4 Mean value(MV) and standard deviation(SD) of $\psi(1,0)$ for 12 numerical integrations. Period of the statistics is from 1,251 to 25,000(in dimensional 2,672 days). Figure in parenthesis is the result for a control experimemt without surface topography. All the values are multiplied by 10^4.

$\Theta_{A_1}^*$		σ_0 x 1.25			σ_0 x 1.5		
		W1	W2	Hadley	W1	W2	Hadley
0.15	MV	290	288	286	-	-	-
	SD	182	173	178	-	-	-
0.2	MV	308(288)	263(291)	297(294)	296	321	323
	SD	219(21)	234(21)	243(18)	310	294	303

Table 5 Zonal components in three categories. All the values are multiplied by 10^4. Total number in each category N' is also listed.

category	N'			$\psi(1,0)$			$\theta(1,0)$			$\psi(2,0)$			$\theta(2,0)$		
	W1	W2	H.	W1	W2	H.	W1	W2	H.	W1	W2	H.	W1	W2	H.
(H)	3717	3471	3375	629	604	663	325	310	322	-11	3	5	-3	-3	5
(M)	16486	16579	16799	313	276	308	297	294	298	2	-3	-2	-1	-1	-3
(L)	3547	3700	3576	-52	-119	-100	253	244	256	4	2	8	2	-1	4

Figure captions

Fig.1 Schematic representation of the interactions permitted in three cases of different truncation level : case 1(M=1, N=2), case 2(M=2, N=2) and case 3(M=2,N=3). Zonal flow-wave interaction is denoted by a solid line and wave-wave interaction by a broken line. Surface topography is given by (1,n) component(shaded). Interactions permitted in case 2 are denoted by thin lines in case 3.

Fig.2 Linear stability of the equilibrium solutions($\tilde{n}$=3) with respect to free waves with zonal wavenumber $\tilde{n}$=1-12(abscissa). Growth rate of the most unstable perturbation is contoured. In dimensional, σ_r=0.1 corresponds to e-folding time of 27 hours.

Fig.3 Time-evolution of the zonal and wave components in case 1. Initial condition is the W1 solution with small perturbation (θ_A^*=0.2). 1,000 nondimensional time corresponds to 112.5 days.

Fig.4 As in Fig.3 for the truncation level of case 2. Only ψ components are presented.

Fig.5 Time-variation of the zonal and wave components in case 3(only ψ components are presented). θ_A^*=0.2. 2,500 time steps from t=5,001 to t=7,500 are presented(in dimensional 281.3 days).

Fig.6 Four types of time variation of the zonal component $\psi(1,0)$. External parameters in (a)-(j) are listed in Table 2. Steady flow(S): (g), periodic oscillation(P): (c), (j), quasi-periodic oscillation(Q): (a), (d), and irregular fluctuation(I): (b), (e), (f), (h), (i).

Fig.7 As in Fig.5 except for σ_0x1.25. Initial condition is the W2 solution with small perturbations. Note that scale of the ordinate is 1/2 for the zonal components. Threshold values for three categories(mean value $\pm$ standard deviation) are denoted by dotted lines.

Fig.8 Composite fields of stream function in three categories. σ_0x1.25, $\theta_A{}^*$=0.2 and the W2 initial condition.

Fig.9 Amplitude and phase of the stationary waves in three categories. Three independent runs with different initial conditions are designated by symbols as follows; W1(●), W2(▲) and Hadley(+). $\psi(m,n)$ component is denoted by a solid line and $\theta(m,n)$ by a broken line. Amplitude is multiplied by 10^3. σ_0x1.25 and $\theta_A{}^*$=0.2.

Fig.10 Composite fields of stream function in the upper layer. (1): σ_0x1.25, $\theta_A{}^*$=0.15 and the Hadley initial condition. (2): σ_0x1.5, $\theta_A{}^*$=0.2 and the Hadley initial condition. (3): control experiment without topography. σ_0x1.25, $\theta_A{}^*$=0.2 and the Hadley initial condition.

CASE 1

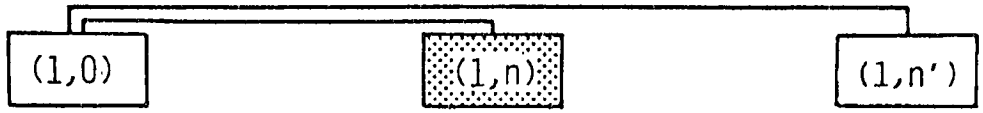

CASE 2

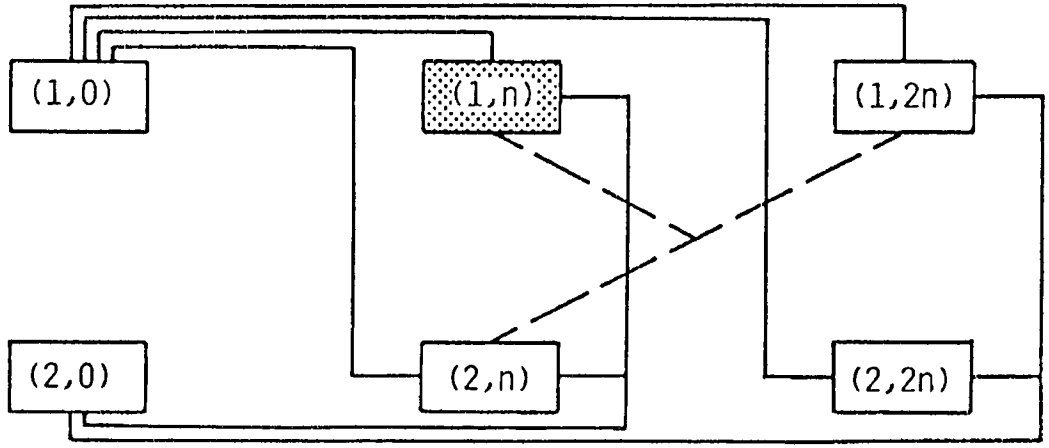

CASE 3

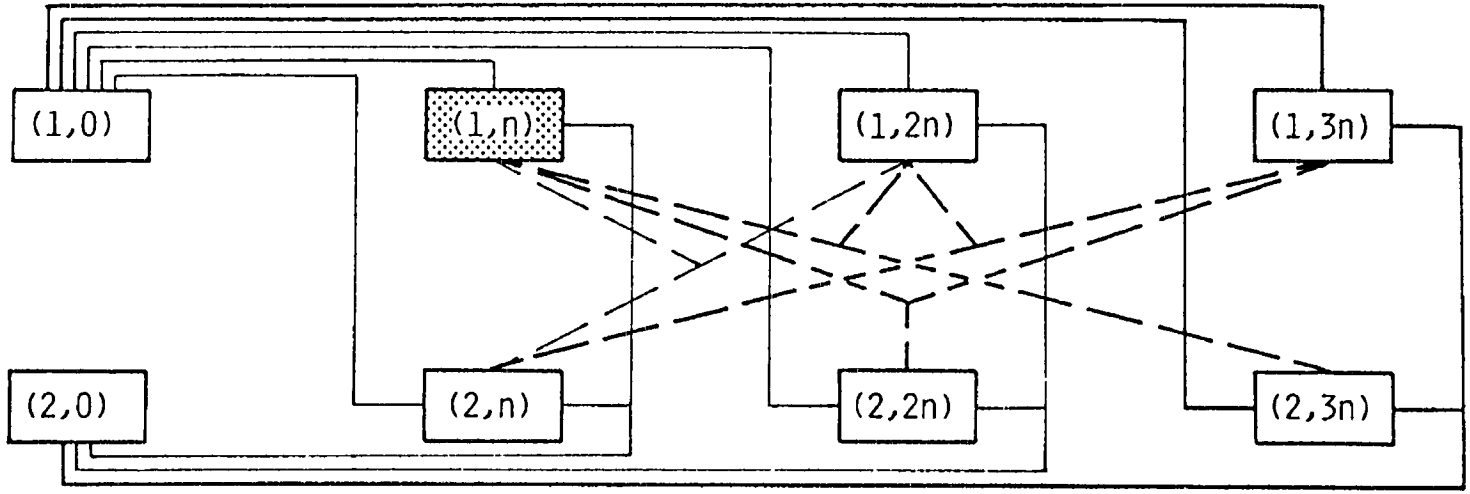

Fig. 1

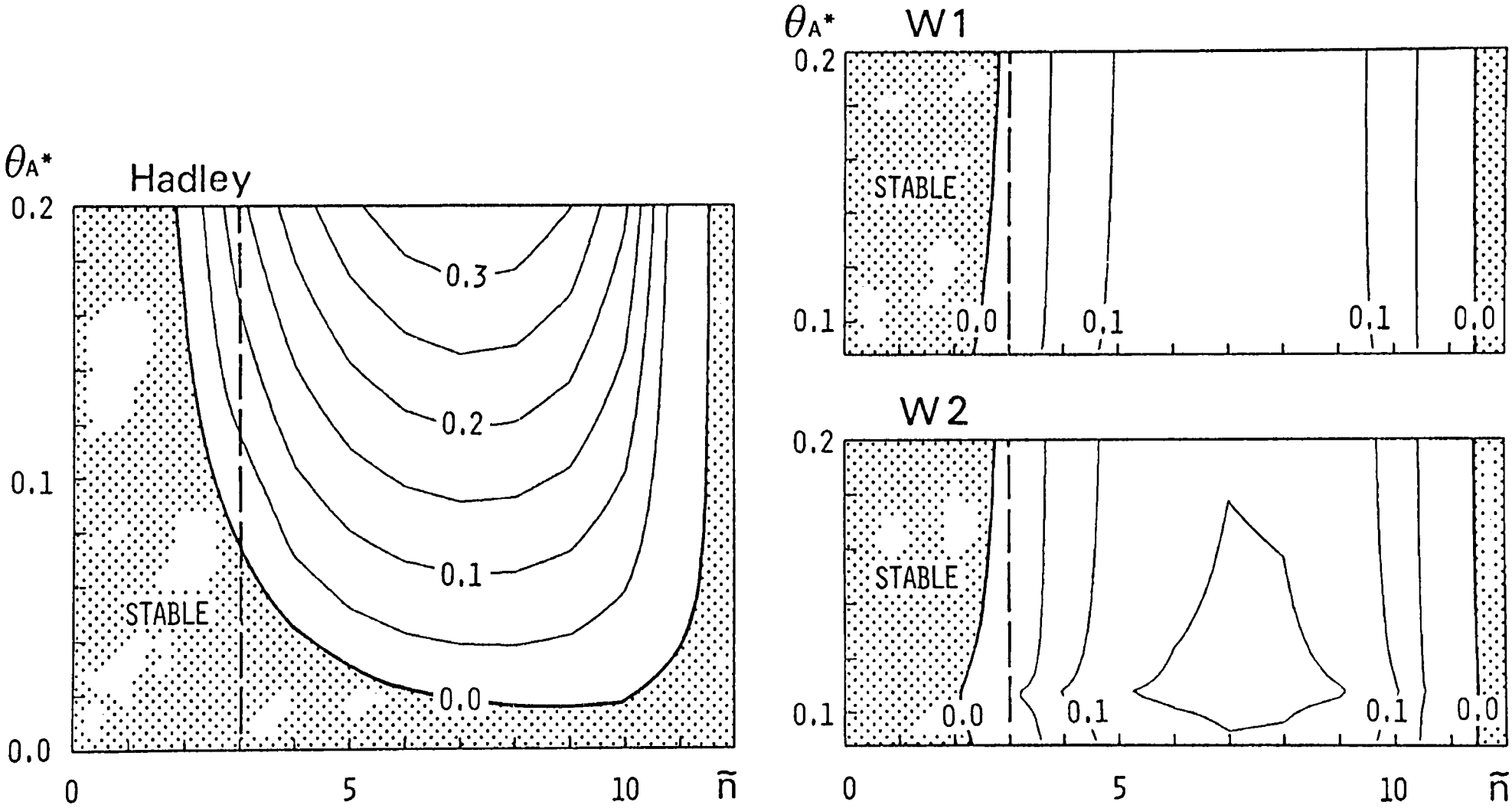
θA*
Hadley
0.2
0.1
0.0
0.3
0.2
0.1
0.0
STABLE
0
5
10
ñ
θA*
W1
0.2
0.1
STABLE
0.0
0.1
0.1
0.0
W2
0.2
0.1
STABLE
0.0
0.1
0.1
0.0
0
5
10
ñ

Fig. 2

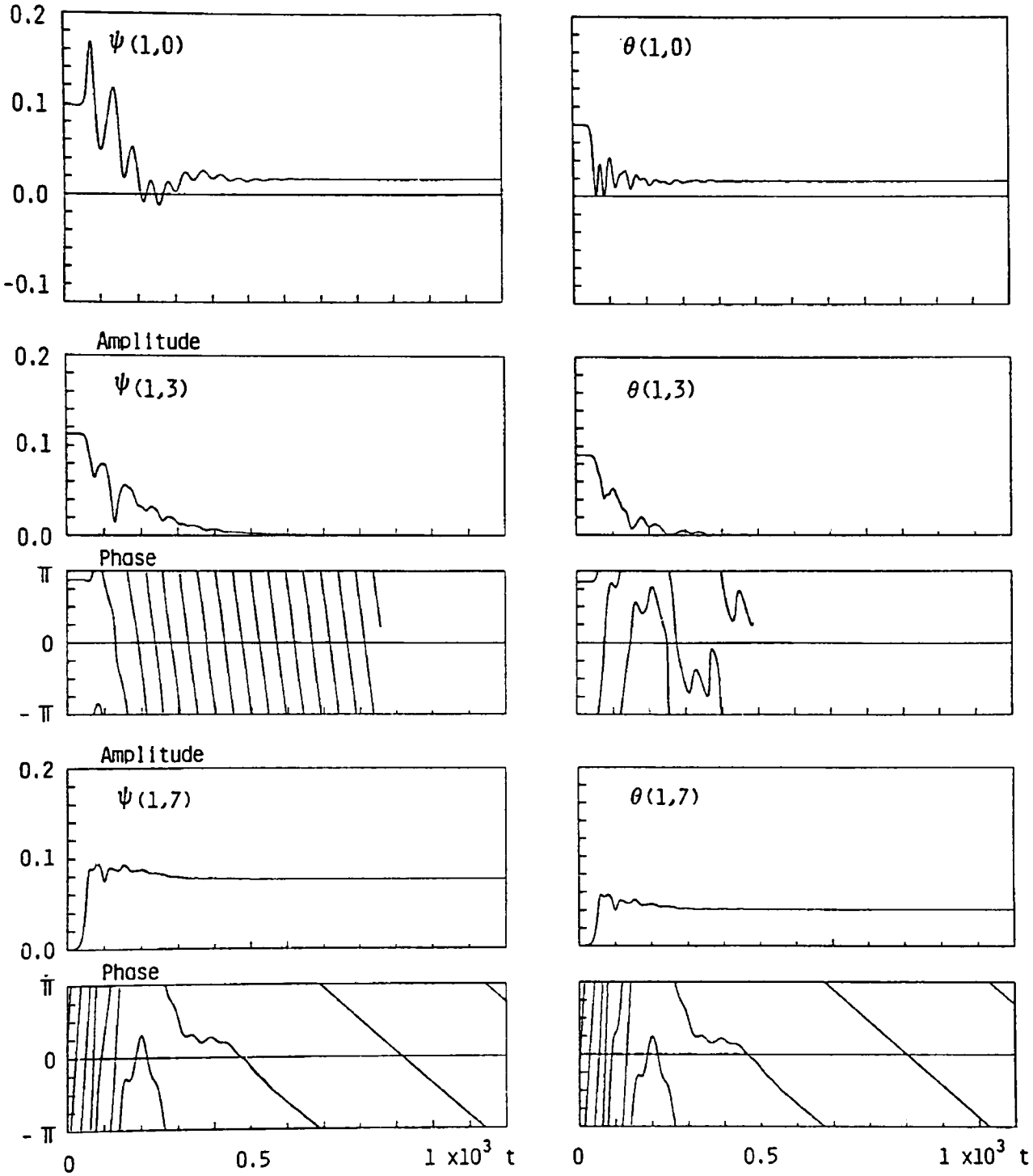
0.2
0.1
0.0
-0.1
ψ(1,0)
θ(1,0)
Amplitude
ψ(1,3)
θ(1,3)
Phase
π
0
- π
Amplitude
ψ(1,7)
θ(1,7)
Phase
0
0.5
1 x10^3 t

Fig. 3

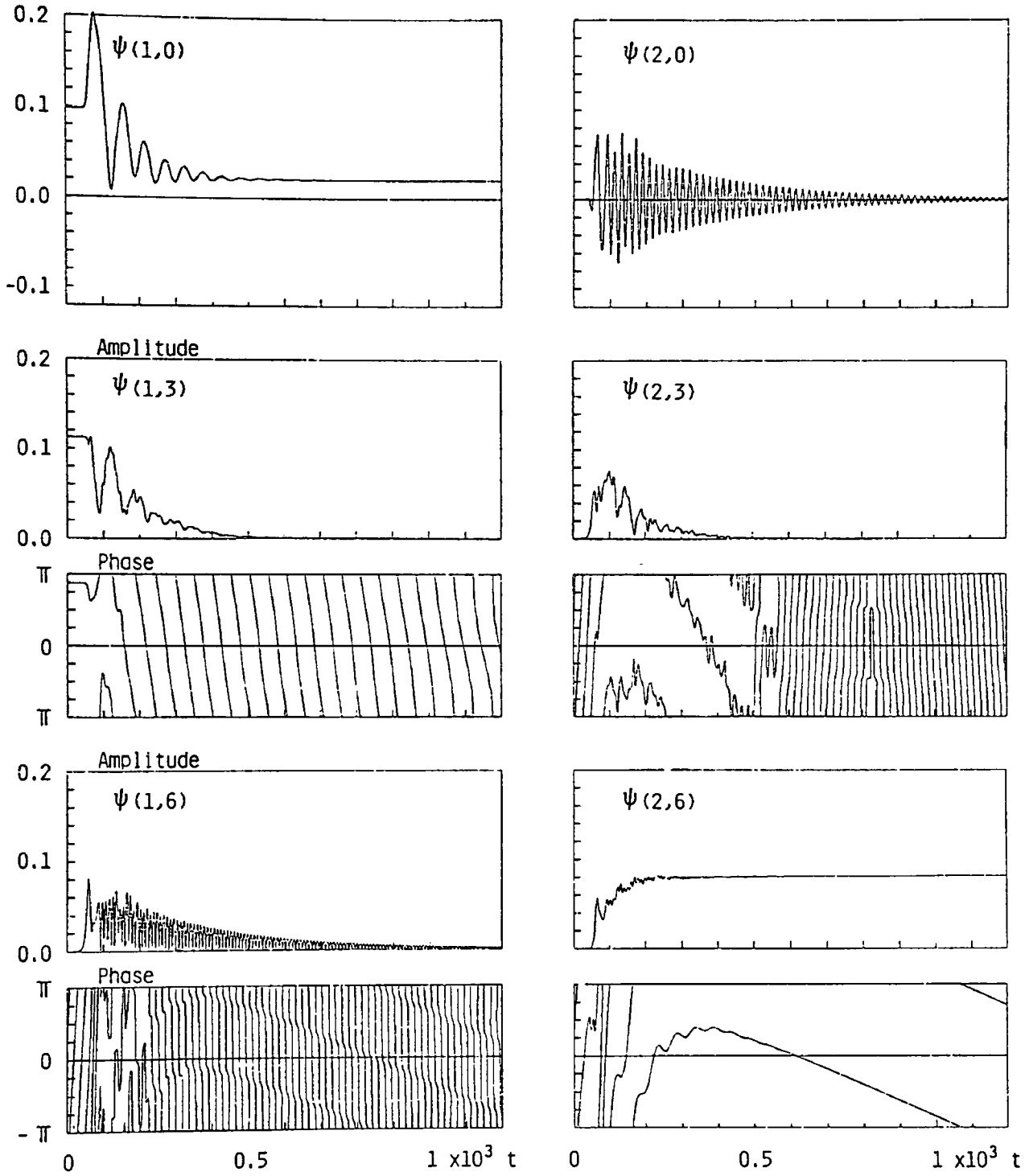
0.2
0.1
0.0
-0.1
ψ(1,0)
ψ(2,0)
Amplitude
ψ(1,3)
ψ(2,3)
Phase
π
0
π
Amplitude
ψ(1,6)
ψ(2,6)
Phase
π
0
- π
0
0.5
1 x10³ t
0
0.5
1 x10³ t

Fig. 4

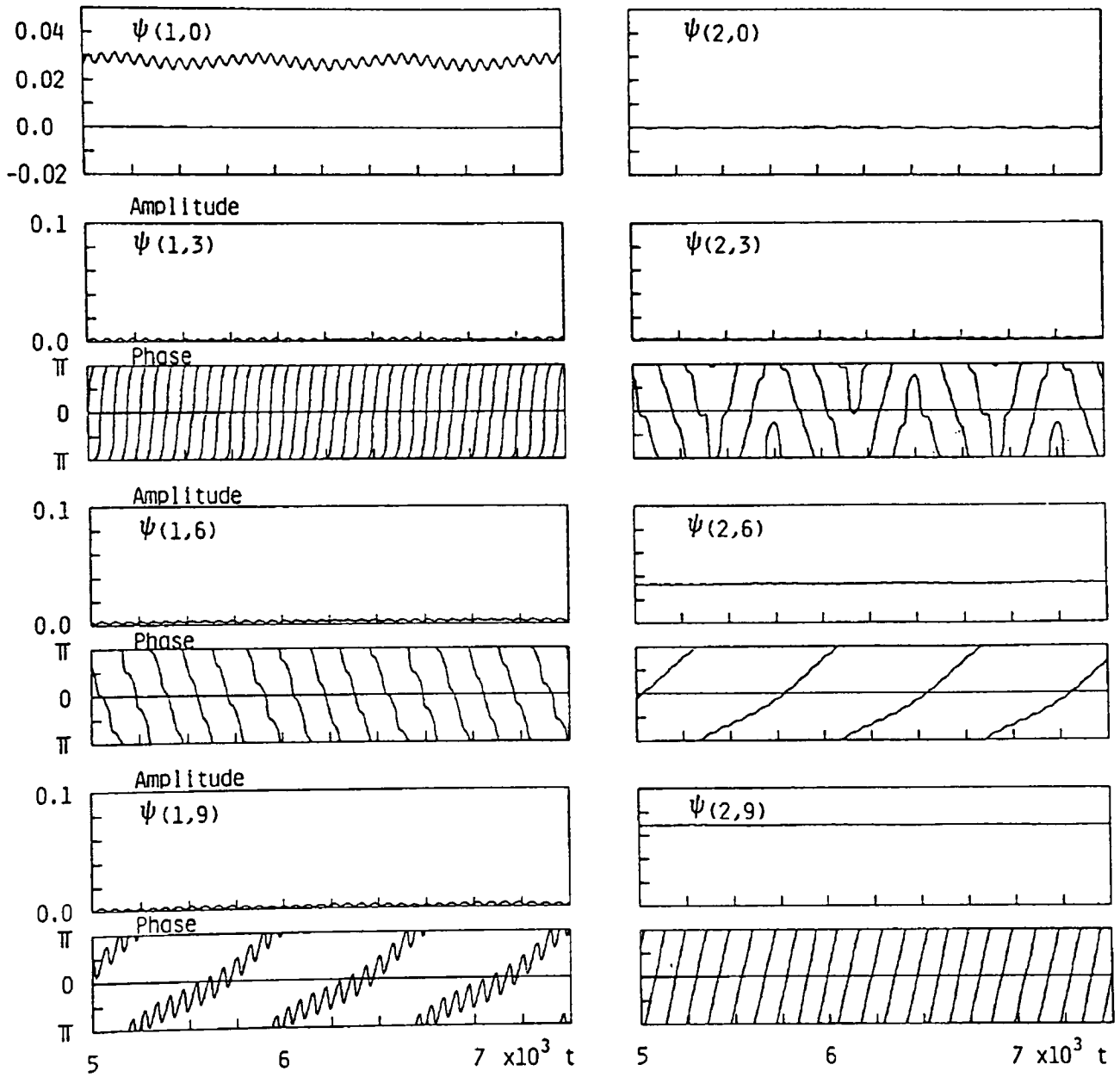
0.04
0.02
0.0
-0.02
ψ(1,0)
ψ(2,0)
Amplitude
0.1
ψ(1,3)
ψ(2,3)
0.0
π
Phase
0
π
Amplitude
0.1
ψ(1,6)
ψ(2,6)
0.0
π
Phase
0
π
Amplitude
0.1
ψ(1,9)
ψ(2,9)
0.0
π
Phase
0
π
5
6
7 x10^3 t
5
6
7 x10^3 t

Fig. 5

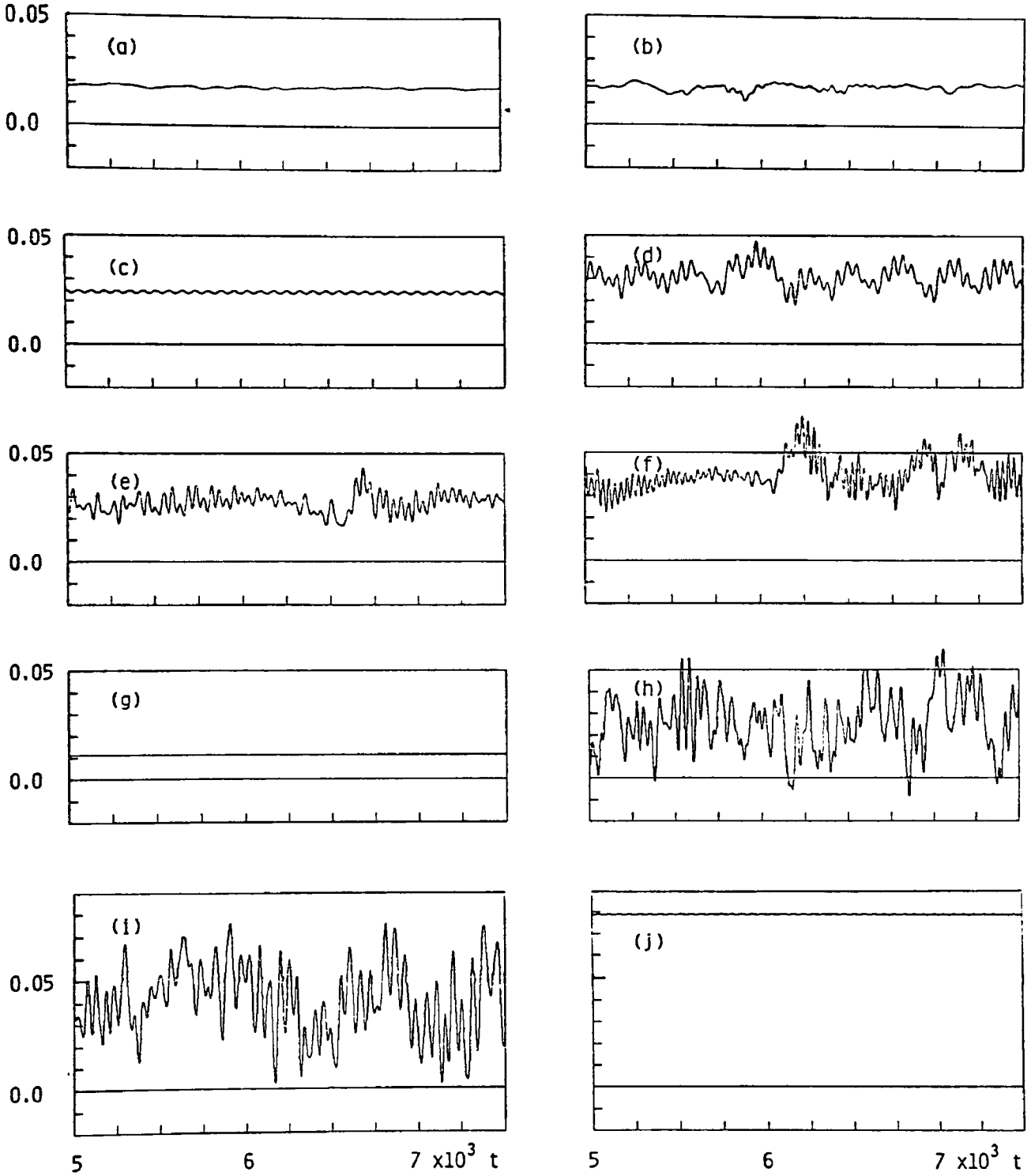

Fig. 6

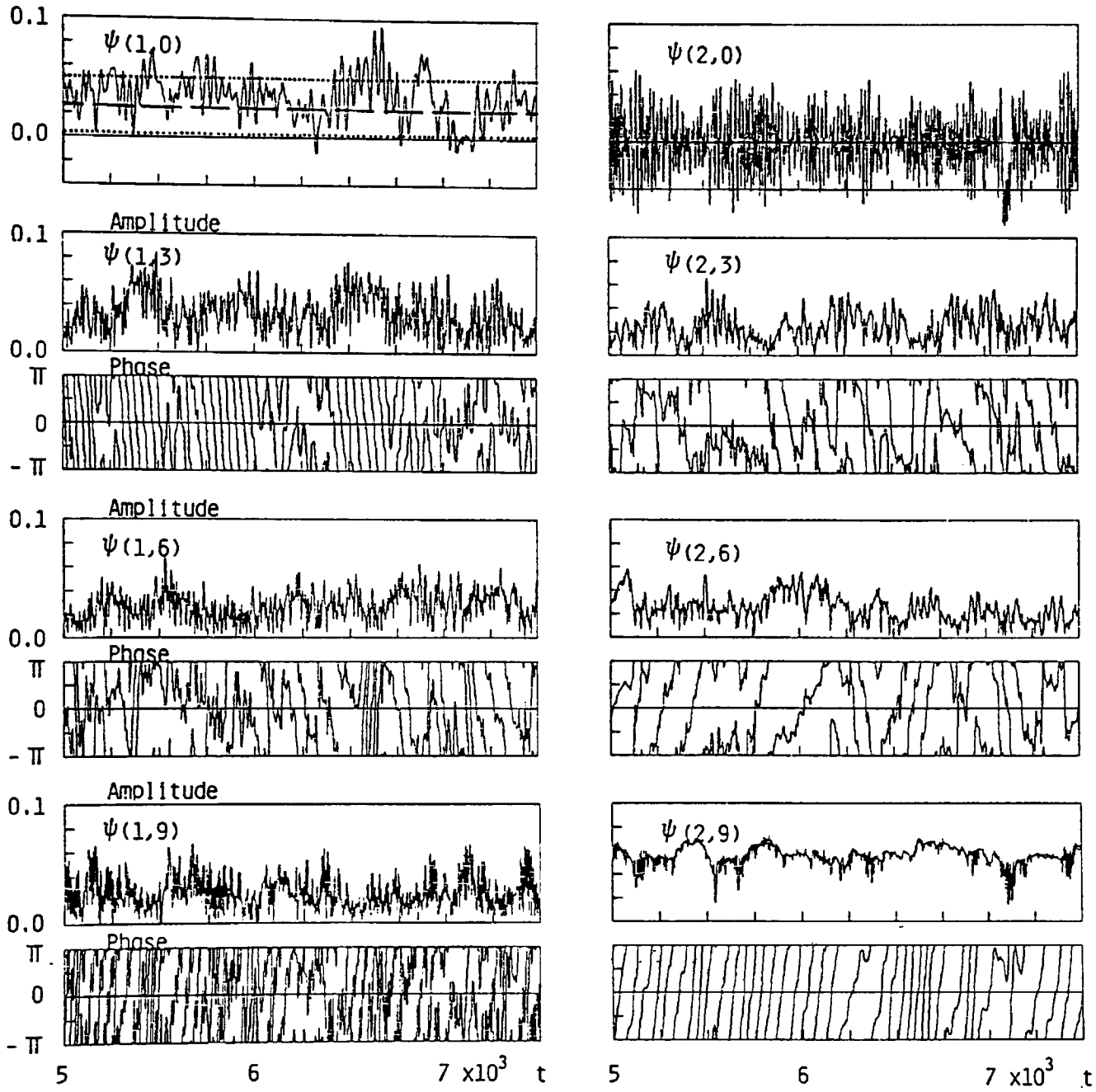
0.1
ψ(1,0)
0.0
ψ(2,0)
Amplitude
0.1
ψ(1,3)
0.0
ψ(2,3)
Phase
π
0
- π
Amplitude
0.1
ψ(1,6)
0.0
ψ(2,6)
Phase
π
0
- π
Amplitude
0.1
ψ(1,9)
0.0
ψ(2,9)
Phase
π
0
- π
5
6
7 x10^3
t
5
6
7 x10^3
t

Fig. 7

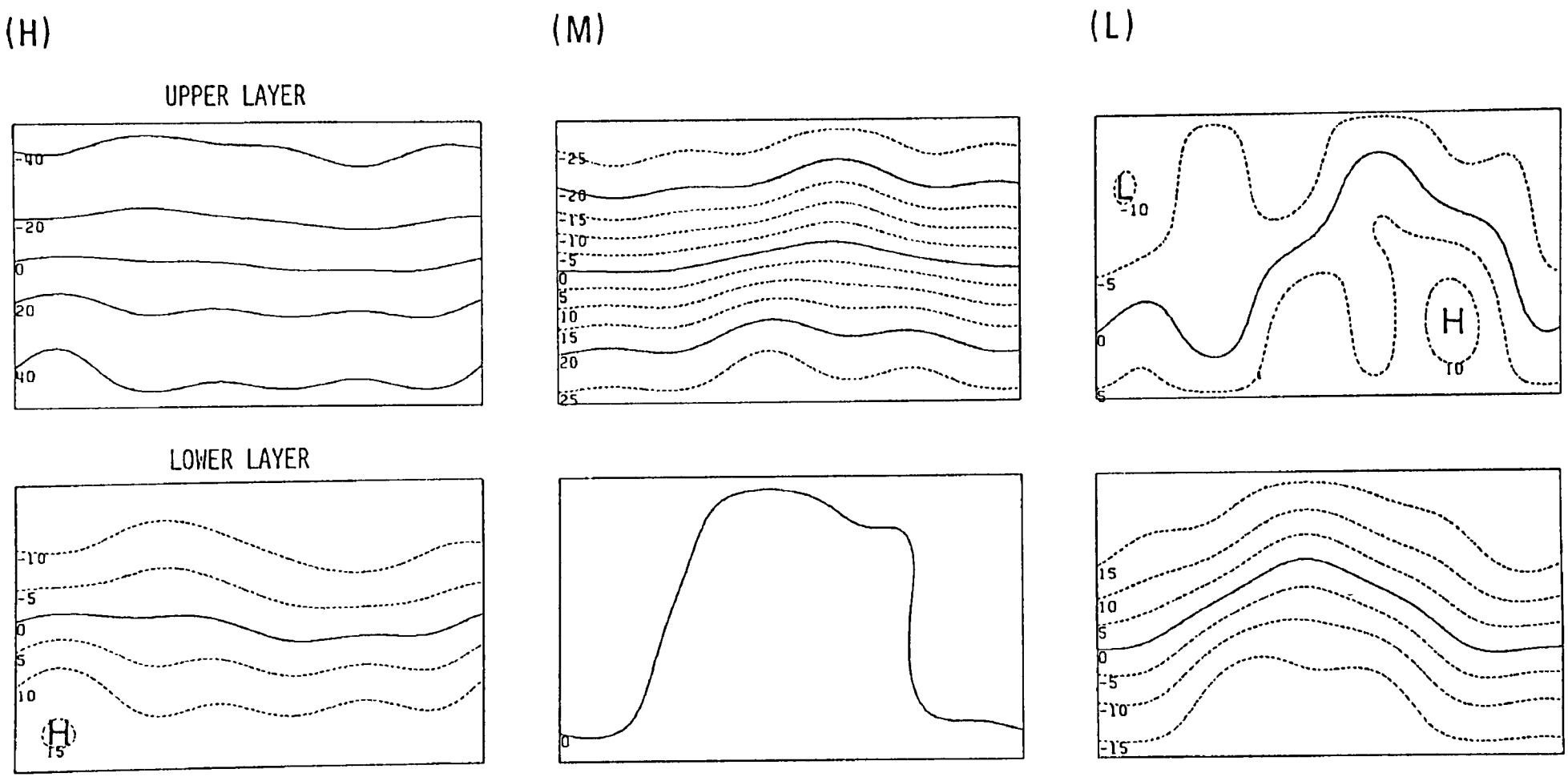
(H)
(M)
(L)
UPPER LAYER
-40
-20
0
20
40
-25
-20
-15
-10
-5
0
5
10
15
20
25
-10
-5
0
5
10
H
LOWER LAYER
-10
-5
0
5
10
15
H
0
15
10
5
0
-5
-10
-15

Fig. 8

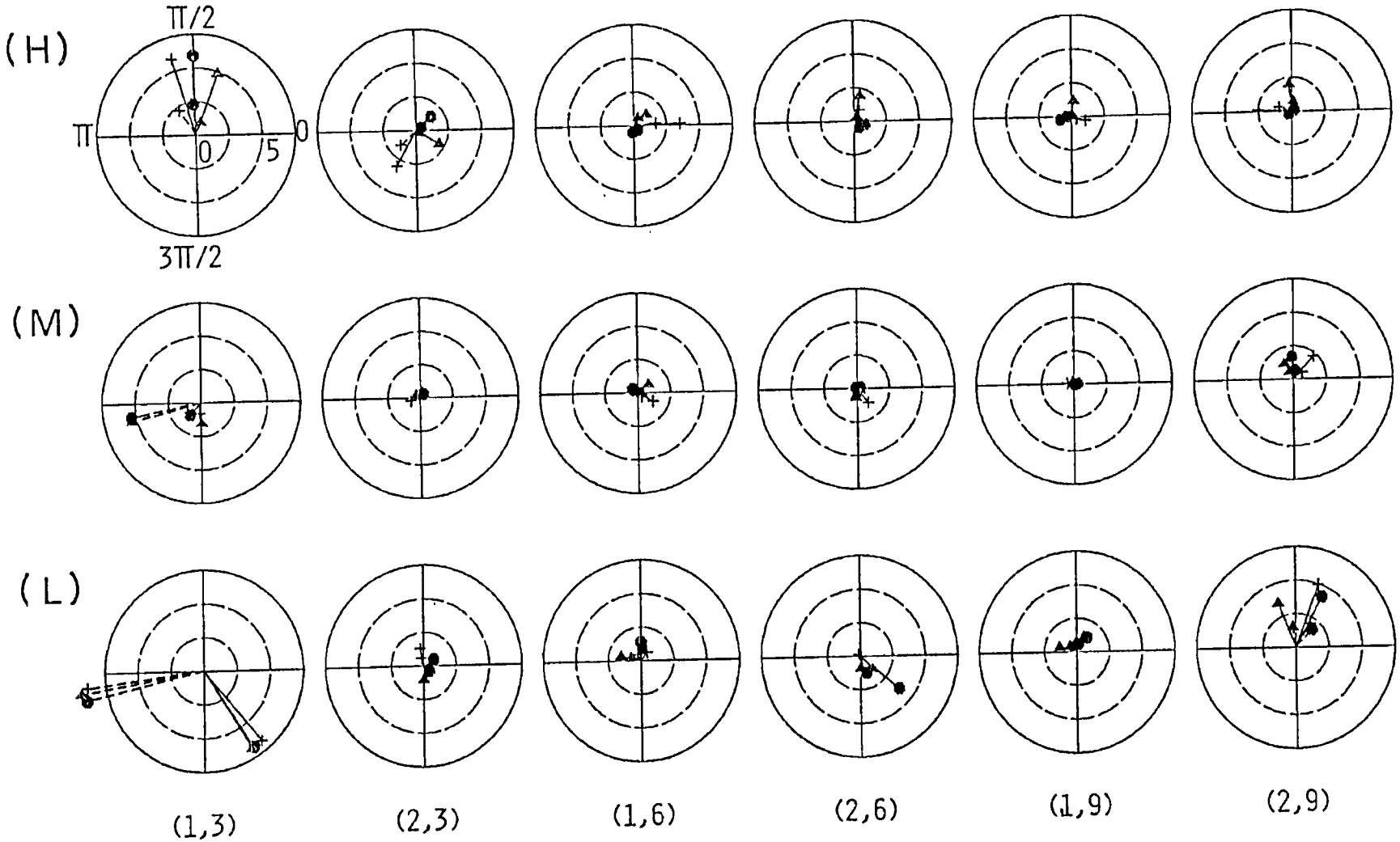

Fig. 9

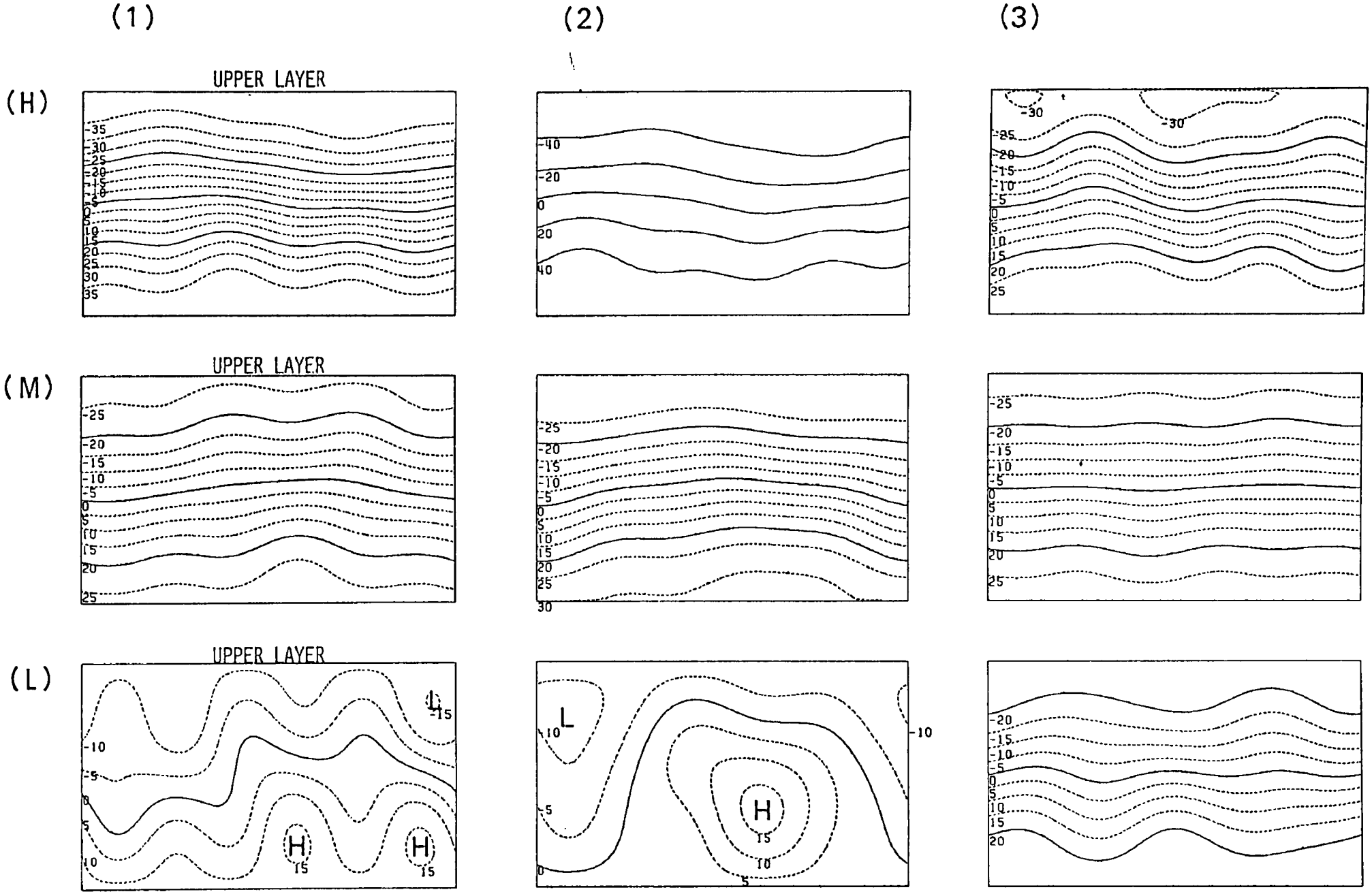

Fig. 10

地形を含む二層準地衡低次モデルにおける非線型相互作用

II：帯状流－強制波－自由波間の相互作用

余田成男

京都大学理学部地球物理学教室

第I部で作成した二層・準地衡風近似の低次モデルを用いて，帯状流と地形による強制波および傾圧不安定波間の非線型相互作用を調べた．理想化された地形として，このモデルで許されるいちばん大きなフーリエ成分のみの地形を入れた．

帯状流が，地形と直接結びついた強制波よりも自由波に対してより不安定になるとき，次のような最終定常状態が出現する．すなわち，一定の振幅と位相速度をもつ自由波（傾圧波）が臨界安定な帯状流とつりあい，強制波は減衰してしまう．他方，帯状流が地形の影響をうける波に対してより不安定になるとき，両方の波が存在する．

この論文中で扱う最も自由度が大きい場合

は，南北に2つのモード，東西に帯状成分と $\tilde{n}$，$2\tilde{n}$，$3\tilde{n}$ の3つの波を許した28次のモデルである．このとき，すべての波成分は地形と相互作用して，流れは時間とともに変化してゆく．変化の様子は次の4つの型に分けられ，その選択は，外部加熱による強制，摩擦，静的安定度という外部パラメータに依存している：(1)一定の強制波と移動波を含む定常流，(2)周期振動流，(3)準周期的振動流，(4)不規則変動流．

地球大気に対応する外部パラメータを与えると，大きな振幅の波成分を含む不規則変動が出現する．この不規則変動をする状態中での帯状流と波動の関係を，長期間にわたる統計として調べた．各時刻での流れを，帯状流の強さを基準にして3つのカテゴリーに分類した．カテゴリー毎に合成した流れの場は次のような特徴をもつ．帯状流の卓越する高次数状態および中間状態と，流れの蛇行する低次数状態である．この低次数状態では，帯

状流の強さおよび鉛直シアーが小さく，他の状態よりも停滞波の振幅が大きくなり，移動波の振幅が減少する．

不規則変動しているなかで，ある期間の平均として定義された停滞波は，第Ⅰ部で得られた平衡解の強制波と重なった振幅・構造としている．